PERIODICA POLYTECHNICA

TRANSPORTATION ENGINEERING

TECHNICAL UNIVERSITY OF BUDAPEST

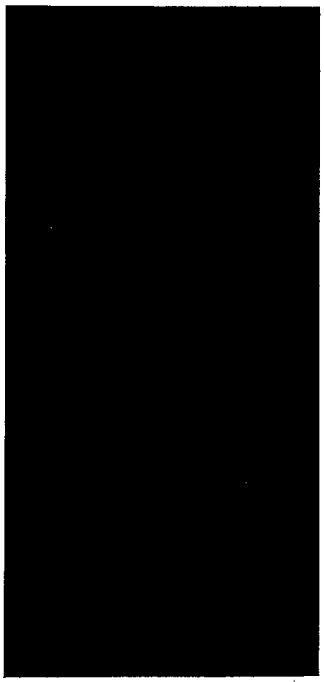

Vol. 23. Nos. 1-2.
1995

PERIODICA POLYTECHNICA

A contribution to international technical sciences, published by the Technical University of Budapest in six separate series, covering the following sciences:

Chemical Engineering
Civil Engineering
Electrical Engineering and Informatics
Mechanical Engineering
Social and Management Sciences (Earlier: Humanities and Social Sciences)
Transportation Engineering

TRANSPORTATION ENGINEERING SERIES

Published twice a year

Contributions in transportation engineering should be sent to the address of the journal:

TECHNICAL UNIVERSITY OF BUDAPEST
Periodica Polytechnica
Transportation Engineering
H-1521 Budapest, HUNGARY
Telefax: + 36 1 463-2141

For subscriptions please contact "Andreas Hess" Ltd. (Mail: P.O.B. 190, Budapest III, H-1300; Telefax: +36 1 250–2188) or its representatives abroad.

Exchange copies should be requested from the International Exchange Department of the Central Library of the Technical University of Budapest
(H–1111 Budapest, Budafoki út 4.; Telefax: + 36 1 463–2440).

Published by the Technical University of Budapest, Hungary, with the financial help of the foundation "Ipar a korszerű mérnökképzésért" (Industry for Modern Education in Engineering).

HU ISSN: 0303–7800

PERIODICA POLYTECHNICA

TRANSPORTATION ENGINEERING

Vol. 23 * Nos. 1–2 * 1995

TECHNICAL UNIVERSITY
BUDAPEST

PRINTED IN HUNGARY
LIGATURA LTD – ÁFÉSZ PRESS, VÁC

PERIODICA POLYTECHNICA SER. TRANSP. ENG. VOL. 23, NO. 1, PP. 3-18 (1995)

ON REAL-TIME SIMULATION OF THE LONGITUDINAL DYNAMICS OF TRAINS ON A SPECIFIED RAILWAY LINE

István ZOBORY and Elemér BÉKEFI [‡]

Department of Railway Vehicles
Technical University of Budapest
H-1521 Budapest, Hungary

Received: 9 November, 1994

Abstract

The dynamical model of the train is a simplified linear lumped-parameter one. The steady-state tractive effort is specified by the points of the bivariate, control and velocity dependent tractive effort performance curves. The train is equipped with an airbrake system. The vehicles in the train are characterized by the traction resistance functions, while the railway line is specified by the arclength-dependent track-slope and track-curvature functions. The equations of motion of the train are numerically solved under real-time conditions. The drive and brake controls are given from the computer keyboard. The results of the real-time simulation can be continuously followed on the computer screen. Statistical analysis of the results and visualization can also be initiated through activizing evaluation software.

Keywords: train dynamics, train operation, real-time simulation.

1. Introduction

In this paper, the train is modelled as a complex dynamical system, which moves along a specified railway line under the influence of tractive and resistance forces. The tractive influences are caused by the tractive effort exertion of the traction unit and by the track-directional components of the gravity force in case the vehicles are actually in down-hill position on the track. Resistance influences are caused on the one hand by the traction resistances, i.e. the basic resistances of the vehicles in the train and by the track-directional components of the gravity force of the vehicles that are actually in up-hill position on the track, or are positioned actually in the curved track sections, as well as by the brake application-induced braking-effort exertion, on the other. The track conditions for the considered whole railway line are specified, i.e. the inclination tangent and the radius of curvature as a function of the track arclength are numerically given by piece-wise linear functions $e(s)$ and $R(s)$. The longitudinal dynamics of

[‡]This research was supported by the Hungarian Ministry of Culture and Education, Grant No. 82/94

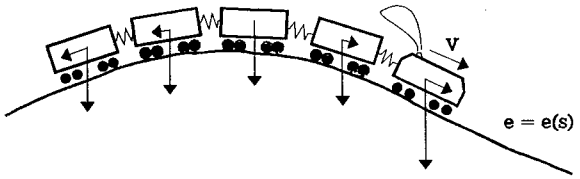

Fig. 1. Train at the peak area of a hill

a specified train operating on a specified railway line depend fundamentally on the activity of the driver, in other words, on the actual variation with time of tractive effort control function $u_1(t)$ and the braking-force control function $u_2(t)$. The complex dynamical model and the motion equations, as well as the real-time simulation method will be introduced, together with the statistical evaluation diagrams of the realised operation process. The results of the investigations can be applied to the design of new traction units by utilizing the information received from the simulation of the future operation conditions on specified railway lines.

2. Complex Model for the Train Longitudinal Dynamics

In *Fig. 1*, a train is sketched, which is passing through the peak area of a hill. The vertical track profile is characterized by the function of inclination tangents vs. track-arclength $e = e(s)$. The gravity forces acting on the vehicles and the track-directional components of those, as well as the longitudinally sprung intervehicle connections are also shown in the Figure.

In *Fig. 2*, the top view of the train is shown, distances $s_1, s_2, \ldots, s_N$ between the gravity point of the locomotive and the cars in the train are also indicated. The curved track section is specified by giving the radius of curvature R and the initial and last points of the circular arc. In this way function $R = R(s)$ (or $1/R(s)$) can be determined for the whole railway line considered.

In *Fig. 3*, the longitudinal vibratory sub-system, i.e. the dynamical model of the train is visualized. The model is a lumped-parameter one with linear inter-vehicle springs of stiffness s and dampers of damping coefficient d. Longitudinal displacements x_i, masses m_i, rotating mass factors γ_i, basic resistance forces F_b^i and braking forces F_B^i; $i = 1, 2, \ldots, N$ as well as tractive effort F_z are clearly indicated.

It should be mentioned that the basic tractive resistance forces F_b^i are velocity-dependent for non-zero velocities, while in case of zero velocity (standstill) they depend on the resultant of the non-resistance forces acting on the vehicles in question.

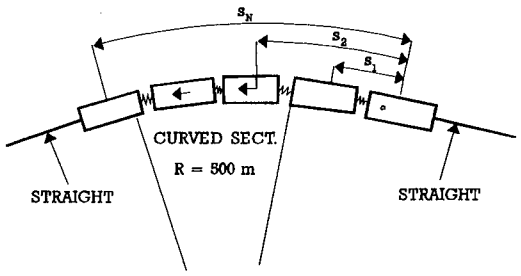

Fig. 2. Top view of the train negotiating a curve

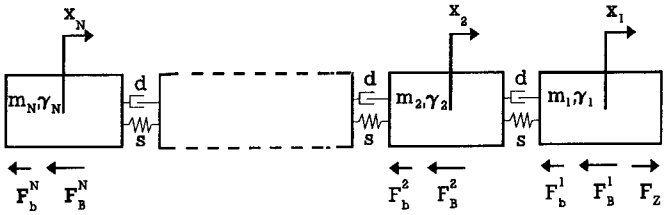

Fig. 3. The train as a longitudinal vibratory system

The tractive effort acting on the train is exerted by the locomotive situated in the front of the train. In the dynamical simulation procedure, the tractive effort is treated as a three-variate function $F(u_1, v, t)$ which depends directly on drive control u_1, velocity v and time t. The braking-force exertion is realized vehicle-wise, i.e. regularly each vehicle in the train has its own brake-gear. The braking force is treated by using a set of three-variate functions $F_b^i(u_2, v_i, t)$ $i = 1, 2, \ldots, N$. In the further analysis, a pneumatic brake system is dealt with, and the pneumatic transients are treated in the framework of a simplified model.

In *Fig. 4*, the inputs and outputs of the train as a dynamical system are visualized.

3. Subsystem 'Traction Resistances'

The basic traction resistance force acting on the i-th vehicle is given by formula:

$$F_b^i(v, \sum F) = \begin{cases} k(a_i v^2 + b_i|v| + c_i) \operatorname{sign} v & \text{if} \quad |v| \geq \varepsilon\,, \\ \min\{kc_i, |\sum F|\} \operatorname{sign} \sum F & \text{if} \quad |v| < \varepsilon\,, \end{cases} \tag{1}$$

where $k = \mathrm{mg}/1000$, and a_i, b_i, c_i are vehicle-specific constants, (m is the mass of the vehicle in kg, g is the gravity acceleration in $\mathrm{m/s}^2$, $[a_i] =$

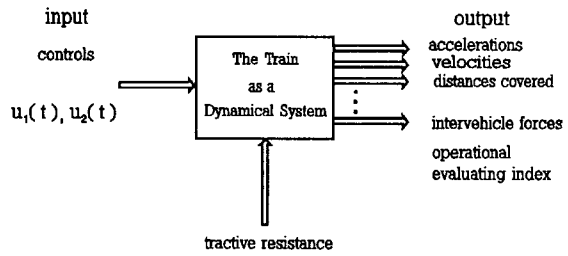

Fig. 4. Inputs and outputs of the train

$\mathrm{Ns}^2/\mathrm{kNm}^2$, $[b_i] = \mathrm{Ns/kNm}$, $[c_i] = \mathrm{N/kN}$), while $\sum F$ is the resultant of the non-resistance forces acting on the ith vehicle (in N). In *Fig. 5* the performance surface of the bivariate function $F_b = f(v, \sum F)$ is shown. The characteristic discontinuity of the surface over axis $\sum F$ is very well recognizable.

In order to determine the track-directional component of the gravity force acting on the vehicle in the train, it is necessary to characterize the inclination condition of the track as a function of the track arclength. The derivative of the vertical track profile $y(s)$ gives the tangent of inclination angle α, which can be considered equal to $\sin\alpha$ in case of small α values coming into question for railway tracks. In the simulation method the track inclination will be treated in mille, i.e. instead of dy/ds the value $e(s)‰ = 1000\ dy/ds = 1000\ \mathrm{tg}\ \alpha$ will be taken. It is clear that the track-directional component of the gravity force can be calculated by using formula $F_e = \mathrm{mg}\sin\alpha \approx \mathrm{mgtg}\alpha = \mathrm{mg}e(s)/1000$. If F_e is positive, its value represents the track inclination resistance, while a negative value of F_e means an additional tractive effort caused by the downhill position of the vehicle considered. The sign of F_e is uniquely determined by that of $e(s)$, namely in uphill position of the vehicle $e(s)$ is positive, while in downhill position $e(s)$ is negative. Due to this rule of signs, force F_e should be substituted into the equation of motion with a negative sign, which automatically ensures the correct mechanical conditions. In *Fig. 6*, the graph of function $e(s)$ is visualized. It should be noted that in case of changing inclinations, the piecewise constant sections of $e(s)$ will be connected by a linear transition line the slope of which is determined by the rounding circle of radius 4000 m laying in the vertical plain.

In *Fig. 7*, the track curvature is shown as a function of the track arclength. The curvature is positive if the curved track deviates to the right from the tangent straight line situated prior to the curve in question. The elaborated simulation method takes into consideration also the transition curves located between the straight and circular track sections.

It is assumed that the curvature in the transition curves is a linear

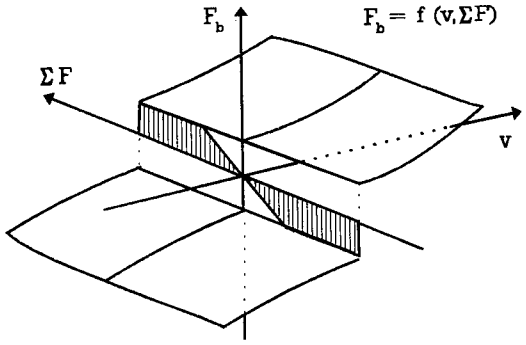

Fig. 5. Performance surface of the basic resistance force

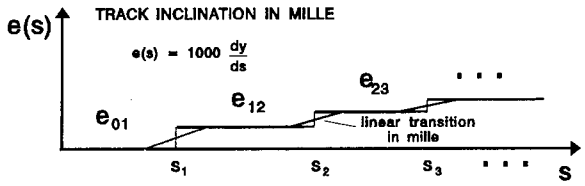

Fig. 6. Track inclination e vs. track arclength s

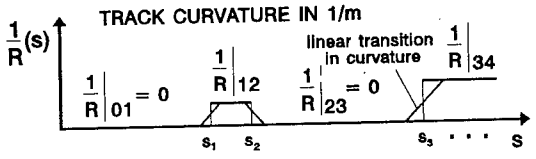

Fig. 7. Track curvature $1/R$ vs. track arclength s

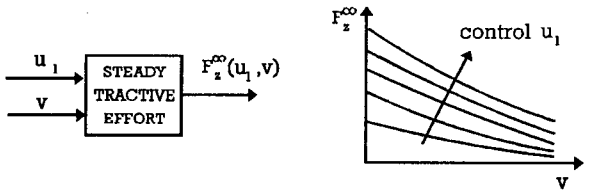

Fig. 8. Block diagram and set of stabilized tractive effort curves

function of arclength s, as it is plotted in *Fig. 7*. The half-length of the transition curve depends upon the radius of the circular section to be connected with the preceding or following straight section.

4. Subsystem 'Tractive Effort Exertion'

The tractive effort exerted actually by the traction unit depends on the actual value of control u_1, velocity v, and due to the transients also a direct time-dependence should be reckoned with. It is to be mentioned that the time constant T_z of the transients is of order of magnitude 0.01 sec. It can be considered that for the steady-state tractive effort exertion a bivariate $F_z^{\infty}(u_1, v)$ function can be taken. The values of the latter belong to the case of limit transition $t \to \infty$, i.e. the stabilized steady-state values are characterized. In *Fig. 8*, the block diagram and the set of performance curves representing function $F_z^{\infty}(u_1, v)$ are shown.

If control u_1 changes in a jump-like way, the tractive effort will also change but the latter change is no longer jump-like. An approximate exponential expression can be formulated for the non-steady-state tractive effort exertion as follows:

$$F_z(u_1, v, t) = F_z^* e^{-\frac{t-t_{ij}}{T_z}} + F_z^{\infty}(u_1, v)\left(1 - e^{-\frac{t-t_{ij}}{T_z}}\right), \tag{2}$$

where

t_{ij}	:	the instant of transition in drive control function level $u_1 = i$ to level $u_1 = j$,
T_z	:	time constant of the tractive effort transients
$t > t_{ij}$	:	the time instant after transition point t_{ij},
F_z^*	:	the tractive effort value prevailing due to control level $u_1 = i$ just prior to time t_{ij},
$F_z^{\infty}(u_1, v)$	:	the steady tractive effort belonging to the control level $u_1 = j$ in case of $t \to \infty$.

In *Fig. 9*, the tractive effort transient is shown, which is caused by transition from control level $u_1 = i$ into that of $u_1 = j$.

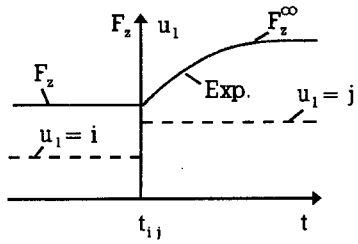

Fig. 9. Transient time function of the tractive effort in case of jump-like change in u_1

5. Subsystem 'Braking Force Exertion'

The approximate quasi-static exponential expression for the decrease in pressure in the main pipe line as a function of time t, the instant of transition t_{ij} in control function $u_2(t)$ and the actual pressure values p^* and p_{stac} as well as time constant T_f will be:

$$p(t) = p^* e^{-\frac{t-t_{i,j}}{T_f}} + p_{stac}(u_2)\left(1 - e^{-\frac{t-t_{i,j}}{T_f}}\right). \tag{3}$$

In the above formula the following designations were used:

t_{ij}	:	the instant of transition in brake control function from level $u_2 = i$ to level $u_2 = j$
T_f	:	time constant of the pressure transient in case of brake application and release
$t > t_{ij}$	:	the time instant after transition t_{ij}
p^*	:	the pressure value prevailing due to control level $u_2 = i$ just prior t_{ij}
$p_{stac}(u_2)$	:	the steady pressure belonging to the control level $u_2 = j$ in case $t \to \infty$
p_0	:	maximum pressure level in the main brake pipe-line
$p_m = p_0 - p$	:	the actual pressure in the main brake pipe-line; in case of the ith vehicle a signal propagation retardation τ_i should be reckoned with $p_m^i(t) = p_0 - p(t - \tau_i)$, $i = 1, 2, \ldots, N$.
p_c^i	:	the brake cylinder pressure at the ith vehicle: $p_c^i(t) = Kp(t - \tau_i)$, where K is constant.

In *Fig. 10*, the brake cylinder pressure vs. time functions are plotted for the locomotive (p_c^1) and for the i-th car (p_c^i). The time shift τ_1 due to the pressure signal propagation velocity is clearly indicated.

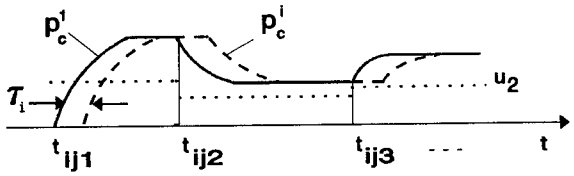

Fig. 10. Cylinder pressure vs. time functions

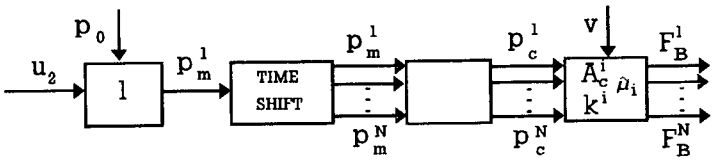

Fig. 11. Flowchart of the braking force exertion

The total brake-block force acting on the ith vehicle can be computed by the following formula:

$$F_t^i = p_c^i A_c^i k^i \,, \tag{4}$$

where A_c^i is the area of the brake cylinder cross-section and k^i is the torque ratio (mechanical advantage) of the brake leverage for the ith vehicle. With the knowledge of the virtual friction coefficient function $\tilde{\mu}^i(p_b^i, v^i)$ belonging to the brake-block wheel tread friction connection, the braking force acting on the ith vehicle can be computed by the following formula

$$F_B^i = F_t^i \tilde{\mu}^i(p_b^i, v^i) \,, \quad i = 1, 2, \ldots, N \,. \tag{5}$$

In the formula, p_b^i stands for the actual value of the brake-block pressure, while v^i is the velocity of the ith vehicle.

The flowchart of the braking-force exertion is shown in *Fig. 11.* Brake control u_2 and pressure p_0 in the main air reservoir of the locomotive determine the main pipeline pressure p_m^l in the locomotive, from which the appropriate pipeline pressures p_m^i; $i = 2, 3, \ldots, N$ can be determined by using the time-shifts mentioned above. With the knowledge of the pipeline pressure time functions for each vehicle in the train, also the time functions of the brake-cylinder pressure can be determined by taking into consideration the approximate proportional and 'counter-tact' variation character of the pipeline and brake-cylinder pressures.

6. Subsystem 'Unified Resistance Forces'

The basic traction resistance force, the curving resistance force and the braking force are originated from certain torque effects influencing the motion

of the wheelsets. The peripheral force corresponding to some of the torques mentioned above can be considered as the 'unified resistance force'.

The 'unified' resistance force F_{bRB} (in N) can be computed by using the train of thoughts similar to that described in case of traction resistances. The formula has the following form:

$$F_{bRB} = \begin{cases} \min\{|F_a(v)|; K(av^2 + b|v| + c) + \\ +|F_R| + |F_B|\} \text{ sign } v & \text{if } |v| \geq \varepsilon \\ \min\{|\sum F|, \min\{|F_a(0)|, Kc + \\ +|F_R| + |F_B(0)|\}\} \text{ sign } \sum F & \text{if } |v| < \varepsilon \end{cases}, \tag{6}$$

where the following designations were used:

v	:	the velocity of the vehicle in m/s
$F_a(v)$	:	the maximum adhesion force transmittable in the wheel–rail connection without macroscopic sliding as a function of travelling velocity ($[F_a]$ =N)
K	:	mg/1000 the weight of the vehicle in kN a, b, c: coefficients of the quadratic specific basic traction resistance vs. velocity function, $[a] = \text{Ns}^2/\text{mkN}$, $[b] = \text{Ns/mkN}$, $[c] = \text{N/kN}$
$\sum F$	:	the resultant of the non-resistance forces acting on the vehicle at zero velocity, i.e. • tractive effort exerted by the drive system, • track-directional component of the gravity force and • forces acting on the vehicle through the buffer and drive-gears from the adjacent vehicles
F_R	:	the curve resistance force acting on the vehicle in N
F_B	:	the braking force acting on the vehicle in N
$F_a(0)$	:	limit value of the maximum adhesion force at zero velocity in N
$F_B(0)$	:	limit value of the braking force at zero velocity in N

It should be noted that F_B depends on velocity v and actual brake control u_2, while $F_B(0)$ also depends on u_2. Curving resistance force F_R depends upon the distance covered by the vehicle (s). The force values building up $\sum F$ can also depend on the distance covered by the vehicle in question and due to the longitudinal connection forces (transmitted by the draw-gears and buffer-gears from the adjacent vehicles), forces $\sum F$ can depend on distance covered s_1, s_2 and velocities v_1, v_2 of the adjacent vehicles, respectively. In addition, in case of a traction unit, $\sum F$ can depend also on the actual drive control u_1. In this way, in a general case the unified resistance force has eight independent variables as indicated in the following expression:

$$F_{bRB} = f(s, v, \sum F(s_1, v_1, s, v, s_2, v_2, u_1), u_2)\,. \tag{7}$$

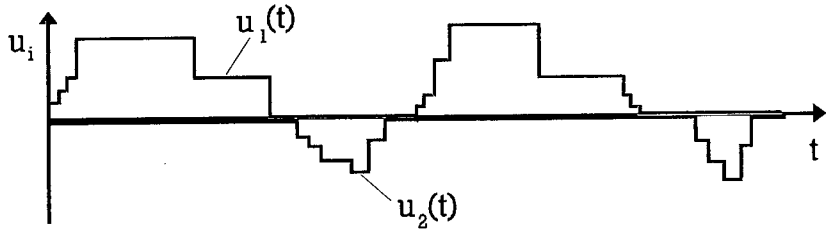

Fig. 12. Characteristic pair of drive and brake control functions

Formula (7) shows the complicated structure of the unified resistance force introduced in (6).

7. Simulation in the Time Domain Controls from the Keyboard

Control functions $u_1(t)$ (drive control) and $u_2(t)$ (brake control) are the inputs of the system to be simulated, and in our model both functions are step functions taking finite number of integer values due to the following definitions:

$$\begin{aligned} u_1(t) &\in \{0, 1, 2, \ldots, 15\} \\ u_2(t) &\in \{0, -1-, 2, \ldots, -15\} \end{aligned}$$

Control functions in question are plotted in *Fig. 12.*

The integers representing the possible levels to be taken by the control functions are corresponding to keyboard positions (buttons), chosen in an appropriate way. If one pushes a keybord button, the control takes an integer value belonging to the position in question, and its value remains unchanged up to the subsequent pushing of any other keyboard button assigned for the possible values of the control function in question. The partition of the keyboard positions used by the authors is shown in *Fig. 13.*

The mathematical description of the train motion in a specified complex environment is carried out by using a set of non-linear differential equations. If the number of vehicles in the train is N (i.e. mechanical system with N degree of freedom is dealt with) then the state vector is of $2N$ dimension. State vector $\mathbf{Y}$ contains the velocities in coordinates $1, \ldots, N$; and the displacements in coordinates $N+1, \ldots, 2N$. The set of motion equations written for state vector $\mathbf{Y}(t)$ has the following form:

$$\dot{\mathbf{Y}} = \mathbf{A}\mathbf{Y} + F(\mathbf{Y}, u_1, u_2, t) \,, \tag{8}$$

where $2N \times 2N$ coefficient matrix $\mathbf{A}$ is the so-called system matrix, which

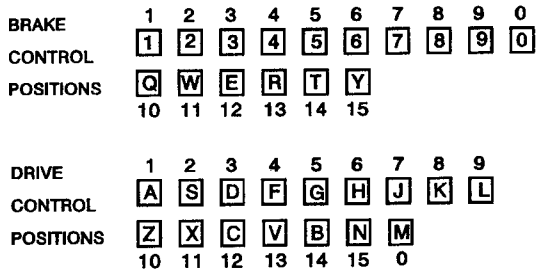

Fig. 13. Brake and drive controls from keyboard

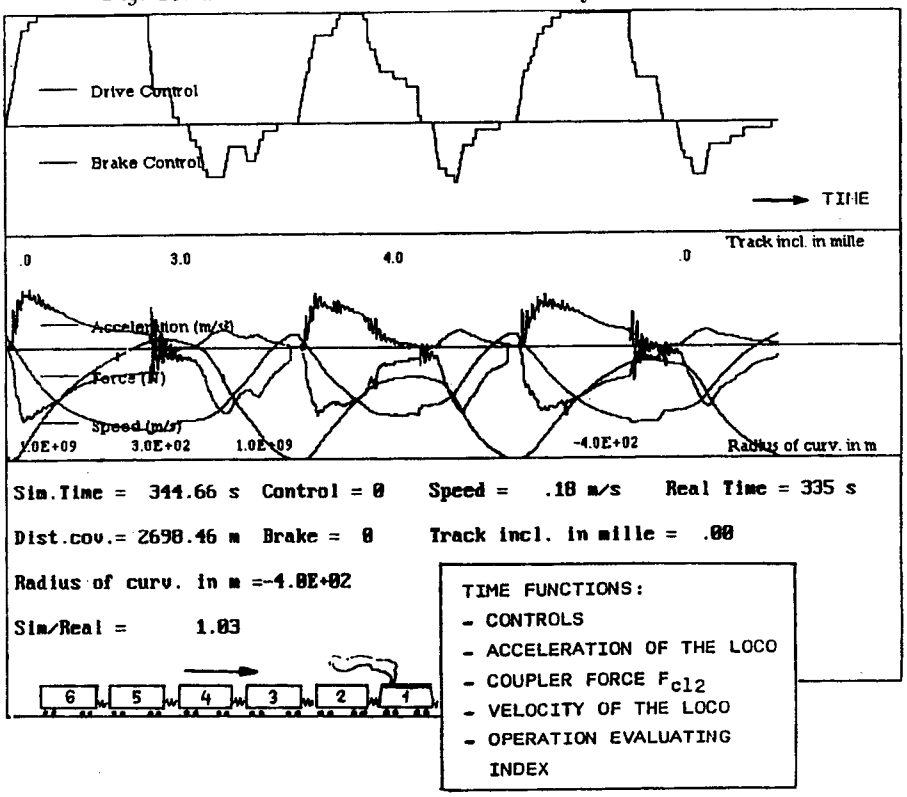

Fig. 14. Diagrams and numerical information on the computer screen

has the following special structure:

$$\mathbf{A} = \begin{bmatrix} -\mathbf{M}^{-1}\mathbf{D} & -\mathbf{M}^{-1}\mathbf{S} \\ \mathbf{E} & \mathbf{0} \end{bmatrix}. \tag{9}$$

In the expression of matrix $\mathbf{A}$, $\mathbf{S}$ is the $N \times N$ stiffness matrix, $\mathbf{D}$ is the $N \times N$ damping matrix, $\mathbf{M}$ is the $N \times N$ mass matrix, $\mathbf{E}$ is the $N \times N$ unit matrix

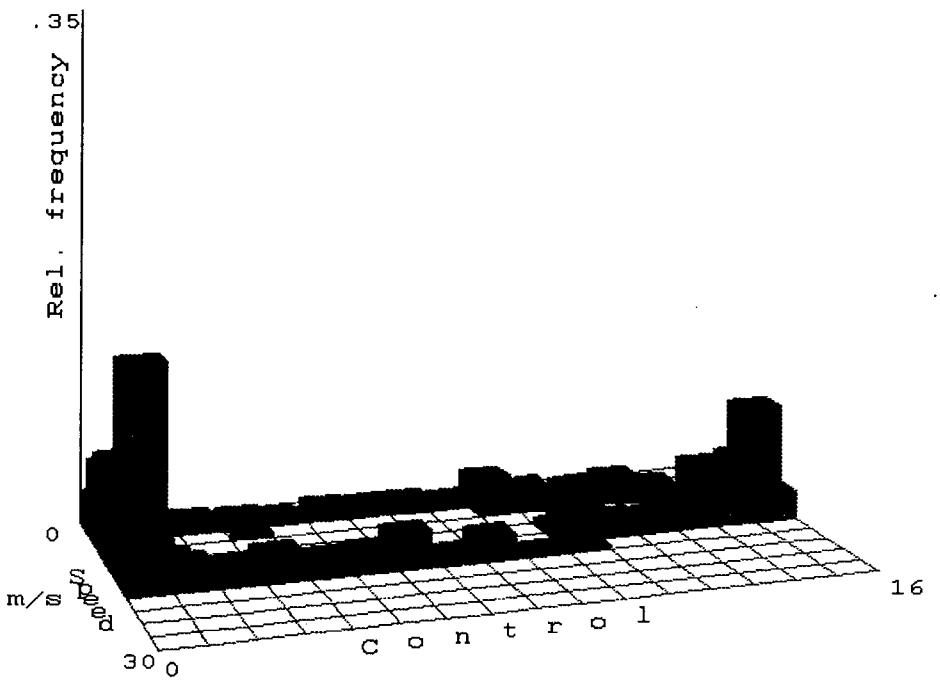

Fig. 15. Joint distribution of the drive control and speed

while **0** is the $N \times N$ zero matrix. Vector-valued function $\mathbf{F}(\mathbf{Y}, u_1, u_2, t)$ is of a very complicated structure and is strongly non-linear. The set of motion equations is to be solved numerically (Euler's method, Rung-Kutta method, etc.) Characteristic time step for the real-time simulation is of $\Delta t = 0.01$ sec order of magnitude.

The set of diagrams displayed on the computer screen is shown in *Fig.14*. The control functions, the acceleration and velocity functions of the locomotive, as well as the time function of the coupler force arising in the draw and buffer gear of the locomotive, and that of the operational evaluation index can clearly be identified. In the lower part of the Figure the numerical information characterizing the simulation process is visible.

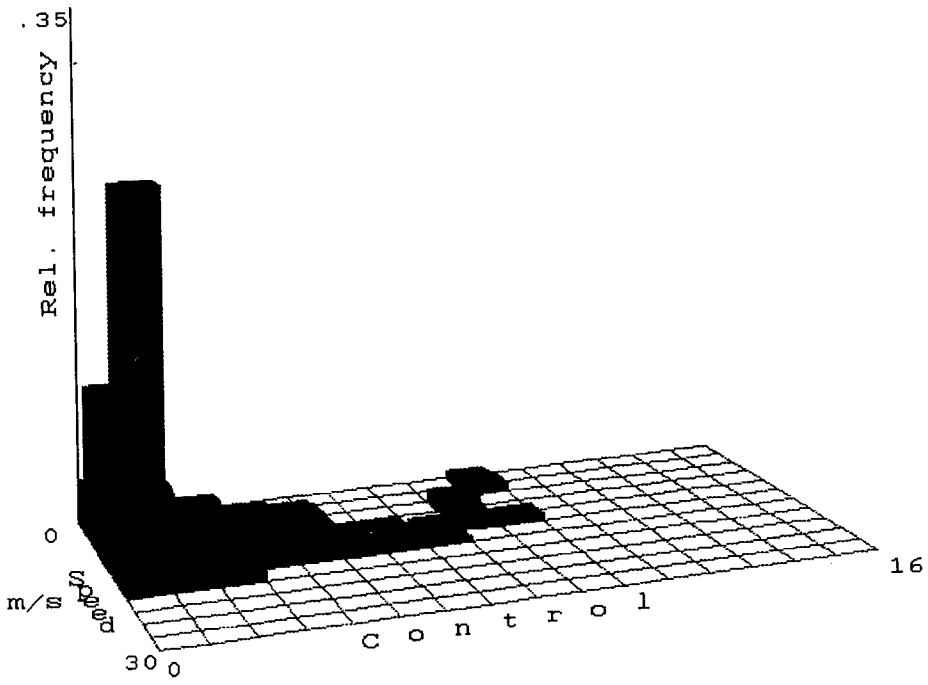

Fig. 16. Joint distribution of the brake control and speed

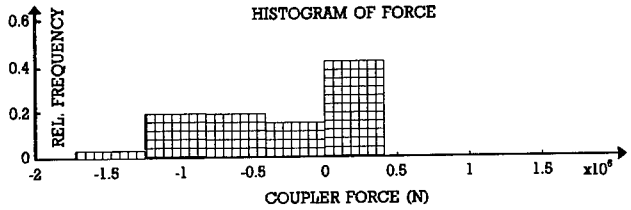

Fig. 17. Relative frequency histogram of the coupler force between the loco and the adjacent carriage

8. Statistical Evaluation of the Responses

In the course of the simulation procedure the relative frequencies of certain events are continuously computed. The events in question are defined by using a partition of the ranges of the state vector coordinates and other state dependent quantities, as well as the controls.

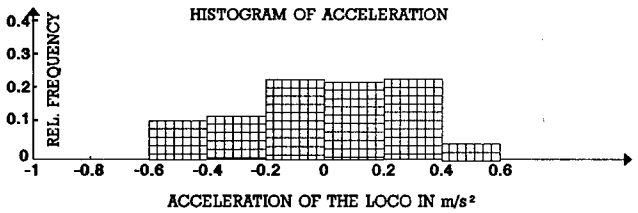

Fig. 18. Relative frequency histogram of the loco's acceleration

For the sake of visualization, joint probability distribution of the drive control and the locomotive velocity $\mathbf{P}\{u_1 \in \Delta u_i, v_{\text{loco}} \in \Delta v_j\}$ is approximated by determining the relative frequency histogram shown in *Fig. 15.* The joint probability distribution of the brake control and the locomotive velocity $\mathbf{P}\{u_2 \in \Delta u_i, v_{\text{loco}} \in \Delta v_j\}$ is treated in a similar way in *Fig. 16.* The simulated coupler force between the locomotive and the first carriage, as well as the acceleration process of the locomotive were also evaluated by determining relative frequency histograms, which approximate to probability distributions $\mathbf{P}\{F_{cl2} \in \Delta F_i\}$ and $\mathbf{P}\{a_{\text{loco}} \in \Delta a_i\}$, respectively. The diagrams are plotted in *Figs. 17* and *18.*

The relative frequency distribution can be used in the course of designing the drive system components, e.g. the roller bearings, the gear-wheels and the shafts, as well as the components of the brake gear, e.g. the linkages and the leverages. The knowledge of the relative frequencies belonging to the different loading conditions makes it possible to carry out dimensioning procedures taking into consideration the fatigue phenomena.

9. Concluding Remarks

The investigations of the authors into the longitudinal dynamics of trains in complex environment, the elaboration of the simulation models and programs and real-time simulations carried out made it possible to summarize the following statements:

- The real-time simulation of the train longitudinal dynamics can be carried out by using simplified dynamical model and approximate process description for the airbrake system.
- The continuous simulation requires the unified treatment of the resistance forces acting on the vehicles.
- The numerical integration in the real-time simulation requires a time step of order of magnitude 0.01 sec.
- The elaborated simulation procedure makes it possible to predict the loading conditions of the components built into the vehicle's structure and the drive/brake system already *in the period of the vehicle design.*

- The predictions mentioned appear in the form of probability approximating relative frequency distributions and further statistical parameters.
- The simulation procedure can yield also values characterizing the energy consumption and environment pollution characteristics of the vehicle realized in the course of the operation process.

References

[1] ZOBORY, I.: Stochasticity in Vehicle System Dynamics. *Proceedings of the 1st Mini Conference on Vehicle System Dynamics, Identification and Anomalies.* Held at the TU of Budapest, 1988, pp. 8–21.

[2] ZOBORY, I.: Prediction of Operational Loading Conditions of Powered Bogies. *Vehicles, Agricultural Machines*, 1990. Vol. 37, Issue 10, pp. 373–376 (in Hungarian).

[3] MICHELBERGER, P. – ZOBORY, I.: Loading Conditions of Ground Vehicles in Operation. *Proceedings of the 2nd Mini Conference on Vehicle System Dynamics, Identification and Anomalies.* Held at the TU of Budapest, 12–15 of November 1990, pp. 246–262.

[4] MICHELBERGER, P. – ZOBORY, I.: Operation Loading Conditions of Ground Vehicles – Analysis of Load History. *Proceedings ASME Winter Annual Meeting*, Dallas, New York, 1990, pp. 175–182.

[5] HORVÁTH, K. – ZOBORY, I. – BÉKEFI, E.: Longitudinal Dynamics of a Six-unit Metro Train-set. *Proceedings of the 2nd Mini Conference on Vehicle System Dynamics, Identification and Anomalies.* Held at the TU of Budapest, 12–15 of November 1990. pp. 45–62.

[6] ZOBORY, I. – FRANG, Z. – SZABÓ, A. – GYŐRIK, A: Investigation of Operation Loading Conditions of Electric Locomotive of Series V43. *Review of Transportation Sciences.* Volume XLI. Issue 6. Budapest, 1991, pp. 201–215 (in Hungarian).

[7] ZOBORY, I. – BÉKEFI, E.: Software for Stochastic Simulation of Motion and Loading Processes of Vehicles. *Proceedings of the 3rd Mini Conference on Vehicle System Dynamics, Identification and Anomalies.* Held at the TU of Budapest, 9–11 of November, *Periodica Polytechnica, Transportation Engineering*, Vol. 22, No. 2, pp. 111–127, 1994.

[8] ZOBORY, I.: Stochastic Simulation of the Motion and Loading Processes of Railway Traction Units. *Review of Transportation Sciences*, Vol. XLII, Issue 1, Budapest, 1993, pp. 19–29 (in Hungarian).

PERIODICA POLYTECHNICA SER. TRANSP. ENG. VOL. 23, NO. 1-2, PP. 19-35 (1995)

ON STOCHASTIC SIMULATION OF THE WHEEL-PROFILE WEAR PROCESS OF A RAILWAY VEHICLE OPERATING ON A SPECIFIED NETWORK

András SZABÓ and István ZOBORY

Department of Railway Vehicles
Technical University of Budapest
H-1521 Budapest, Hungary

Received: November 8, 1994

Abstract

The alteration in wheel and rail profiles due to wear involves considerable vehicle and track-maintenance costs, and influences the loading capacity of the rails, as well as the operation safety and riding comfort of the vehicles. In the past five years, a vehicle dynamics-based numerical procedure was elaborated at the TU of Budapest to predict the wear-caused wheel profile alterations and to maximize the mileage performance by selecting the optimum axle-box guidance stiffnesses in case of traditional running-gears operating on a specified railway line [1]. This paper introduces the fundamental principles and conditions decisive in the dynamical and tribological procedure mentioned, and deals with an extension of it. This extension regards the wheel wear analysis and mileage performance maximization of the vehicle in case of stochastic operation on a given railway network. The network is characterized by its graph. The operation process is described in the framework of a semi-Markovian model [12], [13]. The elaborated stochastic simulation and optimization method is visualised for a simple railway network by introducing the two important two-parameter stochastic fields, namely those of the wheel profile and the mileage performance.

Keywords: stochastic simulation, railway wheel-profile wear.

1. Introduction

The wear simulation technique based on a non-linear dynamical track/vehicle model – elaborated by the Department of Railway Vehicles at the TU of Budapest for the numerical investigations into the wheel-profile wear of railway vehicles operating on a specified railway line [1], [10], [11] – is extended by the authors. The goal of the extension is to describe the propagation of the wheel-profile-wear under stochastic operation conditions of the vehicle on a whole railway network as a function of the distance covered by the vehicle. The stochastic operation process taking place on the network is treated on the basis of the theory of semi-Markovian stochastic processes [12], [13]. The statistical characteristics of the bivariate stochastic field describing the wheel profile alterations and also the stochastic field describing the mileage performance defined as a function of the longitudinal and lateral

axle-box guidance stiffnesses are analyzed. The expected value function and the standard deviation function of the latter stochastic field makes possible to optimize the axle-box guidance system by maximizing the expected mileage performance between two profile renewals.

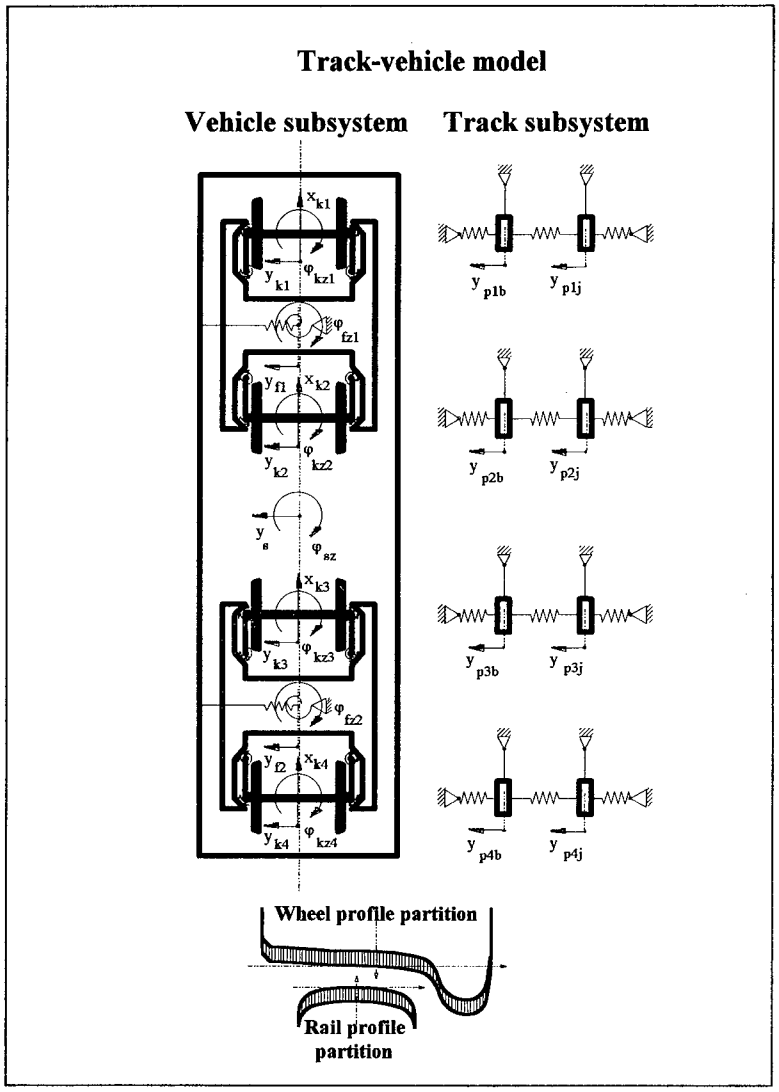

Fig. 1. Lumped-parameter track–vehicle model

2. Summary of the Wheel-Wear Simulation on a Specified Railway Line

2.1. Introductory Remarks

The possibility of predicting the wheel wear process of a railway vehicle is connected with the numerical feasibility of simulations based on:

- appropriate dynamical models,
- rolling contact theory, and
- wear hypothesis.

The early investigations into the wear phenomena of railway wheels focused on the wear propagation under simple and steady operation conditions, e.g. constant velocity operation on an ideal straight track [2], [3], [4], [5], [6].

The most frequently used wear hypothesis was formulated in terms of the proportionality between the specific energy dissipated over the contact surface and the specific mass removal for the unit of the distance covered [6].

In the following, the model elaborated for simulating the wear propagation on the wheels running on a specified railway line consisting of straight and curved sections will be summarized.

This model was the basis of the research into the more complicated wear process simulation concerning the stochastic operation on a specified railway network.

2.2. The Track–Vehicle Dynamical Model

The lumped-parameter track–vehicle model is shown in *Fig. 1.*

The vehicle body, the bogies, the wheel sets and the discrete masses representing the track inertia are modelled as rigid bodies. The spring structural connections between the rigid bodies mentioned are modelled by piecewise linear characteristics, while the dampers supposed to be parallel to the former ones are definitely linear. The used wheel and rail profiles can be practically arbitrary, the only requirement is to give their points on a laterally equidistant sequence of 1 mm spacing.

The track can be composed of specified straight and curved sections coming one after another in an arbitrary order, see *Fig. 2.* The transition curves can be approximated by circular arcs of non-equal radii.

- The track can be laterally 'imperfect', i.e. a stochastic lateral irregularity can be taken into consideration. On the basis of the measured spectral density function, lateral irregularity realization functions are generated for the two rails as based on simulation technique by random number generation [8]. The lateral irregularities as excitation sources

are taken into consideration in both the straight and the curved track sections.

- The vertical wheel loads are constants on the straight sections, while in curves the quasi-static compensation of the centrifugal forces is carried out [7].
- The wheel–rail contact on the wheel tread is treated as a creep-dependent force transfer spot, the creep coefficients are treated by Kalker's linear theory [9].
- The longitudinal and lateral contact forces, as well as the spin moment are bounded by the values based on the constant sliding friction coefficient.
- The flanging is considered as a conditional, laterally elastic and damped linear connection between the wheel set and the mass representing the rail inertia.
- In the model, a specified constant torque is acting on each wheel set, which represents the resultant of the rolling resistance, the journal friction and the eventually acting tractive or braking torques.
- It is always assumed that no braking torque is exerted by frictional tread braking, i.e. the wear phenomenon on the wheel tread and the flange are caused exclusively by the wheel–rail contact.

2.3. Remarks on the Simplified Operation Conditions

The vehicle–track model in question takes into consideration track section-wise constant travelling velocities and torques on each wheel set. It is reasonable to use a constant average travelling velocity along the whole railway line examined, and also an average torque to act on the wheel sets on the

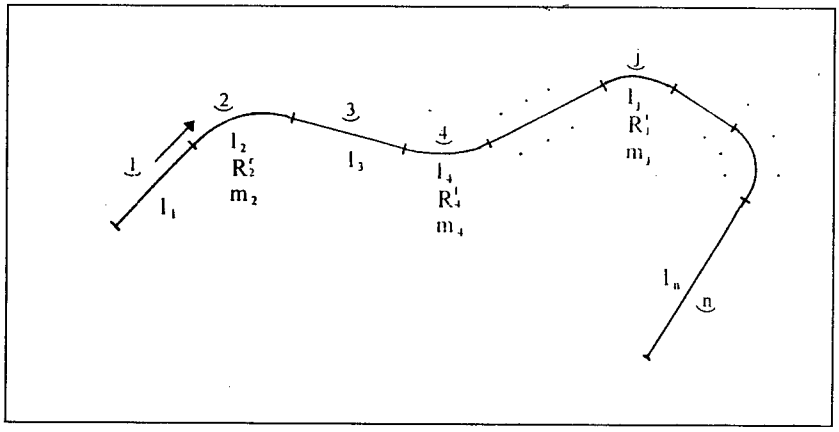

Fig. 2. Straight and curved sections of the track

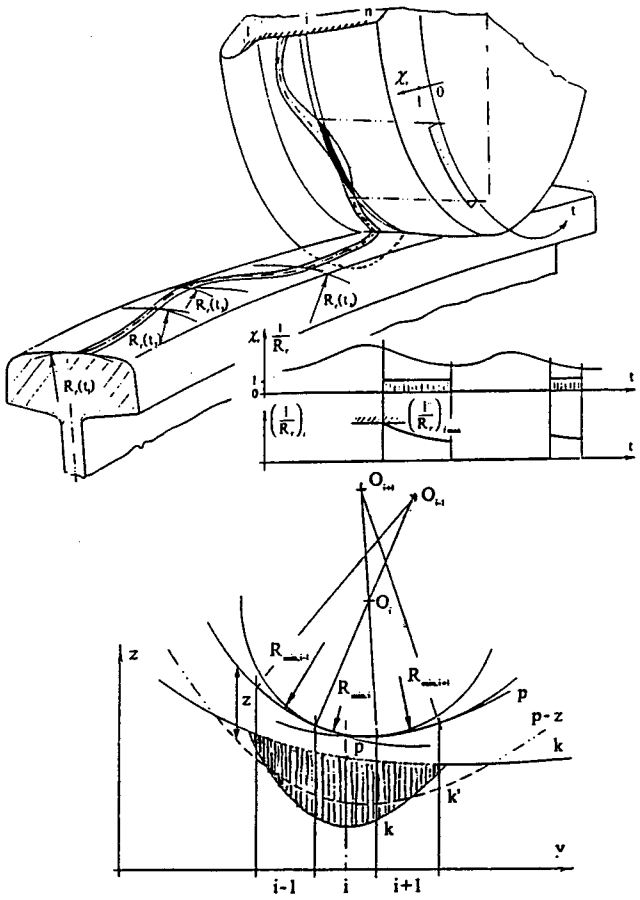

Fig. 3. The principle of physical smoothing

basis of a preliminary 'speed – distance covered' analysis. Tractive and braking torques vs. distance covered functions can also be determined for the whole length L of the line between terminals A and B.

Average velocity and torque can be calculated by formulae

$$\nu_{aAB} = \frac{1}{L}\int_A^B |\nu(s)|ds \quad \text{and} \quad M_{raAB} = \frac{1}{L}\int_A^B |M_r(s)|ds\ . \tag{1}$$

2.4. Wheel Profile Alteration Due to Wear

The wheel profile alteration due to wear caused by the rolling contact of the wheel and railhead is a rather slow process. Debris continuously leaves the wheel tread and recurrently the flange surface being in sliding contact with the railhead.

Principally, each angular displacement increment $d\varphi$ of the wheel implies a certain material removal Δdm from the contact spot on the wheel. This material loss is very slow, and a recognisable variation in profile geometry appears only over hundred km-s of distance covered by the wheel. This survey is the basis of the discretization technique used in the elaborated wear simulation procedure.

The fundamental idea is to consider the actual wheel profile and railhead profile as the basis of the contact geometrical and dynamical operations. The latter ones result in the wear-load distribution along the wheel meridional profile. This wear-load distribution is considered valid for a given distance covered by the wheel, and the profile alteration, i.e. the reduction in rolling radii is carried out by using appropriate smoothing procedures.. In this way, a discrete step of profile alteration due to wear is done [10].

The resulted new wheel profile takes over the role of the initial profile, and a subsequent discrete step can be done, etc. The outlined procedure means that the material is removed step-wise, whereas the contact conditions are considered to be constant in each step.

The errors caused by the discretization are balanced by the physical and mathematical smoothing procedures, which are built up on the basis of the rail and wheel profile compatibility and C_2 spline method.

Regarding the tread contact, the used wear hypothesis connects the specific mass removal $\partial m/\partial s$ from the contact band with the specific work done by the creep forces by proportionality

$$\frac{\partial m}{\partial s} = k_r \left(F_x \nu_x + F_y \nu_y\right) . \tag{2}$$

In the formula, k_r is the wear coefficient, F_x and F_y are the longitudinal and lateral creep forces, while ν_x and ν_y are the longitudinal and lateral creepages, respectively. In case of flange contact

$$\frac{\partial m}{\partial s} = k_s F_f \frac{\Delta \nu_s}{\nu} . \tag{3}$$

Here k_s is the sliding wear coefficient, F_f is the friction force on the flange, $\Delta \nu_s$ is the sliding velocity and ν is the travelling velocity.

Mass removal Δm from the contact surface A over a small distance of rolling Δs can be calculated based on relationship

$$\Delta m = \frac{\partial m}{\partial s} \Delta s . \tag{4}$$

Mass Δm should be distributed along that interval(s) of the wheel profile which intersects the contact area.

The Hertzian pressure ellipsoid is divided into 'slices' by parallel planes being in a lateral distance Δy from each other. The volume of the pressure ellipsoid is V, while that of the i-th slice is V_i. Then, weighting factors $\lambda_i = V_i/V$; $i = 1, 2, \ldots, n$ are defined, and the i-th 'slice' will have a mass fraction removed by wear

$$\Delta m_i = \lambda_i \Delta m = \lambda_i \frac{\partial m}{\partial s} \Delta s \ . \tag{5}$$

The wear load for the partition elements along the profile is

$$w_i = \frac{1}{S} \sum \Delta m_i \ : \quad i = 1, 2, \ldots, n \ , \tag{6}$$

where S is the total distance covered by the wheel. The unit of measure of w_i is mg/m. With the knowledge of the topology of the railway line the conditional wear-load distributions can be calculated for each straight and curved section:

$$w_{ij} \ ; \quad j = 0, 1, 2, \ldots, m \ . \tag{7}$$

The resultant wear distribution is yielded in the form

$$W_i = \sum_{j=0}^{m} w_{ij} l_j \ . \tag{8}$$

In formula (8) l_0 is the total length of the straight track sections and l_j; $j = 1, 2, \ldots, m$ are the total lengths of the curved ones of radii R_j; $j = 1, 2, \ldots, m$.

The decrement in radius of the i-th slice due to wear is

$$\Delta r_i = W_i / \rho \ 2\pi \ r_i \ \Delta y \ , \tag{9}$$

where ρ stands for the material density of the wheel and r_i is the initial radius of the wheel for partition element Δy. The sequence of worn profile radii are

$$r_i^w = r_i - \Delta r_i \ ; \quad i = 1, 2, \ldots, n \ . \tag{10}$$

Discretized profile alterations are carried out by 1500 km distances. The errors caused by profile incompatibility should be balanced by smoothing.

Profile incompatibility can occur in certain altered wheel profile point(s) if the local curvature yielded is greater than the maximum rail profile curvature contacted.

The maximum rail profile curvatures contacted by the partition elements of the wheel profile are continuously computed.

For the wheel profile smoothing the following steps are required [7]:

- Construction of 'circle arc chain' (see *Fig. 3*).
- Pushing the circle arc chain into the profile to be smoothed.
- Mathematical smoothing by using C_2 spline.
- Checking of the curvature compatibility with the smoothed profile. If necessary, repetition of the above points up to achieving compatibility.

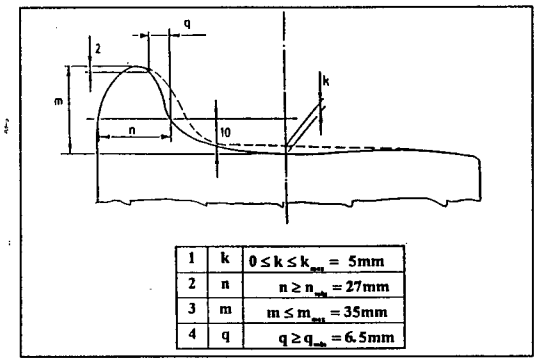

1	k	$0 \le k \le k_{max} = 5mm$
2	n	$n \ge n_{min} = 27mm$
3	m	$m \le m_{max} = 35mm$
4	q	$q \ge q_{min} = 6.5mm$

Fig. 4. Permitted profile dimensions

Distance covered M, which belongs to the exhaustion of one of the four conditions prescribed for permitted rail profiles (see *Fig. 4*) defines the mileage performance of the wheel under examination [10], [11].

2.5. Numerical Optimization of Mileage Performance

The mileage performance M belongs to the fixed axle-box guidance stiffness values taken into consideration. Define axle-box guidance stiffness vector $\mathbf{s} = [s_x, s_y]^T$, and seek for the conditional maximum of function $M(\mathbf{s})$ over the permitted domain E of rectangle form (see *Fig. 5*). If the initial stiffness vector is designated by $\mathbf{s}_0$, then – based on the gradient method-vector $\mathbf{s}_1$ can be computed by formula:

$$\mathbf{s}_i = \mathbf{s}_{i-1} + \Delta s \frac{\mathbf{grad}\ M(\mathbf{s}_{i-1})}{|\mathbf{grad}\ M(\mathbf{s}_{i-1})|}\,. \tag{11}$$

3. Specification of the Railway Network

The railway network can be interpreted as a set of nodes (line junctions) and lines interconnecting the nodes or radially leaving them as single branches. A simple network consisting of only two nodes and three lines is shown in *Fig. 6.*

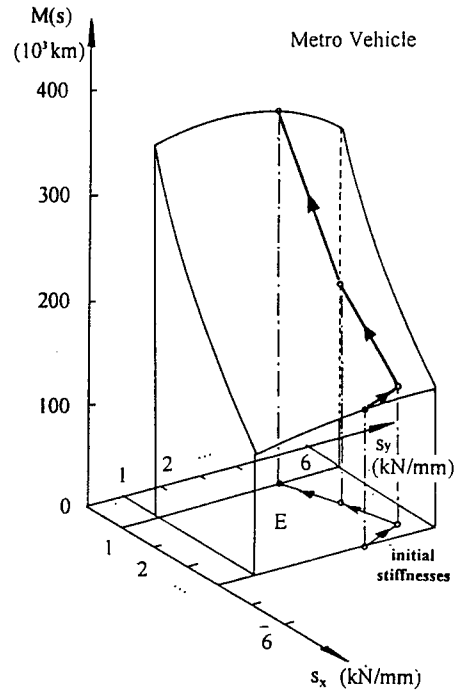

Fig. 5. Objective function $M(s)$ and the maximization procedure over domain E

4. Approximate Description of the Operation Conditions by a Semi-Markovian Stochastic Process

Let us denote the sequence of the states of the semi-Markovian process by

$$u_1, u_2, \ldots, u_n, u_{n+1} \cdots . \tag{12}$$

The sequence of random durations spent in the appropriate states is

$$\tau_1, \tau_2, \ldots, \tau_n, \tau_{n+1} \cdots . \tag{13}$$

The state transition probabilities are defined by the following conditional probabilities:

$$p_{ij} = P\left\{\{u_{n+1} = j\} | \{u_n = i\}\right\} \; ; \quad i, j = 1, 2, \ldots, N \; , \tag{14}$$

where N stands for the number of line sections in the railway network considered. The system of transition probabilities can be represented by defining

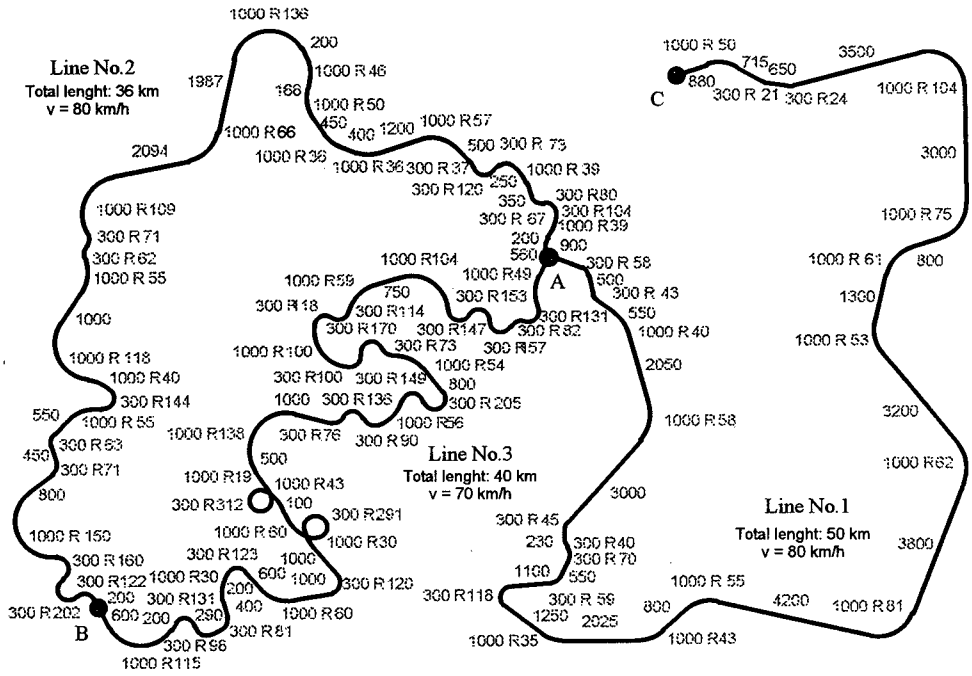

Fig. 6. Topology of the railway network (Example)

the $N \times N$ stochastic matrix Π as follows

$$\Pi = \begin{bmatrix} p_{11} & p_{12} & p_{13} & \cdots & p_{1N} \\ p_{21} & p_{22} & p_{23} & \cdots & p_{2N} \\ p_{31} & p_{32} & p_{33} & \cdots & p_{3N} \\ \vdots & \vdots & \vdots & \ddots & \vdots \\ p_{N1} & p_{N2} & p_{N3} & \cdots & p_{NN} \end{bmatrix} . \tag{15}$$

For the systematic process description, also the 'staying-in-state' probabilities should be dealt with. In case of semi-Markovian processes, a matrix-valued function built up from the conditional probability distribution functions $F_{ij}(t)$ plays a decisive role [12]. Functions $F_{ij}(t)$ are non-zero only for those index pairs which also non-zero transition probabilities belong to. Function $F_{ij}(t)$ means the conditional probability that staying in the j-th state is less than duration t, under the condition that the previous state was the i-th one.

According to the aforesaid, the durations spent in the appropriate states are characterized by the set of conditional probability distribution

functions:

$$F_{ij}(t) = P\left\{\{\tau_{n+1} < t\} | \{u_n = i\} \bigcap \{u_{n+1} = j\}\right\} \; ; \quad i,j = 1,2,\ldots,N \; . \tag{16}$$

Using the convenient matrix formulation, the $N \times N$ matrix-valued conditional distribution function $\mathbf{F}(t)$ is yielded:

$$\mathbf{F}(t) = \begin{bmatrix} F_{11}(t) & F_{12}(t) & F_{13}(t) & \ldots & F_{1N}(t) \\ F_{21}(t) & F_{22}(t) & F_{23}(t) & \ldots & F_{2N}(t) \\ F_{31}(t) & F_{32}(t) & F_{33}(t) & \ldots & F_{3N}(t) \\ \vdots & \vdots & \vdots & \ddots & \vdots \\ F_{N1}(t) & F_{N2}(t) & F_{N3}(t) & \ldots & F_{NN}(t) \end{bmatrix} . \tag{17}$$

The railway operation taking place on the network plotted in *Fig. 6* is characterized by semi-Markovian stochastic process $\xi(t)$ describing the transitions between the following five 'states':

1. Operation on line 1 from A to the end of line and back,
2. Operation on line 2 from A to B,
3. Operation on line 2 from B to A,
4. Operation on line 3 from A to B,
5. Operation on line 3 from B to A.

The state transitions will be controlled by the transition probability matrix $\Pi = \{p_{ij}\}$. The entries of matrix Π should be determined by using the operation time table or traffic statistics. In our example the following transition probability matrix was used:

$$\Pi = \begin{bmatrix} 0 & 0.5 & 0 & 0.5 & 0 \\ 0 & 0 & 0.9 & 0 & 0.1 \\ 0.05 & 0.9 & 0 & 0.05 & 0 \\ 0 & 0 & 0.1 & 0 & 0.9 \\ 0.05 & 0.05 & 0 & 0.9 & 0 \end{bmatrix} . \tag{18}$$

In accordance with the definition, entries in matrix Π are conditional probabilities, e.g. p_{ij} stands for the conditional probability of occurring state j in the course of the state transition, under the condition that prior to the transition the state was i.

In the following tractation, variable $x \geq 0$ means the number of running cycles along a 'state-defining' line in the network considered. As states 2,3,4,5 are defined by performing a single running cycle along line 2 and line 3, respectively, the characteristic number of cycles will be 1 for the states mentioned, irrespective of the previous state i. So functions F_{ij} can be expressed by shifted unit jump functions U (Heaviside functions) as follows:

$$F_{ij}(x) = U(x-1) \; ; \quad j = 2,3,4,5 \; . \tag{19}$$

If state 1 is realized, then function $F_{ij}(x)$ should be defined as a piece-wise linear distribution function over the positive axis with break points at the positive integers. The actual variation of $F_{ij}(x)$ can depend on the previous state. In our example matrix-valued function $\mathbf{F}(x)$ takes the following form:

$$\mathbf{F}(x) = \begin{bmatrix} 0 & U(x-1) & 0 & U(x-1) & 0 \\ 0 & 0 & U(x-1) & 0 & U(x-1) \\ F_{31}(x) & U(x-1) & 0 & U(x-1) & 0 \\ 0 & 0 & U(x-1) & 0 & U(x-1) \\ F_{51}(x) & U(x-1) & 0 & U(x-1) & 0 \end{bmatrix} . \quad (20)$$

When simulating the number of cycles, uniformly distributed random number η is generated, and x_{ij} is obtained by relationship

$$x_{ij} = F_{ij}^{-1}(\eta) . \quad (21)$$

In *Fig. 7* the operation process of a vehicle moving on the specified railway network is visualized. On the horizontal axis the distance covered by the vehicle is represented, while on the vertical axis positive integers 1, 2, 3, 4 and 5 identify the states of the embedded Markovian chain. These states indicate the actual motion of the vehicle on the line sections, as they are defined in specification (18). The total length in km belonging to operation

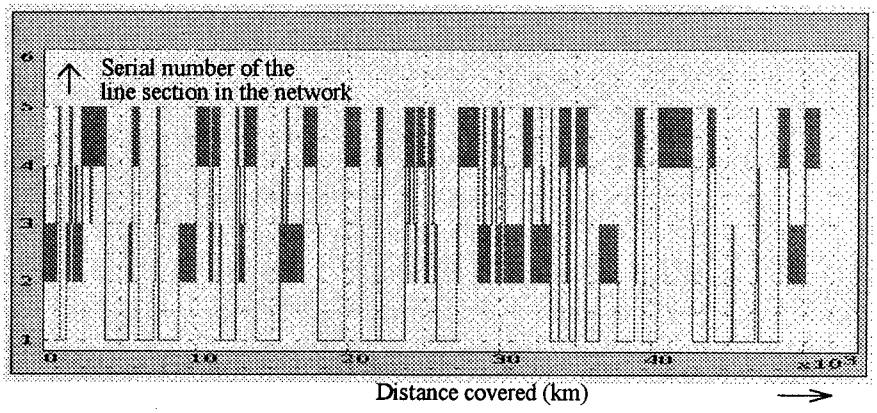

Fig. 7. Realization of the semi-Markovian stochastic process of the operation on the specified railway network

in state 1 can uniquely be read off from the Figure, by determining the total length of intervals fitting on level 1. The total length of operation in the other states can be determined similarly, by reading off the summarized length of the related intervals fitting on levels 2, 3, 4 and 5. In the Figure due to the horizontal scale applied unfortunately the intervals belonging to the latter states can hardly be recognised because of the considerable

width of the vertical lines visualizing the actual state transitions between the adjacent levels.

5. Simulation of the Wheel Profile Wear Stochastic Process

With the knowledge of matrices Π and $\mathbf{F}(x)$ operation process realization sections of 1500 km length can be simulated one after another, sequentially, up to the exhaustion of at least one condition prescribed for the permitted wheel profiles. The sequence of the altered wheel profiles can be determined for the realization function in question, see *Fig. 8*. The alteration of the wheel profile meridional curves in the course of the stochastic operation conditions examined becomes a stochastic process, namely a two-parameter stochastic field $\zeta(S, y)$.

Profile realizations for distance covered $S = 24000$ km are visualized in *Fig. 9* for the case of stochastic operational process determined by matrices (19) and (21). Expected value and standard deviation of the profile realizations can be evaluated, and so can the one-dimensional marginal probability density functions of the profile.

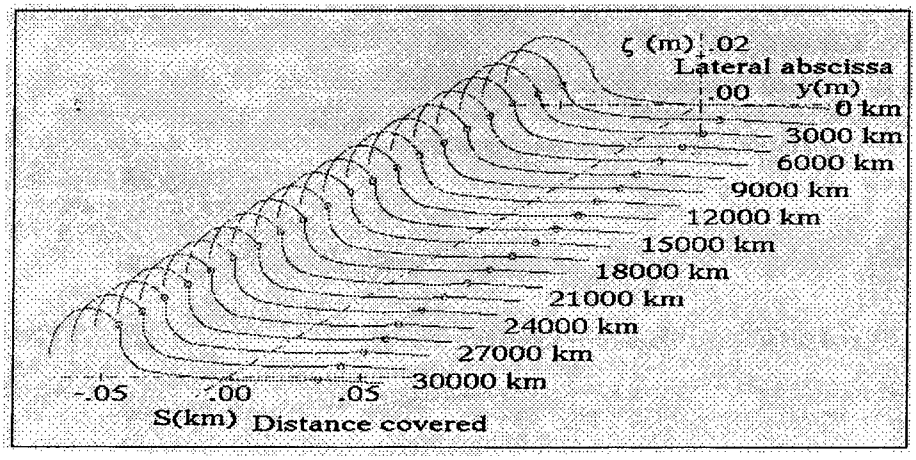

Fig. 8. Sequence of altered wheel profiles

6. Evaluation of the Stochastic Mileage Performance

In case of stochastic operational process also the mileage performance becomes a stochastic field defined on stiffness parameters s_x and s_y. Stochastic

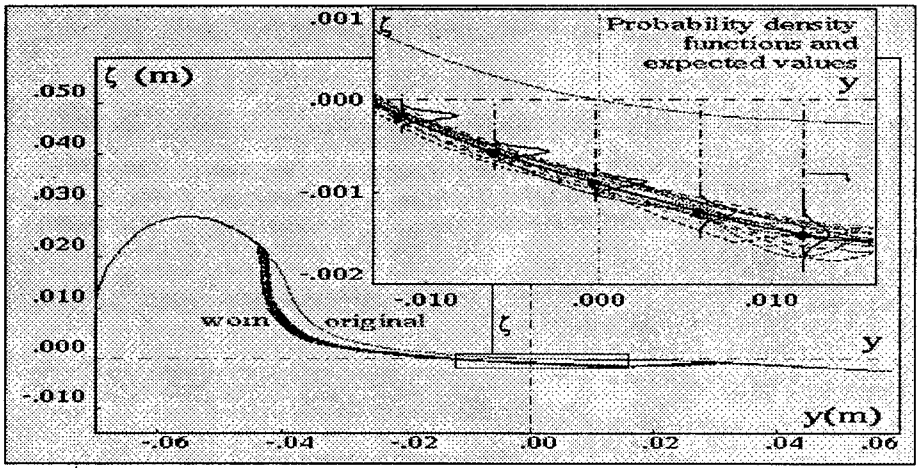

Fig. 9. Worn profile realizations after 24000 km distance covered in stochastic operation

mileage performance $\mu(s_x, s_y)$ can be defined as infimum of four random variables, namely of $\mu_1(s_x, s_y)$, $\mu_2(s_x, s_y)$, $\mu_3(s_x, s_y)$ and $\mu_4(s_x, s_y)$. The latter are the distances covered up to the individual exhaustion of the permitted profile dimensions in *Fig. 4*. According to the aforesaid

$$\mu(s_x, s_y) \stackrel{\text{def}}{=} \inf \{\mu_1(s_x, s_y), \mu_2(s_x, s_y), \mu_3(s_x, s_y), \mu_4(s_x, s_y)\}$$

is a bivariate stochastic field. In a spatial co-ordinate frame, over the rectangle lying in the parameter plane the one-dimensional marginal probability density functions are plotted on the basis of simulation results obtained for the simple network shown in *Fig. 6*.

It is obvious to determine also the expectation and standard deviation of $\mu(s_x, s_y)$ as a function of s_x and s_y over the parameter domain, as it is indicated in *Fig. 10*.

7. Possibility of Axle-Box Guidance Optimization

The objective function of the mileage performance optimization can be the expected value function of the field μ in the form:

$$M(\mathbf{s}) = \mathbf{E}\mu(s_x, s_y) = \max! \,. \tag{22}$$

The numerical procedure can be again the gradient method described by formula (11). As a supplementary objective, the requirement of low standard

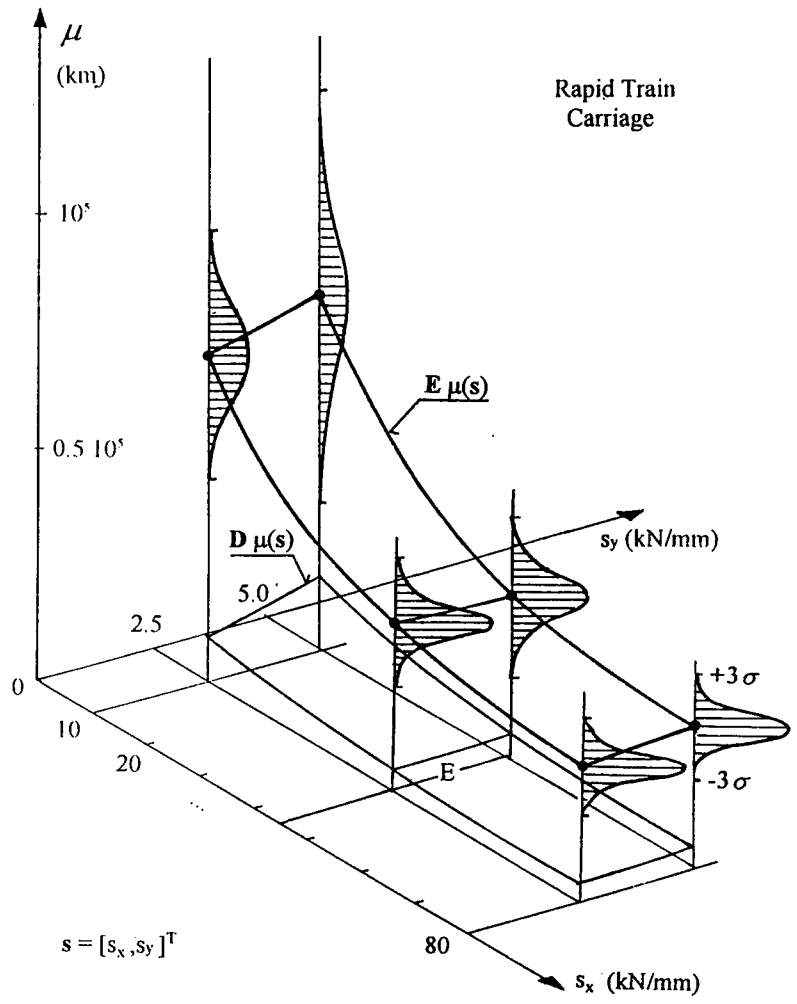

Fig. 10. Expectation, standard deviation and marginal density functions of stochastic field $\mu(s)$

deviation of mileage performance can be written as follows:

$$D(\mathbf{s}) = \mathbf{D}\mu(s_x, s_y) = \min! \,. \tag{23}$$

Objective functions (18) and (19) determine a region of the stiffness parameter plane in which in average high and relative homogeneous mileage performances can be predicted.

8. Concluding Remarks

On the basis of our theoretical investigations and numerical simulations, the following conclusions can be drawn:

- The operation of the vehicle can be approximately described by using the semi-Markovian stochastic model, based on the state transition probability matrix and the matrix-valued function of the conditional probability distribution functions of the durations spent on certain line sections after specified state transitions,
- The description of wheel wear propagation by a two-parameter stochastic field represents a new approach to the analysis,
- The stochastic field reflecting the mileage performance is introduced, its expectation and standard deviation functions form the objective functions of the traditional running-gear optimization, so the lateral and longitudinal axle-guidance stiffnesses can be optimized by a numerical procedure, also in case of stochastic operation on a specified railway network,
- Further investigations are required to take into consideration also the wheel wear caused by tread braking.

Authors are working on the prediction of rail wear propagation by means of similar tools presented in this paper.

References

[1] Computer-Based Prediction of the Wheel Tread and Flange Wear in Case of a Railway Vehicle Negotiating a Curve. Research report I-III. No 497006/90/1-3.(In Hungarian) Institute of Vehicle Engineering, Technical University of Budapest, 1990-1991.

[2] SOSTARICS, GY.: *Periodica Polytechnica (Transportation Engineering)* 1983. Vol. 11. No. 2 pp. 261–267.

[3] SPECHT, W.: Beitrag zur rechnerischen Bestimmung des Rad- und Schienenverschleisses durch Güterwagendrehgestelle. Dissertation, Aachen, 1985.

[4] FRIES, R. H. – DAVILA, C. G.: Analytical Methods for Wheel and Rail Wear Prediction. *Proceedings of the 9th IAVSD-Symposium: The Dynamics of Vehicles on Roads on Tracks.* Swets and Zeitlinger B. V. Lisse, 1986. pp. 112–125.

[5] CHUDZIKIEWICZ, A.: Progress Wear of Wheel in Simulation Research. *Proceedings of the 2nd Mini Conference on Vehicle System Dynamics, Identification and Anomalies*, held at the TU of Budapest, 1990. pp. 209–230.

[6] KALKER, J. J.: *Wear*, Vol. 150 (1991) pp. 355–365.

[7] SZABÓ, A.: Determination of Lateral Dynamical and Wheel Wear Processes of Railway Vehicles by Means of Digital Simulation. C.Sc. Thesis. (In Hungarian) Budapest, 1993.

[8] ZOBORY, I.: Stochasticity in Vehicle System Dynamics. *Proceedings of the 1st Mini Conference on Vehicle System Dynamics, Identification and Anomalies*, held at the TU of Budapest, 1988. pp. 8–21.

[9] KALKER, J. J.: On the Rolling Contact of two Elastic Bodies in the Presence of Dry Friction. Doctoral Dissertation, Technical University, Delft, Ned. Drukkerij Bedrijf, Nr. Leiden, 1967.

[10] SZABÓ, A. – SOSTARICS, GY. – ZOBORY, I.: Optimum Axle Box Guidance Stiffnesses for Traditional Running Gears Operating on a Given Railway Line. *Periodica Polytechnica (Transportation Engineering)*, Vol. 21. No. 2. 1993, *Proceedings of the 3rd Mini Conference on Vehicle System Dynamics, Identification and Anomalies*, held at the TU of Budapest, 9-11 November, 1992. pp. 173–184.

[11] SZABÓ, A. – SOSTARICS, GY. – ZOBORY, I.: *International Journal of Vehicle Design.* Vol. 15. Nos. 3/4, 1994. pp. 1–9.

[12] ZOBORY, I. – BÉKEFI, E.: Software STOPSIM for Stochastic Simulation of Motion and Loading Process of Vehicles. *Periodica Polytechnica, (Transportation Engineering)*, Vol. 22. No. 2. 1994, *Proceedings of the 3rd Mini Conference on Vehicle System Dynamics, Identification and Anomalies*, held at the TU of Budapest, 9-11 November, 1992. pp. 111–127.

[13] SZABÓ, A. – GAJDÁR, T. – SOSTARICS, GY. – ZOBORY, I.: On Numerical Simulation of the Wheel Wear Process under Specified Operation Conditions Possibility of Wheel-Set Guidance Optimization. 4th International Conferece on Contact Mechanics and Wear of Rail/Wheel Systems, held in Vancouver, Canada, July 24-28, 1994. in print).

PERIODICA POLYTECHNICA SER. TRANSP. ENG. VOL. 23, NO. 1-2, PP. 37-44 (1995)

ON DYNAMICAL PROCESSES IN RAILWAY TRACTION UNITS CAUSED BY WHEELSET GRAVITY POINT ECCENTRICITIES

I. ZOBORY and V. ZOLLER

Technical University of Budapest
Department of Railway Vehicles
H-1521 Budapest, Hungary

Received: Nov. 9, 1994

Abstract

Authors analyse the effect of the wheelset gravity point eccentricity on the longitudinal dynamical processes of the vehicle by using a simple model describing the longitudinal motion of the wheelset and the bogie-frame interconnected through a linear spring/damper system. The torque driving the wheelset is given by a specified time function. The wheel/rail contact is treated by the approximate pure rolling condition. By using perturbation techniques, appoximate solutions of the equations of motion are determined.

Keywords: vehicle dynamics, simulation of operational loads, perturbation techniques.

1. Introduction

In case of railway vehicles certain gravity point eccentricity (GPE) always appears with the wheels due to inaccuracies in the machining or irregular wear on the running surfaces.

It is an important question in the design and operation of railway vehicles, how great the allowed GPE can be. It is obvious that the presence of non-zero GPE values implies the existence of rotating centrifugal forces in the course of the rotatory motion of the wheels [2]. As the wheelsets are elastically connected in horizontal direction with the bogie-frame of the railway vehicle, it is clear that, due to the horizontal component of the rotating centrifugal forces acting on the wheelset, under certain conditions excited vibrations can be generated in the wheelset/bogie-frame two mass system. The latter excited vibrations can cause unwanted excess loads in the drive system, and the running behaviour of the vehicle can become untolerable.

The actual problem which motivated the investigations described in this paper was connected with the undesirable longitudinal vibrations experienced in the running gear of a metro trainset during the test period [3]. As a possible source of the unwanted dynamic processes, the presence of certain GPE values was suspected. In order to check the possible motions caused by the excitation effect of the rotating centrifugal forces, a simple model was

established, for which the strongly nonlinear problem could be treated by some approximation methods developed in the theory of nonlinear ordinary differential equations (see e.g. [1]).

2. The Model

In *Fig. 1* the simple in-plane longitudinal dynamical model of the wheelset/bogie-frame system is shown. Mass m_1 represents the bogie undergoing longitudinal translatory motion, while m_2 represents the mass of the wheelset having a GPE value designated by e. The moment of inertia of the wheelset is denoted by Θ, while s and k stand for the stiffness and damping coefficients of the connection, respectively. The longitudinal displacements x_1 and x_2, as well as the velocities $\dot{x}_1$ and $\dot{x}_2$ are also identified in *Fig. 1*. The rolling radius of the wheel is R, while c stands for the air drag coefficient. The time dependent torque M, acting on the wheelset, is in dynamical connection with the peripheral force F arising in the wheel–rail contact. The rolling motion of the wheelset is considered as pure rolling, i.e. creep dependent phenomena are omitted.

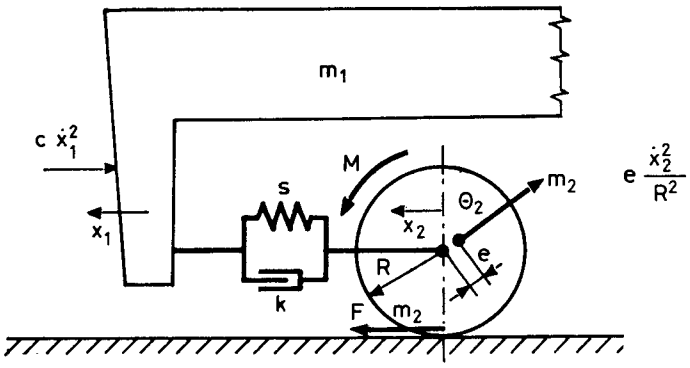

Fig. 1. The system model

3. Equation of Motion

The governing equations of the system have the form

$$m_1\ddot{x}_1 = s(x_2 - x_1) + k(\dot{x}_2 - \dot{x}_1) - c\dot{x}_1^2 , \tag{1}$$

$$m_2\ddot{x}_2 = -s(x_2 - x_1) - k(\dot{x}_2 - \dot{x}_1) + \frac{m_2 e}{R^2}\dot{x}_2^2 \cos\frac{x_2}{R} + F , \tag{2}$$

where, in case of pure rolling in the wheel–rail contact, force F can be determined by the equation

$$\Theta\frac{\ddot{x}_2}{R} = M - FR\,,$$

and M stands for the reduced turning moment.

Acceleration a of the longitudinal fundamental motion of the mass gravity point can be obtained by the governing equation

$$(m_1 + m_2)a = \frac{M - \Theta a/R}{R} - cv^2$$

as

$$a = \frac{MR - cR^2v^2}{(m_1 + m_2)R^2 + \Theta}\,,$$

where v is the speed of the fundamental motion.

Let us introduce the following notations:

$$\omega_1^2 := \frac{s}{m_1}\,, \quad \omega_2^2 := \frac{s}{m_2 + \Theta/R^2}\,, \quad \omega^2 := \omega_1^2 + \omega_2^2\,,$$

$$\kappa_1 := \frac{k}{m_1}\,, \quad \kappa_2 := \frac{k}{m_2}\,, \quad \kappa := \kappa_1 + \kappa_2\,,$$

$$\varepsilon := \frac{em_2R}{m_2R^2 + \Theta} \quad \text{and} \quad \delta := \frac{cR}{m_1}\,.$$

Using the above defined new parameters, the governing equations take the form

$$\ddot{x}_1 - \kappa_1\dot{x} - \omega_1^2 x = -\frac{\delta}{R}\dot{x}_1^2\,, \tag{3}$$

$$\ddot{x}_2 + \kappa_2\dot{x} + \omega_2^2 x = \left(\frac{\omega}{\omega_1}\right)^2 a + \frac{\delta}{R}\left(\frac{\omega_2 v}{\omega_1}\right) + \frac{\varepsilon}{R}\dot{x}_2^2\cos\frac{x_2}{R}\,, \tag{4}$$

where $x := x_2 - x_1$ stands for the relative displacement.

4. Perturbation Equations

We are looking for the solution of the set of differential equations (3–4) in the series form

$$x_i = u_{i0} + \varepsilon u_{i1} + \delta u_{i2} + \ldots\,, \quad i = 1, 2,$$

where functions u_{ij}, $j = 0, 1, 2, \ldots$ are already independent of the dimensionless quantities ε and δ. Relative displacement x can be written into the form

$$x = u_0 + \varepsilon u_1 + \delta u_2 + \ldots$$

Omitting the terms involving degree greater than 1, we obtain the following six equations:

$$\ddot{u}_{10} - \kappa_1 \dot{u}_0 - \omega_1^2 u_0 = 0 , \tag{5}$$

$$\ddot{u}_{20} + \kappa_2 \dot{u}_0 + \omega_2^2 u_0 = \left(\frac{\omega}{\omega_1}\right)^2 a , \tag{6}$$

$$\ddot{u}_{11} - \kappa_1 \dot{u}_1 - \omega_1^2 u_1 = 0 , \tag{7}$$

$$\ddot{u}_{21} + \kappa_2 \dot{u}_1 + \omega_2^2 u_1 = \frac{1}{R} \dot{u}_{20}^2 \cos \frac{u_{20}}{R} , \tag{8}$$

$$\ddot{u}_{12} - \kappa_1 \dot{u}_2 - \omega_1^2 u_2 = -\frac{1}{R} \dot{u}_{10}^2 , \tag{9}$$

$$\ddot{u}_{22} + \kappa_2 \dot{u}_2 + \omega_2^2 u_2 = \frac{1}{R} \left(\frac{\omega_2 v}{\omega_1}\right)^2 \tag{10}$$

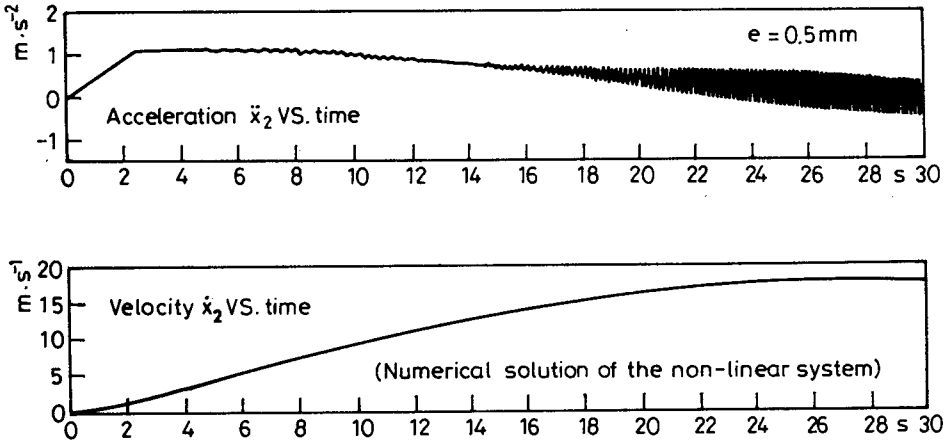

Fig. 2. Vibration form obtained by direct numerical solution

5. Exact Solution of the Perturbation Equations

If we subtract (5) from (6), (7) from (8), and (9) from (10), then we obtain system

$$\ddot{u}_0 + \kappa \dot{u}_0 + \omega^2 u_0 = \left(\frac{\omega}{\omega_1}\right)^2 a , \tag{11}$$

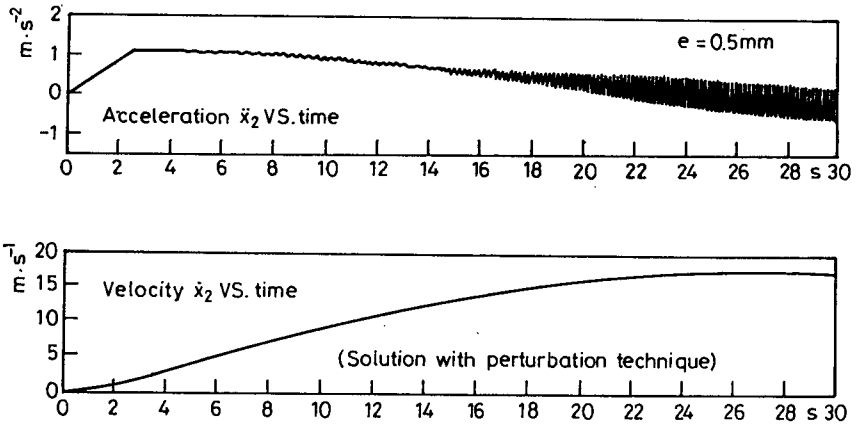

Fig. 3. Vibration form obtained by perturbational techniques

$$\ddot{u}_1 + \kappa\dot{u}_1 + \omega^2 u_1 = \dot{u}_{20}^2 \cos\frac{u_{20}}{R}, \tag{12}$$

$$\ddot{u}_2 + \kappa\dot{u}_2 + \omega^2 u_2 = \frac{1}{R}\left(\dot{u}_{10}^2 + \left(\frac{\omega_2 v}{\omega_1}\right)^2\right). \tag{13}$$

System (11–13) would be a system in three variables, if we could determine $\dot{u}_{10}$ and $\dot{u}_{20}$ with the help of functions u_j, $j = 0, 1, 2$. But $\dot{u}_{10}$ can be given by (5), and a rearrangement of (6) yields

$$\ddot{u}_{20} = \left(\frac{\omega}{\omega_1}\right)^2 a - \kappa_2 \dot{u}_0 - \omega_2^2 u_0 .$$

Hence u_{10} and u_{20} can be determined with the knowledge of u_0.

The solution of the perturbation equations can be given in the following way.

Step 1. Let us solve equation

$$\ddot{u}_0 + \kappa\dot{u}_0 + \omega^2 u_0 = \left(\frac{\omega}{\omega_1}\right)^2 a$$

by formula

$$u_0(t) = e^{-\kappa t/2}\left(C_1 \cos\frac{\lambda t}{2} + C_2 \sin\frac{\lambda t}{2}\right) +$$

$$+ \left(\frac{\omega}{\omega_1}\right)^2 \frac{2}{\lambda}\int_0^t a(\tau) e^{\kappa(t-\tau)/2} \sin\frac{\lambda}{2}(t-\tau)d\tau ,$$

where $\lambda^2 := 4\omega^2 - \kappa^2 > 0$ in practical cases, and constants C_1 and C_2 can be determined by the prescribed conditions as $C_1 = x(0)$ and $C_2 = \frac{1}{\lambda}(\kappa x(0) + 2\dot{x}(0))$.

Step 2. Let us evaluate

$$\dot{u}_{10}(t) = \kappa_1(u_0(t) - x(0)) + \omega_1^2 \int_0^t u_0(\tau)d\tau + \dot{x}_1(0)$$

by *Eq.* (5).

Step 3. Let us evaluate

$$\dot{u}_{20}(t) = \left(\frac{\omega}{\omega_1}\right)^2 (v(t) - v_0) - \int_0^t (\kappa_2 \dot{u}_0(\tau) + \omega_2^2 u_0(\tau)d\tau + \dot{x}_2(0)$$

and

$$u_{20}(t) = \left(\frac{\omega}{\omega_1}\right)^2 (s(t) - v_0 t) -$$

$$- \int_0^t \int_0^\theta (\kappa_2 \dot{u}_0(\tau) + \omega_2^2 u_0(\tau) + \omega_2^2 u_0(\tau))d\tau d\theta + \dot{x}_2(0)t + x_2(0)$$

by *Eq.* (6), where $s(t)$ is the longitudinal displacement of the fundamental motion.

Step 4. Let us solve equation

$$\ddot{x} + \kappa\dot{x} + \omega^2 x = \left(\frac{\omega}{\omega_1}\right)^2 a + \frac{\delta}{R}\left(\frac{\omega_2 v}{\omega_1}\right)^2 + \frac{\varepsilon}{R}\dot{u}_{20}^2 \cos\frac{u_{20}}{R} + \frac{\delta}{R}\dot{u}_{10}^2$$

for the relative displacement as

$$x(t) = e^{-\kappa t/2}\left(C_1 \cos\frac{\lambda t}{2} + C_2 \sin\frac{\lambda t}{2}\right) +$$

$$+\frac{2}{\lambda}\int_0^t \left(\left(\frac{\omega}{\omega_1}\right)^2 a(\tau) + \frac{\delta}{R}\left(\frac{\omega_2}{\omega_1}\right)^2 v(\tau)^2 +\right.$$

$$\left. + \frac{\varepsilon}{R}\dot{u}_{20}(\tau)^2 \cos\frac{u_{20}(\tau)}{R} + \frac{\delta}{R}\dot{u}_{10}(\tau)^2\right) e^{\kappa(\tau - t)/2} \sin\frac{\lambda}{2}(t - \tau)d\tau \,.$$

6. Steady-state Solutions

Suppose that the acceleration a of the fundamental motion is constant. If we are looking for a steady-state solution, then we can assume

$$u_0(t) = \frac{a}{\omega_1^2}, \quad \dot{u}_{10}(t) = v(t) \quad \text{and} \quad u_{20}(t) = s(t) \,.$$

This way we obtain equation

$$\ddot{x} + \kappa\dot{x} + \omega^2 x = \left(\frac{\omega}{\omega_1}\right)^2 a + \frac{\delta}{R}\left(\frac{\omega v}{\omega_1}\right)^2 + \frac{\varepsilon v^2}{R}\cos\frac{s}{R} \tag{14}$$

with solution

$$x(t) = \frac{a}{\omega_1^2}e^{-\kappa t/2}\left(\cos\frac{\lambda t}{2} + \frac{\kappa}{\lambda}\sin\frac{\lambda t}{2}\right) +$$

$$+\frac{2}{\lambda}\int_0^t \left(\left(\frac{\omega}{\omega_1}\right)^2 a + \frac{\delta}{R}\left(\frac{\omega}{\omega_1}\right)^2 v(\tau)^2 +\right.$$

$$\left. +\frac{\varepsilon}{R}v(\tau)^2\cos\frac{s(\tau)}{R}\right) e^{\kappa(\tau-t)/2}\sin\frac{\lambda}{2}(t-\tau)d\tau\ ,$$

where $v(\tau) = v_0 + a\tau$ and $s(\tau) = v_0\tau + \frac{a}{2}\tau^2$.

Let us reparametrize *Eq.* (14) by introducing displacement s as a new variable:

$$v^2 x'' + (\kappa v + a)x' + \omega^2 x = \left(\frac{\omega}{\omega_1}\right)^2 a + \frac{\delta}{R}\left(\frac{\omega v}{\omega_1}\right)^2 + \frac{\varepsilon v^2}{R}\cos\frac{s}{R}\ , \tag{15}$$

where $'$ stands for derivation by s, and $v(s) = \sqrt{v_0^2 + 2as}$ holds.

Let us suppose also that condition $\omega_1 v_0 >> a$ is satisfied. Then we are able to introduce another 'small' dimensionless parameter $\alpha := \frac{a}{\omega_1 v_0}$. In this case, omitting the terms of degree greater than 1 in α, ε and δ, the first perturbational approximation provides differential equation

$$v_0 x'' + \kappa v_0 x' + \omega^2 x = \frac{\alpha\omega^2 v_0}{\omega_1} + \frac{\delta}{R}\left(\frac{\omega v_0}{\omega_1}\right)^2 + \frac{\varepsilon v_0^2}{R}\cos\frac{s}{R}\ . \tag{16}$$

The corresponding steady-state solution at any speed v has the form

$$x(s) = \frac{a}{\omega_1^2} + \frac{\delta v^2}{R\omega_1^2} + \frac{\varepsilon R v^2}{\sqrt{(R^2\omega^2 - v^2)^2 + (R\kappa v)^2}}\cos\left(\frac{s}{R} - \phi\right)\ , \tag{17}$$

where $\tan\phi = \frac{R\kappa v}{R^2\omega^2 - v^2}$ is satisfied.

7. Conclusions

Our solution provides a very good approximation of the nonlinear resonance phenomena appearing due to the existence of a nonzero GPE value. Comparing *Figs. 2* and *3* one can see that the vibration forms obtained by our perturbational approach have the same characteristics as the solution

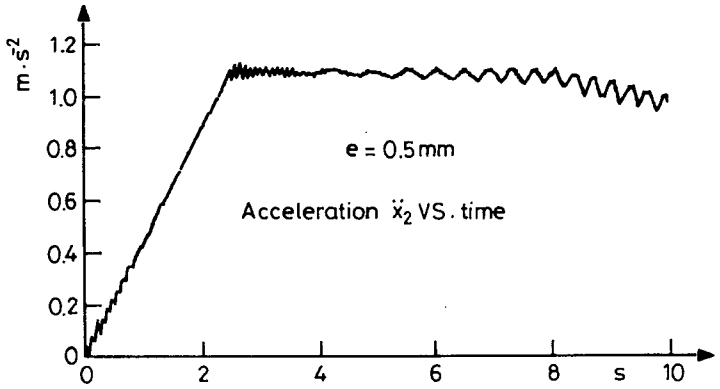

Fig. 4. Blown up section of the perturbational solution

achieved by the direct numerical solution to the equations of motion in case of a metro-vehicle example. Approximate formula (17) possesses almost all the important features of the vibration time functions shown in *Fig. 4*. In the course of further investigations the system model will be generalized to take into consideration the creep-dependence of the tangential force transmitted on the wheel in the wheel–rail rolling contact [4].

References

[1] NAYFEH, A. H.: Introduction to Perturbation Techniques, Wiley, New York, 1981.
[2] ZOBORY, I.: Investigation into the Logitudinal Dynamics of a Six-unit Metro Trainset Developed by Firm Ganz-MÁVAG (in Hungarian), *Res. Report* No 497001/1990-3, TU Budapest, Dept. Railway Vehicles, 1990.
[3] HORVÁTH, K. – ZOBORY, I. – BÉKEFI, E.: Logitudional Dynamics of a Six-unit Metro Trainset, *Proc. 2nd Mini Conf. Vehicle Syst. Dynamics, Identification and Anomalies*, TU Budapest, Nov. 12–15, 1990, pp. 45–62.
[4] ZOBORY, I.: Dynamics of Drive Systems of Railway Traction Units, *Vehicles, Agricultural and Building Machines*, (in Hungarian), Vol. 41, pp. 255–264, April, 1994.

PERIODICA POLYTECHNICA SER. TRANSP. ENG. VOL. 23, NO. 1-2, PP. 45-52 (1995)

COMPARISON OF DISCRETE AND CONTINUOUS RAIL MODELS

Zoltán ZÁBORI

Department of Railway Vehicles
Technical University of Budapest
H-1521 Budapest, Hungary

Received: November 8, 1994

Abstract

This paper shows a comparison between the continuous and discrete rail models. The discrete rail model consists of rigid bodies which are connected with each other by springs and dampers. In the discrete track model the rails are connected with the sleepers by springs and dampers, modelling the pads and fastenings. The continuous rail model is a flexible beam connected with the sleeper masses in discrete points by springs and dampers. The paper introduces a comparative analysis of the two models from the point of view of the shape function of the rail models in case of a moving vertical force. The results give a possibility to identify the parameters of the discrete rail model with the knowledge of the dynamical processes of the continuous rail model.

Keywords: discrete rail model, continuous rail model, dynamical simulation.

1. Introduction

The investigation into the dynamical processes of the railway track – vehicle system has a great importance recently. The structure of the railway track can be modelled as a system of elastically supported continuous beam and sleeper masses connected with the beam and the basic plane elastically and dissipatively. There are moving vertical forces on the beam modelling the vertical wheel loads of a railway vehicle. Due to the vertical forces also vertical displacements of the beam and sleeper masses should be reckoned with.

The goal of this paper is to analyse and compare the dynamical processes of different railway track models.

The railway track is modelled on the one hand as a continuous beam supported elastically in discrete points and as an elastic chain consisting of discrete masses connected with each other elastically and connected with the sleepers in discrete points, on the other. A longitudinally moving vertical force acts on the rail models. The solutions of the equations of motion of the two dynamical track models can be compared from that point of view, if a the good approximation property of the results yielded by the discretized model is ensured.

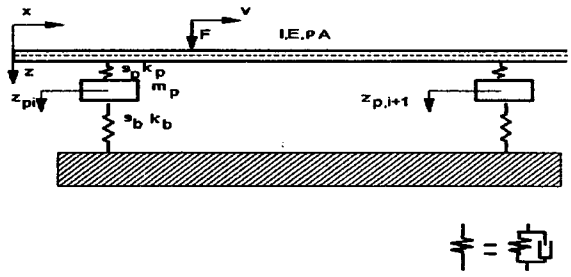

Fig. 1. Continuous rail model

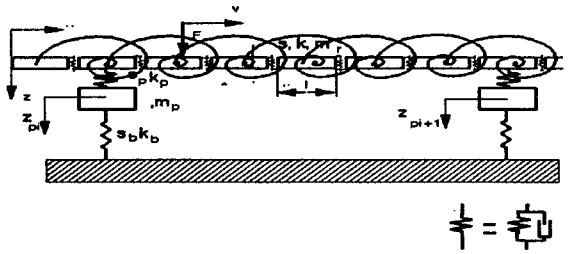

Fig. 2. Discretized rail model

2. Track Modelling

The continuous rail model of the railway track is shown in *Fig. 1.* The in-plane dynamical model consists of an elastic beam supported elastically in discrete points and the model of the sleeper masses is connected with the beam and the stationary basic plane by parallelly connected springs and dampers modelling the rail pads and the ballast. The parameters of the beam are: moment of inertia I, Young modulus E, density ρ and cross-section area A in the model. s_p is the stiffness of the spring, k_p is the damping between the beam and the sleeper mass, while s_b stands for the stiffness and k_b for the damping of the ballast between the sleeper mass and the stationary basic plane. The effect of the wheelset is represented by vertical force F, moving at a constant longitudinal velocity v.

The second model of the railway track is shown in *Fig. 2.* The discretized model of the rail consists of brick-form masses connected with each other by vertical and bending springs (s_p) and vertical and bending dampers (k_p). The length of one mass element is designated by l. Moving vertical force F acts on the discrete track model representing the wheelset load of the vehicle.

3. Motion Equations

a. The equations of motion of the continuous rail model are determined by the known equation of the Euler–Bernoulli beam and by using Newton's 2nd law for the motion of the sleeper masses of the model.

Thus, the equation of motion for the beam is a fourth order linear partial differential equation

$$IE\frac{\partial^4 z(x,t)}{\partial x^4} + \rho A\frac{\partial^2 z(x,t)}{\partial t^2} = -\sum_{(i)} k_i \left(\frac{\partial z(x,t)}{\partial t} - z'_{pi}(t)\right)\delta(x - x_i) -$$

$$-\sum_{(i)} s_i(z(x,t) - z_{pi}(t))\delta(x - x_i) + F(t)\delta(x - vt)\,, \tag{1}$$

where $z(x,t)$ is the vertical displacement of the beam and x_i is the sequence of the longitudinal position of the sleepers [1], [2], [3].

The equation of motion of the ith sleeper mass is the following second order ordinary linear differential equation:

$$m_i\ddot{z}_{pi} = s_i(z(x_i,t) - z_{pi}(t)) + k_i(z_t(x_i,t) - \dot{z}_{pi}(t))\,. \tag{2}$$

Eqs. (1) and (2) determine an equation system consisting of one fourth order linear partial differential equation and number n second order linear ordinary differential equations.

b. The equation of motion for the discretized track model (shown in *Fig. 2*) can be written into the following form:

$$\mathbf{M}\ddot{z} + \mathbf{K}\dot{z} + \mathbf{S}z = b(t)\,, \tag{3}$$

where $\mathbf{M}$ is the mass, $\mathbf{K}$ is the damping and $\mathbf{S}$ is the stiffness matrix, $z(t)$ is the vertical displacement and angular position vector and $b(t)$ is the excitation vector. Vector $b(t)$ can be written in the following form:

$$b_i(t) = \begin{cases} F & \text{if } \frac{(i-1)l}{v} < t < \frac{1}{v} \\ 0 & \text{otherwise} \end{cases} \quad (i = 1,2,\ldots,2n-1)\quad, \tag{4}$$

$$b_j(t) = \begin{cases} F[(i-1)l + 0.5l - vt] & \text{if } \frac{(i-1)l}{v} < t < \frac{1}{v} \\ 0 & \text{otherwise} \end{cases} \quad (j = 2,4,\ldots,2n)\,, \tag{5}$$

The excitation function can be seen in the *Fig. 3.*

The structure of the stiffness matrix can be seen in the *Table 1.*

Table 1. The structure of the stiffness mat $\mathbf{S} =$

$+s$	$-s^*(1/2)$	$-s$	$-s^*(1/2)$							
$-s^*(1/2)$	$st+s(1/2)\hat{}2$	$+s^*(1/2)$	$-st+s(1/2)\hat{}2$							
$-s$	$+s^*(1/2)$	$+2s+sp$		$-sp$		$-s$	$-s^*(1/2)$			
$-s^*(1/2)$	$-st+s(1/2)\hat{}2$		$2st+2s(1/2)\hat{}2$			$+s^*(1/2)$	$-st+s(1/2)\hat{}2$			
		$-sp$		$+sp+sb$						
					$2st+2s(1/2)\hat{}2$					
		$-s$	$+s*(1/2)$			$+2s$		$-s$	$-s*(1/2)$	
		$-s^*(1/2)$	$-st+s(1/2)\hat{}2$				$2st+2s(1/2)\hat{}2$	$+s^*(1/2)$	$-st+s(1/2)\hat{}2$	
						$-s$	$+s^*(1/2)$	$+2s$		$-s$
						$-s^*(1/2)$	$-st+s(1/2)\hat{}2$		$2st+2s(1/2)\hat{}2$	$+s^*(1/2)$
								$-s$	$+s^*(1/2)$	$+2s$
								$-s^*(1/2)$	$-st+s(1/2)\hat{}2$	
										$-s$
										$-s^*(1/2)$

$-s^*(1/2)$										
$-st+s(1/2)\hat{}2$										
	$-s$	$-s^*(1/2)$								
$2st+2s(1/2)\hat{}2$	$+s^*(1/2)$	$-st+s(1/2)\hat{}2$								
$+s^*(1/2)$	$+2s$		$-s$	$-s^*(1/2)$						
$-st+s(1/2)\hat{}2$		$2st+2s(1/2)\hat{}2$	$+s*(1/2)$	$-st-s(1/2)\hat{}2$						
	$-s$	$+s^*(1/2)$	$+2s$		$-s$	$-s^*(1/2)$				
	$-s^*(1/2)$	$-st+s(1/2)\hat{}2$		$2st-2s(1/2)\hat{}2$	$+s^*(1/2)$	$-st+s(1/2)\hat{}2$				
			$-s$	$-s*(1/2)$	$+2s+sp$		$-sp$		$-s$	$-s^*(1/2)$
			$-s^*(1/2)$	$-st-s(1/2)\hat{}2$		$2st+2s(1/2)\hat{}2$			$+s^*(1/2)$	$-st+s(1/2)\hat{}2$
					$-sp$		$+sp+sb$			
								$2st+2s(1/2)\hat{}2$		
					$-s$	$+s^*(1/2)$			$+s$	$+s^*(1/2)$
					$-s^*(1/2)$	$-st+s(1/2)\hat{}2$				$+s^*(1/2)\ st+s(1/2)\hat{}2$

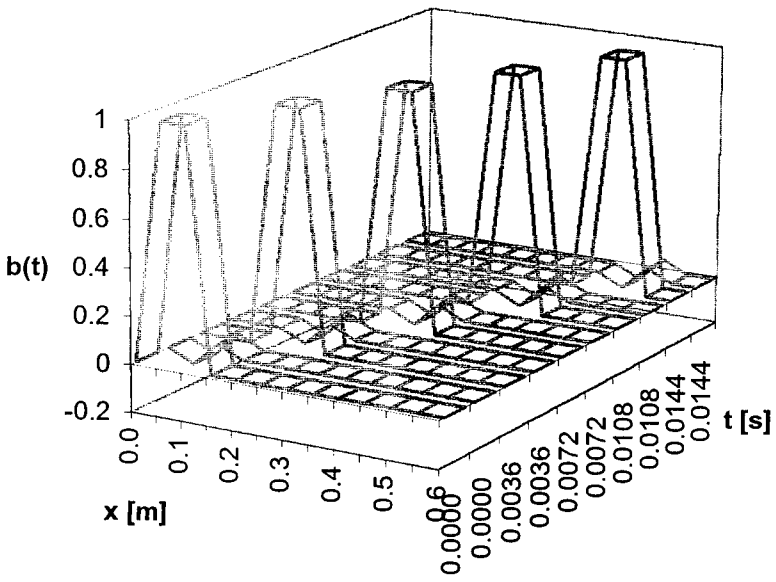

Fig. 3. Excitation function

4. Solution to the Equations of Motion

Equation system (1)-(2) can be solved by using Laplace-transform method. Define

$$Z(p,t) = L\{z(x,t)\}\,, \tag{6}$$

the Laplace-transform of function of $z(x,t)$ with respect to variable x.

The Laplace-transform of (1) can be written into the following form by considering $F(t)$ is constant:

$$(IEp^4 + \rho Av^2p^2 - \sum_{(i)} k_i vpe^{-px_i} + \sum_{(i)} s_i e^{-px_i})Z(p,t) =$$

$$= Fe^{-pvt} + \sum_{(i)}(k_i Z'_{tpi}(p,t) + s_i Z_{pi}(p,t))e^{-px_i}\,. \tag{7}$$

So the characteristic polynom of *Eq.* (7) is the following transcendent equation:

$$f(p) = IEp^4 + \rho Av^2p^2 - \sum_{(i)} k_i vpe^{-px_i} + \sum_{(i)} s_i e^{-px_i} = 0\,, \tag{8}$$

Table 2. Data set of computation

I	=	$1.7415 \cdot 10^{-5}$ m^4	s_b	=	$3 \cdot 10^8$ N/m
E	=	$2.1 \cdot 10^{11}$ N/m^2	s_t	=	0
ρA	=	60 kg/m	k	=	0
m_r	=	6 kg	k_p	=	0
m_b	=	250 kg	k_b	=	0
s	=	$5 \cdot 10^{10}$ N/m	v	=	100 km/h
s_p	=	$3 \cdot 10^8$ N/m	F	=	1 N

where the unknown variable is p. The *Eq.* (8) can be solved graphically or numerically. The solution to (1) and (2) can be written into the following form:

$$z(x,t) = \sum_{(j)} C(p_j) e^{p_j (x - vt)} , \tag{9}$$

where C is the function of p_j, j is the index of the solution of *Eq.* (8), i is the index of the serial number of the support. The solution was approximated by substituting

$$\sum_{(i)} s_i e^{-px_i} = s' \sum_{(i)} s_i e^{-px_i} = s' \quad \text{and} \quad \sum_{(i)} k_i v p e^{-px_i} = k' v p , \tag{10}$$

where s' and k' are constants [1], and let $z_{pi}(x,t) = 0$ and $z'_{tpi}(x,t) = 0$ (the vertical motion and velocity of the ballast is approximately zero).

The differential equation system of the discrete rail model can be written into the following form by using the state space representation [2], [3], [4]:

$$\begin{bmatrix} \ddot{z}(t) \\ \dot{z}(t) \end{bmatrix} = \begin{bmatrix} -\mathbf{M}^{-1} & \mathbf{K} & -\mathbf{M}^{-1} & \mathbf{S} \\ \mathbf{E} & \mathbf{0} & & \end{bmatrix} \begin{bmatrix} \dot{z}(t) \\ z(t) \end{bmatrix} + \begin{bmatrix} b(t) \\ 0 \end{bmatrix} . \tag{11}$$

Set of *Eqs.* (10) can be solved in the time domain by using numerical method (e.g. Euler's method).

The computations were performed by using realistic data set for a 3 m long track section model shown in the *Table 2.*

The solutions obtained by the numerical computations are shown in *Fig. 4.* There are two curves in the Figure. The solid line represents the momentary deflection function of the continuous rail model. The strip of rectangles represents the momentary shape of the discretized rail. Each rectangle describes the displacement of the gravity point of the discrete brick element in the discretized model. The moving force for the instant of the representation is at position $x = 1$ m. In the Figure, the longitudinal distance x is taken on the horizontal axis.

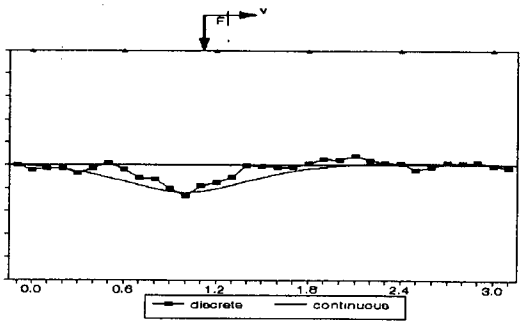

Fig. 4. Shape-function of 3 m long continuous and discrete rail model in case of moving load

It can be seen in the Figure, that the displacement function of the continuous rail model has a smooth shape with small curvature (two inflection points), while the discretized model has more changeable curvatures and more than two inflection points (the initial values were based on by the condition that the maximal vertical displacements of the two models should be equal).

5. Conclusions

It can be seen that the shapes of the displacement functions belonging to the two models are similar to each other but the degree of fitting is not satisfactory between them. Comparing the two computation methods, it is to be emphasized that the treatment of the continuous rail model is complicated because of the necessity of the solution of nonlinear *Eq.* (7), which can be solved only approximately.

The mathematical treatment of the discretized rail model is much more easy.

Further research is necessary to determine the optimum parameters of the discretization and the number of the elements used for representing a sleeper section of the rail.

References

[1] FORTIN, J-P.: Dynamic Track Deformation, *French Railway Review*, North Oxford Academic, 1983., Vol. 1. No. 1. pp. 3–12.

[2] ZOBORY, I.: Track-Vehicle System from the Point of View of a Vehicle Engineer. Transport Scientific Society, Vas County, Szombathely, 1991. pp. 19–42. (in Hungarian).

[3] TIMOSHENKO, S.: Method of Analysis of Statical and Dynamical Stresses in Rail, East-Pittsburgh, Pennsylvania, USA, 1978.

[4] FODOR, GY.: Laplace-Transformation. Technical Publisher, Budapest, 1967. (in Hungarian).

[5] RÉDEI, L.: Algebra, Akademische Verlagsgesellschaft, Geest & Portig K.-G., Leipzig, 1959, pp. 678–685.

[6] HIRATA, C.: An Experimental Study of the Rail Vibration Characteristics in Various Tracks. *Quarterly Reports JNR*, Vol. 21. No. 3.

[7] DESTEK, M.: Complex Investigation and Measuring Method of Track-Vehicle System. Transport Scientific Society, Vas County, Szombathely, 1991. pp. 43–51. (in Hungarian).

[8] TOYODA, M.: Test for Determining Optimum Spring Constant of Tie Pad. Quarterly Report of the Technical Railway Research Institute, 9, 1968/4.

[9] MEGYERI, J.: Track-Vehicle System from the Point of View of a Track Engineer. Transport Scientific Society, Vas County, Szombathely, 1991. pp. 10–18. (in Hungarian).

[10] ZOBORY, I. – ZOLLER, V. – ZÁBORI, Z.: Time Domain Analysis of a Railway Vehicle Running on a Discretely Supported Continuous Rail Model at a Constant Velocity *ICIAM95 Conference*, Hamburg, 1995 (to appear).

[11] ZÁBORI, Z.: The Lateral Dynamics of a Railway Wheelset Running on an Elastically Supported Track. *Periodica Polytechnica Transportation Engineering*, Budapest, Vol. 21. No. 3., 1994. pp. 281–287.

[12] ZOBORY, I. et al.: Theoretical Investigations into the Dynamical Properties of Railway Tracks Using a Continuous Beam Model on Elastic Foundation. *III. Mini Conference*, *Periodica Polytechnica*, Budapest Vol. 22., No. 1., 1994, pp. 35–54.

PERIODICA POLYTECHNICA SER. TRANSP. ENG. VOL. 23, NO. 1-2, PP. 53-62 (1995)

INFLUENCE OF VARIOUS ANOMALIES IN THE VEHICLE AND TRACK PARAMETERS ON THE POSSIBILITY OF DERAILMENT

Victor A. KABLUKOV, Victor D. DANOVICH and
Vladislav A. LITWIN

Dnepropetrovsk State Technical University of Railway Transport
Dnepropetrovsk, Ukraine

Received: November 7, 1994

Abstract

A detailed nonlinear model of the four-axle real vehicle, considering both vertical and lateral vibrations has been proposed. Inertial and elastic-viscous properties of the track have been taken into account. Comparison of the theoretical investigations and on-track tests has confirmed the rather good authenticity of the model. The calculations for anomalies either in track or in vehicle parameters as well as for their combinations have been performed.

1. Introduction

Despite safety measures, strictly observed on railways, the cases of derailment take place sometimes. These cases are becoming more frequent with increasing of operational speeds, axle loads, train length and mass. Thus, the necessity of detailed modelling of such accidents arises in order to determine the causes of them and, that is most important, to prevent the recurrence of such situations in future.

Such an analysis becomes possible on condition that the reliable information about the track and the vehicle is available and that the analytical model detailed sufficiently of the vehicle–track system, allowing to use this information, exists.

The analytical model of the four-axle freight wagon, the software package, designed on the base of this model and some results, obtained with their help, are described in this paper.

2. Freight Wagon Vertical and Lateral Dynamics Model

The four-axle open goods wagon was chosen by the authors as an object for modelling. Such a choice has made it possible to investigate a lot of various types of freight rolling stock, operated on the Ukrainian railways. The model of the wagon is shown in *Fig. 1.*

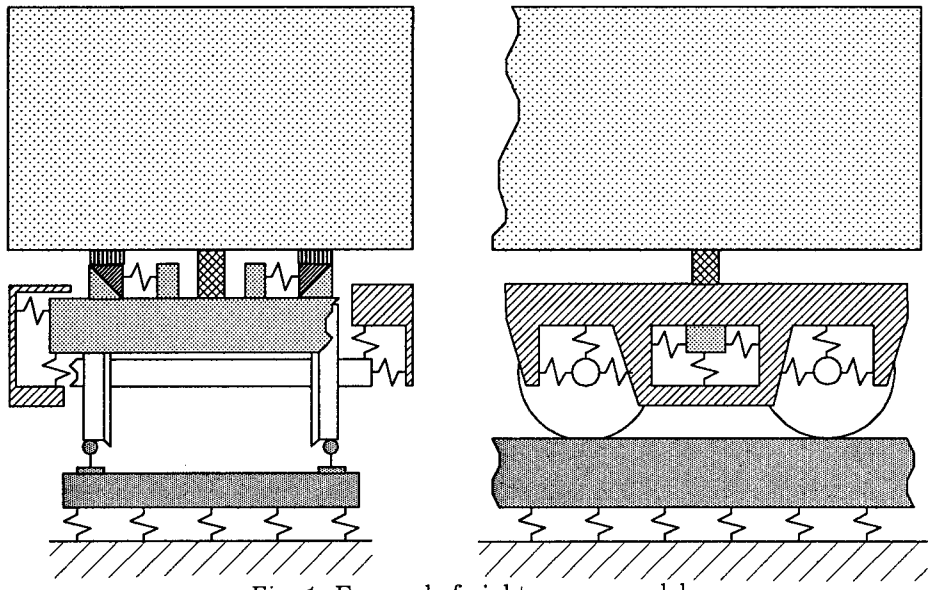

Fig. 1. Four-axle freight wagon model

A brief description of the model is given below (more details one can find in [1]).

The investigated system consists of eleven solid bodies (a car body, two bolsters, four side frames, four wheelsets). If necessary, it is possible to take into account car body flexibility. The following specific features of the vehicle have been reflected in the model as well.

Car body - bolster. One neglects with a clearance between the pivot and the centerplane, thus the mutual longitudinal displacements of these bodies are absent and their pitching is identical. As regards rolling and yawing of the bolster – they may occur independently from rolling and yawing of the car body. The action of the slippers of various types can be modelled.

Bolster - side frame. Vertical, lateral and longitudinal springs allow all possible mutual linear displacements and mutual yawing, In addition to springs, dry friction dampers with asymmetric characteristic are installed in this unit.

Side frame - wheelset. All possible mutual displacements between these bodies are allowable. Installation of the rubber spacers can be simulated by adding the Coulomb friction elements.

Thus, the following non-linearities are modelled: rolling and pitching of the car body on the pivot, kicks after taking up the clearances in the slippers, geometric and physical non-linearities in the wheel–rail contact points (the creepage forces are modelled by the CARTER's theory [2]).

The VLASOV's hypothesis [3] is accepted for the description of elastic-

viscous and inertial properties of the track in vertical and lateral directions.

After taking into account all the above-mentioned features and restraints one obtains a 59-degree-of-freedom model. The corresponding ordinary differential equations system has been composed. The Runge–Kutta (for the first steps) and Adams–Bashforth methods are used for its solving.

The nominal values for some parameters of the standard freight open goods wagon without anomalies are listed in *Table 1.* They have been taken from [4] and [5].

3. A Brief Description of the Software Package

The described model has become the base for the program package for IBM PC computers with MS DOS. The computational part has been written in FORTRAN and the interface modules have been written in C language. The package provides a user-friendly interface, allowing to change the input parameters in easy way. The output of the program contains values for more than one hundred dynamic characteristics.

In addition some other, stand-alone programs have been created. They allow:

- to generate the file with the track irregularities, necessary for the main program in different ways;
- to draw plots of the computed displacements, accelerations and forces;
- to compute the power spectrum densities of the various processes;
- to determine the increment of the rolling radius depending on mutual lateral wheel–rail displacement for various real profiles of the wheel and rail.

The authors would like to thank Mr. R. Granovsky and Mr. A. Reidemeister for their help in creation of these programs.

4. Modelling of the Track Irregularities

Four types of the track irregularities are used as an input for the simulation program, described in Section 3. Those are:

- deviation of the left rail from a uniform profile in a vertical plane;
- deviation of the right rail from a uniform profile in a vertical plane;
- deviation of the left rail from a straight line in a horizontal plane;
- deviation of the right rail from a straight line in a horizontal plane;

For some reason such a set of irregularities was chosen as more convenient in comparison with a traditional vertical profile – cross level – alignment – gage set.

The file with necessary track irregularities may be created with the separate program in several different ways, namely:

Table 1.
Data for the standard wagon

Mass of the car body	76500 kg
Rolling moment of inertia for the car body	7.5E4 kg·m^2
Pitching moment of inertia for the car body	1.05E6 kg·m^2
Yawing moment of inertia for the car body	1.1E6 kg·m^2
Bogie centre distance	8.66 m
Mass of the bolster	450 kg
Rolling moment of inertia for the bolster	300 kg·m^2
Pitching moment of inertia for the bolster	50 kg·m^2
Yawing moment of inertia for the bolster	300 kg·m^2
Vertical stiffness of the secondary suspension springs	4000 kN/m
Shearing stiffness along the lateral axis between the bolster and the side frame	6000 kN/m
Torsional stiffness between the bolster and the side frame	200 kN m/rad
Clearance in the slippers	0.005 m
Mass of the side frame	680 kg
Pitching moment of inertia for the side frame	220 kg·m^2
Yawing moment of inertia for the side frame	220 kg·m^2
Bogie wheelbase	1.85 m
Mass of the wheelset	1370 kg
Rolling and yawing moment of inertia for the wheelset	1000 kg·m^2
Nominal wheel radius	0.45 m
Distance between planes of rolling radii	1.580 m
Flange clearance	0.007 m
Reduced vertical track stiffness	43830 kN/m
Reduced horizontal track stiffness	16570 kN/m
Reduced vertical track mass	659 kg
Reduced horizontal track mass	76 kg

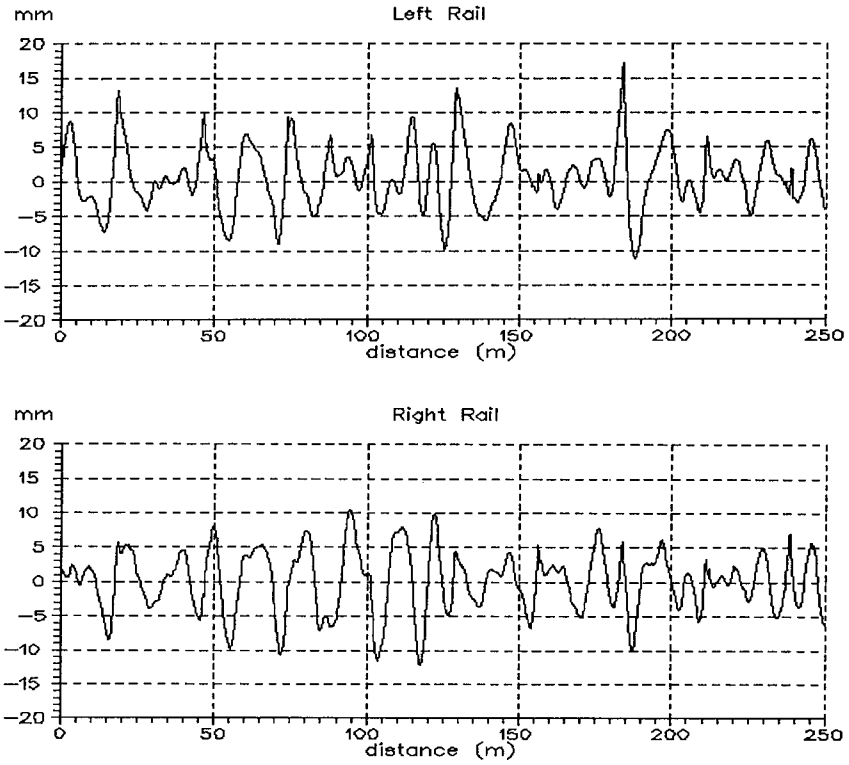

Fig. 2. Measured rail profiles

- after processing the data, recorded with a track-test car (an example of the vertical irregularities, obtained in such a way, is shown in *Fig. 2*);
- by inverse Fourier transform of the vertical profile, cross level, alignment and gage power spectral densities and subsequent change-over to the chosen type of irregularities (the authors use well-known expressions for the PSDs from [6]);
- by modelling the track with the periodically repeating joints;
- by modelling the isolated track geometry variations like bump, jog, plateau, etc.

5. Validation of the Model

The track irregularities shown in *Fig. 2* were recorded during the on-track tests simultaneously with some wagon's performance (vertical and lateral

accelerations of the axle boxes and car body). The measurements were carried out with various speeds both on jointed and on continuously welded track. Thus, the authors got an opportunity to compare the results, obtained by computer simulation, with the corresponding experimental data. For the vertical dynamics performance good coincidence was received. As to horizontal accelerations of the car body, the situation proved to be not so optimistic. The amplitudes of the theoretical accelerations coincide closely with the test ones. As to power spectrum densities of both processes, the coincidence in the low frequencies interval (0.5–3 Hz) is good enough but for higher frequencies (3–10 Hz) the difference occurred. The authors prone to see the origins of this in rather rough modelling of a dry friction in the system.

6. Criterion of Safety and Estimation of the Dynamic Performance

The so-called *coefficient of stability of a wheelset during flanging* (for briefness we shall refer to it simply as to the 'coefficient of stability') is used as a criterion of safety on the railways of the former USSR according to [7]. This coefficient is determined by the following expression:

$$C_S = \frac{|P_1 C_1 - P_2 C_2 - C_3|}{|H_b|}, \tag{1}$$

where

C_s – coefficient of stability;
P_1 – left-axle-box-to-side-frame vertical force;
P_2 – right-axle-box-to-side-frame vertical force;
H_b – frame force (the sum of left and right axle-boxes-to-side-frames lateral forces).

The coefficients C_1, C_2, C_3 depend upon the mass and geometric characteristics of the vehicle [8]. The motion of the wheelset is assumed to be unstable when the coefficient of stability is less than 1.

The program determines the minimum values of the coefficient of stability for all four wheelsets together with distances where those values were registered. The total length (in meters and seconds) of the longest continuous series for $C_s < 1$ also is printed for each wheelset.

Besides the coefficients of stability the program analyses more than a hundred dynamic characteristics of the wagon. For each of them its minimum and maximum values, the distances, where these values were registered, arithmetic mean, dispersion, mean square and confidence limit are determined. The *Fig. 3* illustrates the above-mentioned statistics for some dynamic performance (frame forces (Hb) and coefficients of stability (CS) values for all four wheelsets as well as car body roll angle (THETA)).

Wagon: empty
Speed: 75.0 km/h
Track: Straight

	$F_{\min}$	$X_{\min}$	$F_{\max}$	$X_{\max}$	M	D	S	$M+2.5S$
Hb(1,1)	-17.06	80.29	13.22	86.71	-.3517E-01	10.22	3.196	8.026
Hb(1,2)	-14.93	80.21	10.74	86.61	-.4579E-01	11.90	3.450	8.671
Hb(2,1)	-7.963	68.45	7.769	62.76	.4284E-01	2.110	1.453	3.674
Hb(2,2)	-8.088	69.10	8.232	63.02	.4936E-01	3.044	1.745	4.411
				...				
THETA	-8.191	89.99	7.060	84.80	-.4488E-01	19.26	4.388	11.02
				...				

Coefficients of stability

	$CS_{\min}$	$X_{\min}$	Longest continuous series < 1
1,1	3.086	73.56	from .000 m to .000 m (.00000 sec)
1,2	3.254	71.35	from .000 m to .000 m (.00000 sec)
2,1	3.720	70.30	from .000 m to .000 m (.00000 sec)
2,2	4.770	71.41	from .000 m to .000 m (.00000 sec)

Fig. 3. Fragment of the program's output

7. Anomalies Modelling

The vast number of the model input parameters makes it possible to simulate various anomalies in the track and in the vehicle. Typical anomalies in the track could be modelled with the help of the program, described in section 4. Among the most important anomalies of the vehicle which are possible to imitate one should mention the following ones:

- nonstandard wheel–rail profiles, appeared because of wear or improper machining;
- wear of the different vehicle suspension elements;
- displacement of the car body centre of gravity both in longitudinal and in lateral directions due to inaccurate loading of the vehicle.

8. Some Results

The material of current section has been obtained as a result of analysis of the derailment accident which occurred in reality. The empty tank wagon derailed at the speed of 75 km/h. Careful analysis has revealed some severe anomalies both in the rolling stock (mainly in the wheel profiles that is shown in *Fig. 4* in comparison with a standard profile) and in the track (deflections in alignment and cross-level).

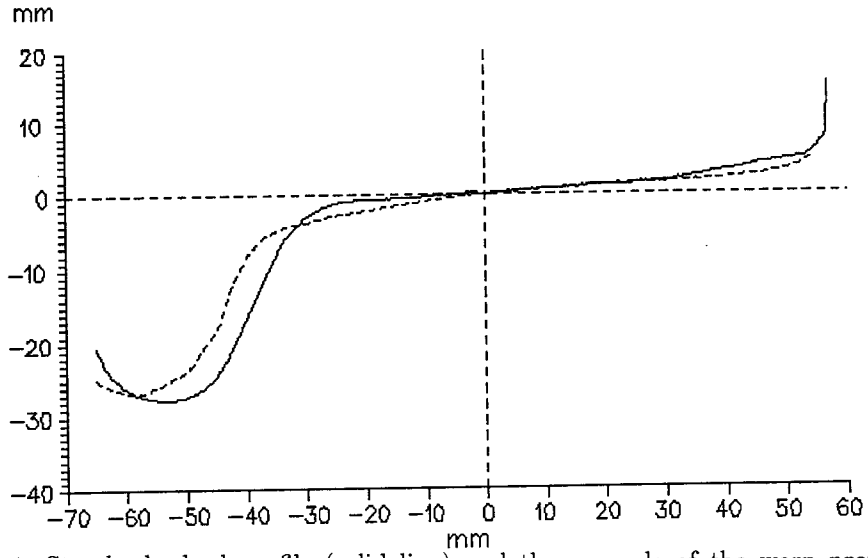

Fig. 4. Standard wheel profile (solid line) and the example of the worn profile (dashed line)

Then numerous calculations were carried out in order to clarify the circumstances of the accident. They were performed for four following combinations of anomalies:

- 'nominal case', i.e. the standard wheel profile and the 'good' track (the real track with average deflections was chosen as a 'good' one);
- the wheel profile from the derailed tank wagon and the 'good' track;
- the standard wheel profile and the track from the accident;
- combination of anomalies in the wheel profile and the track.

The influence of speed on the coefficient of stability for the first wheelset is shown in *Fig. 5.* The dependence of the maximum car body roll angle on the vehicle speed also was studied. The correspondent plots are shown in *Fig. 6.*

While analysing these plots one can draw a conclusion that the non-standard profile has decreased the dynamic performance of the wagon in comparison with the 'nominal case', and the qualitative behaviour of the 'parameter value vs speed' line has remained almost the same. The particular track geometry has caused the sufficient changes in this behaviour: the speed interval of 65 to 80 km/h has become a critical one, the most dangerous interval is 70 to 75 km/h. The combination of the anomalies has resulted in decrease of the stability coefficient much below the safe level.

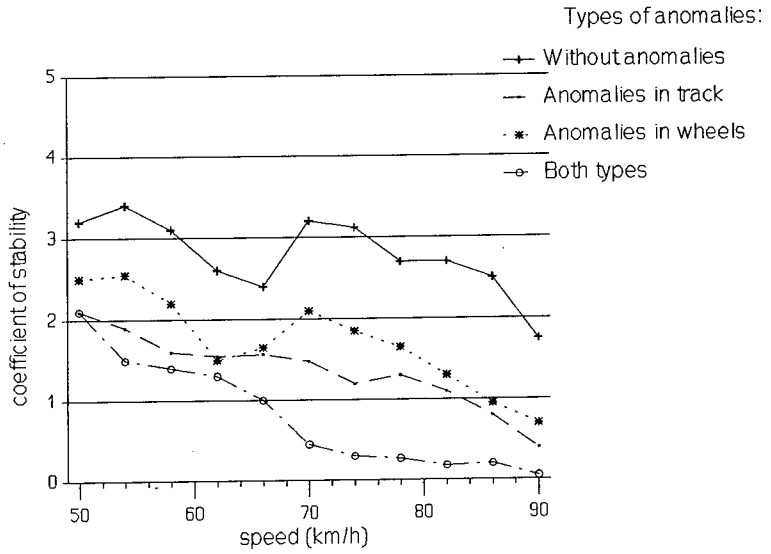

Fig. 5. Effect of speed on the coefficient of stability

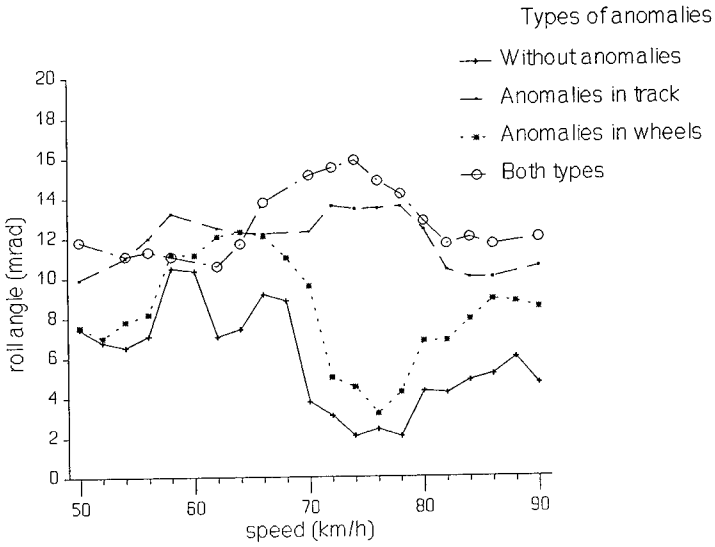

Fig. 6. Effect of speed on car body maximum roll angle

9. Conclusions

The created software package allows to simulate the behaviour of the four-axle freight wagon while travelling over the straight or curved track and to analyse therefore its dynamic performance. Existing of deflections from a nominal value in the parameters of the vehicle or track causes the deterioration of the performance as a rule. Thus, it becomes possible to determine the anomalies limits exceeding of which may cause a railway accident.

References

[1] BLOKHIN, E. P. – DANOVICH, V. D. – MOROZOV, N. I.: Matematicheskaya model prostranstvennych kolebaniy chetyriohosnogo relsovogo ekipazha (A Mathematical Model of the Spatial Vibrations of the Four-Axle Rail Vehicle, in Russian), TsNI-ITEI MPS, Dnepropetrovsk, 1986.

[2] CARTER, F. W.: On the Action of Locomotive Driving Wheel, *Proc. Royal Soc.*, Ser. A, Vol. 112, pp. 151–157, London, 1926.

[3] VLASOV, V. Z.: Balki, plity i obolochki na uprugom osnovanii (Beams, Slabs and Shells on an Elastic Foundation, in Russian), Fizmatgiz, Moscow, 1960.

[4] Otchet po eksperimentalnomu opredeleniyu nerovnostey, deistvuyushchih na chetyryohosnye gruzovye i passazhyrskiye vagony (Report on Experimental Determination of the Track Irregularities, Acting on the Four-Axle Freight and Passanger Wagons, in Russian), DIIT, Dnepropetrovsk, 1990.

[5] LAZARYAN, V. A.: Dinamika Vagonov (Dynamics of Wagons, in Russian), Transport, Moscow, 1964.

[6] GARG, V. K. – DUKKIPATI, R. V.: Dynamics of Railway Vehicle Systems, Academic Press, Toronto, 1984.

[7] Normy dla rascheta i proektirovaniya novych i moderniziruyemych vagonov dorog MPS kolei 1520 mm (Norms for the Calculation and Design of New and Modified Wagons for the MPS Railways with 1520 mm Gauge, in Russian), VNIIV-VNIIZhT, Moscow, 1983.

[8] VERIGO, M. F.: Dinamika vagonov (Dynamics of Wagons, in Russian), VZIIT, Moscow, 1970.

PERIODICA POLYTECHNICA SER. TRANSP. ENG. VOL. 23, NO. 1–2, PP. 63–72 (1995)

A NEW APPROACH TO THE SIMULATION OF RANDOM ROADS

Benno FELLENBERG and Stefan SCHERF

Westsächsische Hochschule Zwickau (FH)
FG Mathematik, PF 35
D 08001 Zwickau
Tel.: 00 49 375 536 2500
Fax: 00 49 375 536 2501

October 16, 1997

Abstract

The stochastic simulation of random road surfaces as well as of parallel tracks is considered. Starting from the spectral density

$$S(\alpha) = \frac{\sigma^2}{\pi} \frac{\gamma}{\gamma^2 + \alpha^2}\,; \quad \gamma > 0\,,$$

a fast simulation method is derived and demonstrated for the surfaces as well as their derivatives. Thereby the theory of weakly correlated functions supplies the theoretical background.

Keywords: stochastic simulation, random road surfaces, weakly correlated functions.

1. Introduction

Considering the influence of roads on the behaviour of vehicles the mathematical modelling results in differential equation systems containing the road surfaces and their derivatives as random excitations. In this paper we are concerned with a new simulation procedure of road surfaces. In the literature several principles and methods can be found for simulation and application in vehicle dynamics (cf. for instance [7], [8] [9]). We are especially interested in a more general method supplying a fast (on-line-) simulation procedure as well as the basis for a theoretical stochastic analysis.

Using the concept of weakly correlated functions VOM SCHEIDT and WÖHRL derived some approximate models of random road profiles (see [10]–[14]). In section 2 the main results of these approximations are summarized and analyzed for our purposes. Thereby we will see that these models are also suitable to get two correlated parallel tracks.

Subsequently in section 3 our simulation procedure is derived on the basis of the simulation of sufficiently smooth weakly correlated processes. Finally in section 4 some numerical results are given to show the usefulness and efficiency of the simulated realizations. Applications of this new

simulation to vehicle dynamics can be found in [3], [5] and [11]. A closed presentation of the simulation methods described in this paper, a comparison with theoretical results and also more concrete applications are included in [11].

2. Mathematical Models and Statistical Adaptation

Starting from the often used spectral density of road profiles f

$$S(\alpha) = \frac{\sigma^2}{\pi} \frac{\gamma}{\gamma^2 + \alpha^2}, \quad \gamma > 0, \tag{1}$$

with the corresponding correlation function

$$R(t) = \sigma^2 e^{-\gamma|t|} \tag{2}$$

an approximation of f is derived in WÖHRL [14] and VOM SCHEIDT; WÖHRL [12] in form of a linear functional

$$f(t,\omega) = \int_{-\infty}^{t} e^{-\gamma(t-s)} f_\varepsilon(s,\omega) ds, \tag{3}$$

where $f_\varepsilon(s,w)$ is a wide-sense stationary and weakly correlated process. Weakly correlated processes are random functions without 'distant effect' or functions of 'noise-natured character'. The exact definition and the resulting limit theorems or expansions of stochastic characteristics are given in [10]. Especially, their expectation function is zero, the correlation function of such processes has the form

$$\langle f_\varepsilon(s_1) f_\varepsilon(s_2) \rangle = \begin{cases} R_\varepsilon(s_1, s_2) & \text{for } |s_1 - s_2| \leq \varepsilon \\ 0 & \text{otherwise} \end{cases}$$

and the so-called intensity is in case of wide sense stationary processes defined by

$$a = \lim_{\varepsilon \downarrow 0} \frac{1}{\varepsilon} \int_{-\varepsilon}^{\varepsilon} R_\varepsilon(z) dz. \tag{4}$$

Then the following limit theorem

$$\lim_{\varepsilon \downarrow 0} \frac{1}{\varepsilon} \langle f(t_1) f(t_2) \rangle = \frac{a}{2\gamma} e^{-\gamma|t_2 - t_1|}$$

results in the approximation for small values of the correlation length $\varepsilon > 0$

$$\langle f(t_1) f(t_2) \rangle \approx \frac{a\varepsilon}{2\gamma} e^{-\gamma|t_2 - t_1|}, \tag{5}$$

which corresponds to the desired correlation function (2).

Whereas the original correlation function (2) is not differentiable, the approximation (3) is twice differentiable if f_ε is continuously differentiable for $\varepsilon > 0$. It follows

$$\begin{aligned} \dot{f}(t,\omega) &= f_\varepsilon(t,\omega) - \gamma \int_{-\infty}^{t} e^{-\gamma(t-s)} f_\varepsilon(s,\omega)ds \,, \\ \ddot{f}(t,\omega) &= \dot{f}_\varepsilon(t,\omega) - \gamma f_\varepsilon(t,\omega) + \gamma^2 \int_{-\infty}^{t} e^{-\gamma(t-s)} f_\varepsilon(s,\omega)ds \,. \end{aligned} \tag{6}$$

Because of the appearance of these explicit derivatives $\dot{f}_\varepsilon$ and $\ddot{f}_\varepsilon$ VOM SCHEIDT [10] introduced a smoothing function (polynomial) $Q_0(t,\delta)$ depending on the parameter $\delta > 0$ and having the properties $Q_0(0,\delta) = Q_0'(0,\delta) = 0$. Putting

$$f(t,\omega) = \int_{-\infty}^{t} Q(t-s,\delta) f_\varepsilon(s,\omega)ds \,,$$

where $Q(t-s,\delta) = Q_0(t-s,\delta)e^{-\gamma(t-s)}$, the approximation corresponding to the correlation function (3)

$$\langle f(t_1)f(t_2)\rangle \approx \frac{a\varepsilon}{2\gamma} e^{-\gamma|t_2-t_1|}$$

is true if $\delta \downarrow 0$. Here we have only linear functionals of f_ε

$$f^{(k)}(t,\omega) = \int_{-\infty}^{t} Q^{(k)}(t-s) f_\varepsilon(s,\omega)ds \,, \quad k = 0,1,2$$

as derivatives. This second model is especially advantageous for the theoretical stochastic analysis of random vibration systems (cf. for instance [10], [11] and [13]). In our former papers (cf. [1], [2]) we also used this model. But, it needs some special efforts with respect to the numerical calculations because of the structure of the smoothing function Q_0. Therefore, we use now the first model (3) to derive a quicker simulation procedure. To this end we need in (6) also simulations of differentiable weakly correlated processes. In section 3 the resulting procedure is given.

After modelling the random road profile as linear functional (3) and subsequently its derivatives by (6) the next problem is to specify the model

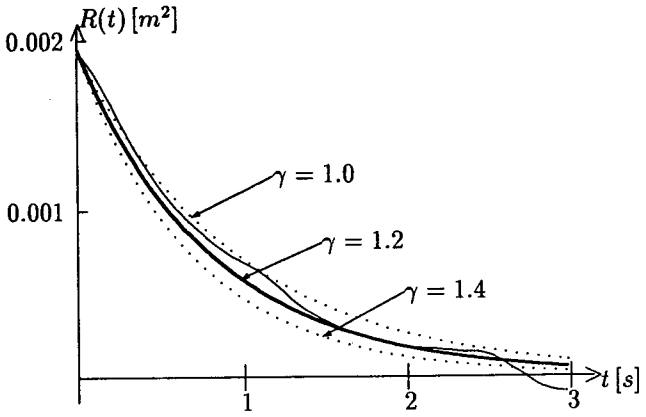

Fig. 1. Adaptation of the scale parameter

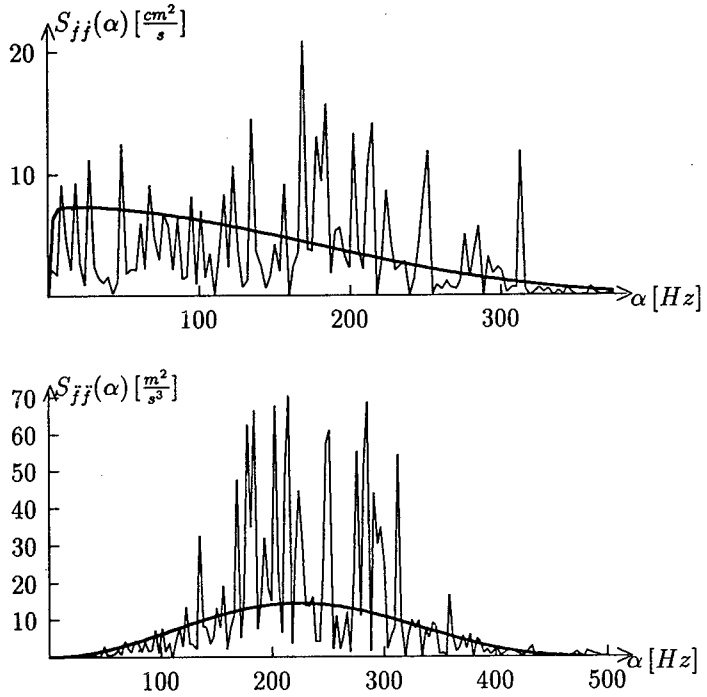

Fig. 2. Estimated and adapted spectral densities

parameters γ, ε and a by comparisons with statistical estimates from measurements of real roads. This can be carried out by means of an interactive procedure. Firstly, the scale parameter γ is adapted by consideration of the correlation function $R(t)$ (see *Fig. 1*).

Secondly, the correlation length ε is determined by calculating the theoretical spectral densities of the 1^{st} and 2^{nd} derivative

$$S_{\dot{f}\dot{f}}(\alpha) = S_{f_\varepsilon f_\varepsilon}(\alpha) - \frac{\varepsilon a}{2\pi}\frac{\gamma^2}{\gamma^2+\alpha^2},$$

$$S_{\ddot{f}\ddot{f}}(\alpha) = (\alpha^2-\gamma^2)S_{f_\varepsilon f_\varepsilon}(\alpha) + \frac{\varepsilon a}{2\pi}\frac{\gamma^4}{\gamma^2+\alpha^2}$$

and comparing them with the estimates of the measured road. The final result is plotted in *Fig. 2*.

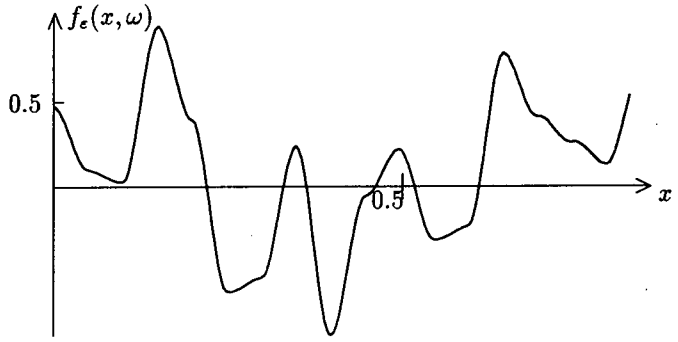

Fig. 3. Realization of a differentiable weakly correlated process

After all, the intensity is calculated from relations (2) and (5) by $a = 2\hat{\sigma}^2\gamma/\varepsilon$, where $\hat{\sigma}^2$ denotes the estimated dispersion of the measured road.

The mathematical models can be extended to considerations of two parallel tracks using methods described e.g. in PARKHILOVSKII [6] and SCHIEHLEN [8]. Taking into account the concepts mentioned above two correlated excitations (tracks) $f_L(t,\omega)$ and $f_R(t,\omega)$ with distance b and an orthotrop behaviour, i.e.

$$R_{f_L f_R}(t_1,t_2) = \langle f_L(t_1) f_R(t_2)\rangle = \sigma^2 e^{-\gamma(|b|+|t_2-t_1|)},$$

can be derived. They have again the form of linear functionals

$$f_L(t,\omega) = \int_{-\infty}^{t} e^{-\gamma(t-s)}[f_{1\varepsilon}(s,\omega) + f_{2\varepsilon}(s,\omega)]ds,$$

$$f_R(t,\omega) = \int_{-\infty}^{t} e^{-\gamma(t-s)}[f_{1\varepsilon}(s,\omega) - f_{2\varepsilon}(s,\omega)]ds$$

with independent weakly correlated processes $f_{1\varepsilon}(s,\omega)$ and $f_{2\varepsilon}(s,\omega)$. The derivation and some further considerations with respect to the coherence function can be found in [2] and [11].

3. Simulation Procedure

Now we turn to the simulation of the mathematical models (3) and (6). First of all, the simulation of a differentiable weakly correlated process $f_\varepsilon(s,\omega)$ is given. Thereby, a bounded domain $s \in [\alpha,\beta]$ of interest is decomposed into n intervals $[a_i, a_{i+1}]$ with length $h = (\beta - \alpha)/n$ and $a_i = \alpha + ih$, $i = 0,1,\ldots,n$. Further $\{\xi_i(w)\}_i$ and $\{\overline{\xi}_i(w)\}_i$, $i = 0,1,\ldots,n$, denote two sets of independent, identically distributed random variables with $< \xi_i >= < \overline{\xi}_i >= 0$ and $< \xi_i^2 >= \sigma_\xi^2$ for all i.

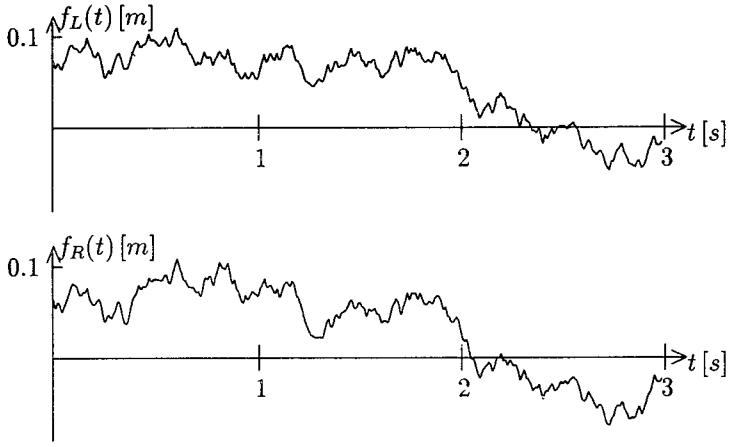

Fig. 4. Simulation of two tracks

Setting

$$\begin{aligned} f_\varepsilon(s,\omega) &= g_i(s,\omega) \\ &= p_i(s-a_i)^3 + q_i(s-a_i)^2 + u_i(s-a_i) + v_i \end{aligned} \tag{7}$$

for $s \in [a_i, a_{i+1}]$ and demanding

$$\begin{aligned} g_i(a_i) &= \xi_i\,, & g_i(a_{i+1}) &= \xi_{i+1}\,, \\ \dot{g}_i(a_i) &= \overline{\xi}_i\,, & \dot{g}_i(a_{i+1}) &= \overline{\xi}_{i+1} \end{aligned}$$

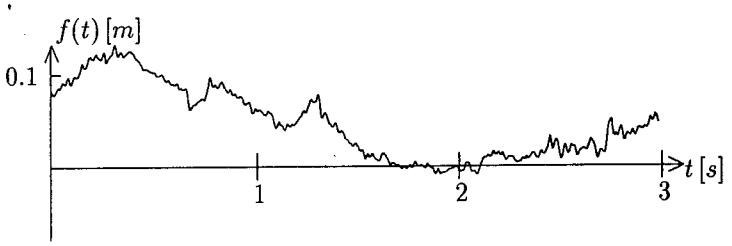

Fig. 5. Measured profile

the coefficients in (7) are determined by

$$\begin{aligned} p_i &= \frac{2(\xi_i - \xi_{i+1}) + (\bar{\xi}_i + \bar{\xi}_{i+1})h}{h^3}, \\ q_i &= \frac{3(\xi_{i+1} - \xi_i) + (2\bar{\xi}_i + \bar{\xi}_{i+1})h}{h^2}, \\ u_i &= \bar{\xi}_i \quad \text{and} \quad v_i = \xi_i . \end{aligned}$$

In consequence of the independence of the random variables ξ_i and $\bar{\xi}_i$ the so defined process f_ε is weakly correlated with correlation length $\varepsilon = 2h$. Its intensity can be determined by $a = \sigma_\xi^2/2$, i.e. the intensity depends only on the stochastic behaviour of ξ. Hence, a simulation of a differentiable weakly correlated process can be obtained by simulation of the random variables ξ_i and $\bar{\xi}_i$. In *Fig. 3* a realization of such a simulation is drawn with $\varepsilon = 0.1$.

Now we consider the simulation of the approximation of f, $\dot{f}$ and $\ddot{f}$ according to (3) and (6). To this end, we need the determination of the integral or linear functional, respectively. Firstly, we separate this integral

$$f(t,\omega) = \int_{-\infty}^{\alpha} e^{-\gamma(t-s)} f_\varepsilon(s,\omega)ds + \int_{\alpha}^{t} e^{-\gamma(t-s)} f_\varepsilon(s,\omega)ds ,$$

where α has to be chosen such that the first integral is neglectably small. There are possibilities to support this choice by some mathematical estimates. Secondly, the integral over $[\alpha, t]$ is determined by

$$\int_{\alpha}^{t} e^{-\gamma(t-s)} f_\varepsilon(s,\omega)ds = \sum_{i=0}^{n_t-1} \int_{a_i}^{a_{i+1}} e^{-\gamma(t-s)} g_i(s)ds + \int_{a_{n_t}}^{t} e^{-\gamma(t-s)} g_{n_t}(s)ds$$

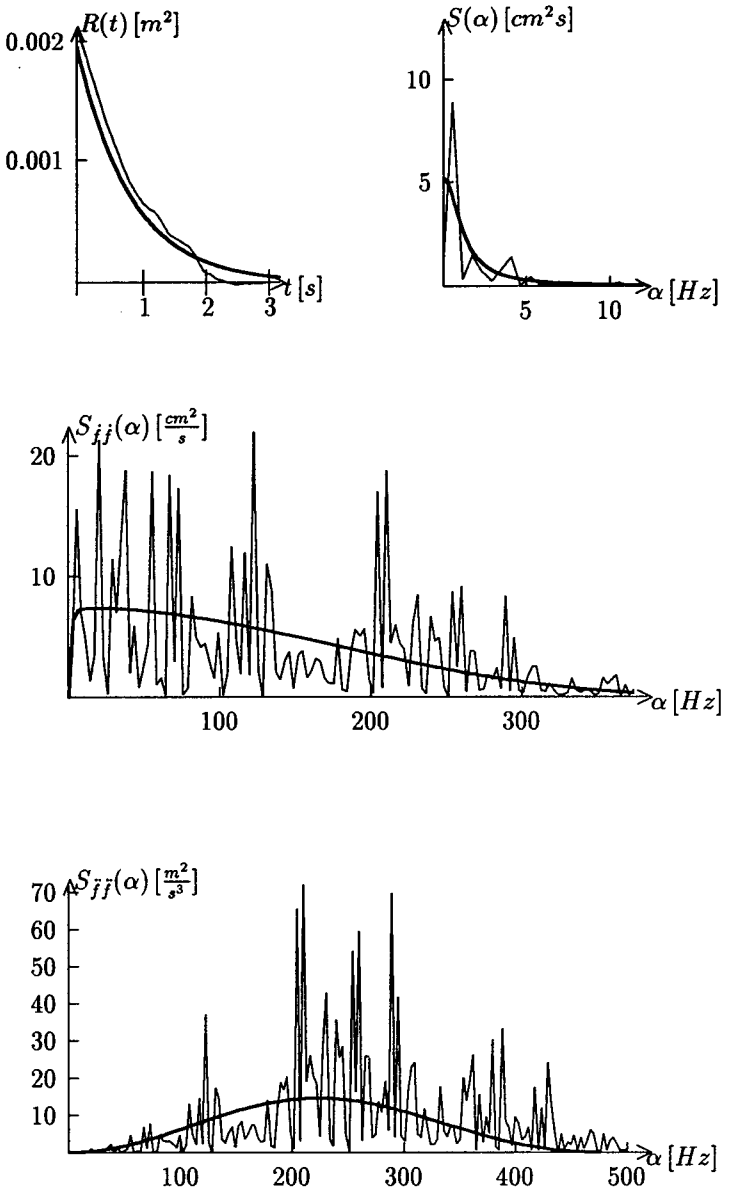

Fig. 6. Estimated and adapted correlation function and spectral densities

with $n_t = \text{entier}\,[(t-\alpha)/h]$. Some straightforward calculations lead to

$$f(t,\omega) \approx \int_{\alpha}^{t} e^{-\gamma(t-s)} f_{\varepsilon}(s,\omega)ds = \sum_{i=0}^{n_t-1} c_i e^{-\gamma(t-a_i)} + c_{n_t}(t) e^{-\gamma(t-a_{n_t})}, \quad (8)$$

where

$$c_i = e^{\gamma h}\left[p_i\left(\frac{h^3}{\gamma} - \frac{3h^2}{\gamma^2} + \frac{6h}{\gamma^3} - \frac{6}{\gamma^4}\right) + q_i\left(\frac{h^2}{\gamma} - \frac{2h}{\gamma^2} + \frac{2}{\gamma^3}\right) + u_i\left(\frac{h}{\gamma} - \frac{1}{\gamma^2}\right) + v_i\frac{1}{\gamma}\right] + \left[\frac{6p_i}{\gamma^4} - \frac{2q_i}{\gamma^3} + \frac{u_i}{\gamma^2} - \frac{v_i}{\gamma}\right]$$

and $c_{n_t}(t)$ corresponds to c_i if h is substituted by $t - a_{n_t}$.

4. Numerical Simulation

Finally we present some concrete simulation results. According to a realized adaptation the values $\gamma = 1.2$, $\varepsilon = 0.021$ and $a = 0.222$ are chosen. To demonstrate two parallel tracks the distance b is put $b = 0.0675$ s which corresponds to 1.5 m ($v = 80$ km/h). In the *Fig. 4* the simulated profiles $f_L(t)$ and $f_R(t)$ are drawn and in *Fig. 5* the measured profile $f(t)$ is drawn for a visual comparison.

A good coincidence can also be stated investigating the characteristics of the simulated profile. In *Fig 6* the estimated correlation function and spectral densities of the simulated profiles are drawn in comparison with the adapted characteristics.

References

[1] DRESCHER, G. – FELLENBERG, B. (1992): Simulation of Weakly Correlated Fields with an Application to Vehicle Dynamics. *Math. Comput. Simulation*, Vol. 34, pp. 397–409.

[2] DRESCHER, G. – FELLENBERG, B. – VOM SCHEIDT, J. (1993): Simulation of Random Functions for Application to Dynamic Systems. *Dynamic Systems and Applications*, Vol. 2, No. 2, pp. 275–289.

[3] FELLENBERG, B.: Simulation and Statistical Analysis of Random Vibration Systems. Submitted to *Bull. Appl. Math.*

[4] FELLENBERG, B. – VOM SCHEIDT, J. (1990): Random Boundary-Initial-Value-Problems for Parabolic Differential Equations – Analytical and Simulation Results. *Periodica Polytechnica (Transportation Engineering)*, Vol. 18, No. 1–2, pp. 23–32.

[5] FELLENBERG, B. – vom SCHEIDT, J. – WÖHRL, U. (1994): Simulation and Analysis of Random Vibration Systems. *Abstracts of the* 8^{th} *Conference of the European Consortium for Mathematics in Industry*, Universität Kaiserslautern, pp. 294–296.

[6] PARKHILOVSKII, I. G.: Investigations of the Probability Characteristics of the Surfaces of Distributed Types of Roads. *Avtom. Prom.*, Vol. 8, pp. 18–22.

[7] PELLEGRINO, E. – TORNAD, U. (1987): A Mathematical Model of Road Excitation. *ECMI 4, Road-Vehicle-Systems and Related Mathematics*, Band 6 (ed. by H. Neunzert), B. G. Teubner, Stuttgart, pp. 7–28.

[8] SCHIEHLEN, W. O. (1988): Modelling, Analysis and Estimation of Vehicle Systems. Analysis and Estimation of Stochastic Mechanical Systems (ed. by W.O. Schiehlen; K. Wedig), *CISM Courses and Lectures* No. 303, International Centre for Mechanical Sciences, Springer Verlag, Wien, New York.

[9] SCHMIDT, H. (1987): Some Examples and Problems of Application of Nonparametric Correlation and Spectral Analysis. *ECMI 4, Road-Vehicle-Systems and Related Mathematics*, Band 6 (ed. by H. Neunzert), B. G. Teubner, Stuttgart, pp. 171–193.

[10] VOM SCHEIDT, J. (1990): Stochastic Equations of Mathematical Physics. Akademie-Verlag, Berlin.

[11] vom SCHEIDT, J. – FELLENBERG, B. – WÖHRL, U. (1994): Analyse und Simulation stochastischer Schwingungssysteme. B. G. Teubner, Stuttgart 1994 (Leitfäden der angewandten Mathematik und Mechanik, Bd. 71).

[12] vom SCHEIDT, J. – WÖHRL, U. (1989): Vehicle Vibration Excited by Random Road Surfaces. *Bulletins for Applied Mathematics*, Vol. 624, pp. 84–94.

[13] VOM SCHEIDT, J. – WÖHRL, U. – WULFF, S. (1992): A Method for the Numerical Treatment of Nonlinear Stochastic Vibrations of Vehicles. *Dynamic Systems and Applications*, Vol. 1, pp. 187–204.

[14] WÖHRL, U. (1986): Approximation von Fahrbahnunebenheiten. *Wiss. Berichte der 2. Tagung Stochastische Analysis*, Zwickau, pp. 177–180.

PERIODICA POLYTECHNICA SER. TRANSP. ENG. VOL. 23, NO. 1-2, PP. 73-87 (1995)

FRACTAL DIMENSIONS IN NON-LINEAR SYSTEM DYNAMICS OF REALITY

Francis FAZEKAS

Mathematical Department of Transportation Faculty
Technical University of Budapest
H-1521 Budapest, Hungary

Received: November 9, 1994

Abstract

This paper treats a) the s.c. 'capacity' and 'alternate' fractal dimensions (fr.dim.), b) together with numerous illustrating examples of geometry, nature and modern arts, c) basin boundaries being often fr.dim, d) finally recent 'control algorithms' for reducing chaotic motions into periodic ones.

Keywords: capacity, pointwise, correlation, information, Ljapunov fr.dim.; fr.basin boundaries, control algorithms.

1. Preliminary Remarks

1.1 Since approx. 3 centuries, the study of a *dynamical system* (dS) given by the *differential equation* (DE), mainly *linear* (lin.) ones and initial date

$$m\ddot{x} = f(x, \dot{x}, t) \; ; \quad x(t_0) = x_0 \; , \quad \dot{x}(t_0) = v_0$$

had performed the classical task: *to predict the motion* (as 'history') of S far into the future, using some counting device. In our century, the (electric, later electronic) computers had brought greater possibilities for such far prediction.

However, in the last 1–2 decades, certain exact sciences (e.g. fluid, then solid mechanics, later electric, electronic, physical-mathematical-technical etc. branches, too) had discovered special, s.c. *chaotic motions* (Ch-m) *in non-linear* (nlin.) dS, which *cannot* be predicted generally into the far future and exiges also new concepts, ideas, theories and methods. It became obvious till now, that α) the Ch-m can appear in all nlin.dS, β) it opened a new age in the dynamics and γ) brought a type of revolution into the exact sciences [2], [6].

1.2 Be characterized shortly the **class of Ch-m** in (deterministic) *nlin.dS*! – a) The motion of nlin.dS α) – e.g. over a value δ of control parameter (e.g. the frictional one $\delta = c/\omega$) – can be *regular* (vibration with period T, tendig at $t \to \infty$ e.g. to a stable limit cycle (LC) $\hat{G}_T(\hat{\varrho}_0)$; then β) – under the values of a certain sequence $\delta_1 > \delta_2 > \ldots \delta_n > \delta_\infty$ – the sequential *bifurcations*

$\hat{\varrho} \to \hat{\varrho}_i \to \hat{\varrho}_j \to \hat{\varrho}_q$ (1; $i = 1,2$; $j = i+2,\ldots$; $q = 2^{n-2}+2$) and stable *period-duplications* $\hat{G}_T \to \hat{G}_{2T} \to \hat{G}_{2^2T} \to \hat{G}_{2^nT}$ happen; finally γ) – under a heaping value $\delta_\infty > \delta$ – the asymptotic motion on the LC $\hat{G}_{2^nT}$ becomes an *irregular* (aperiodical), s.c. **chaotic** one; its trajectories are contracted to a funny (strange) attractor, on which the points jump irregularly; consequ. the *prediction* of this Ch-m appears totally *impossible* (practically, already for $n > N$). (This is the very frequent FEINGENBAUM way toward the Ch., but also other ways exist, too (see in [3]). In other words, the approaching way α)-β) can be qualified as a *deterministic input* of Ch-m (without random or unpredictable inputs and parameters), over δ_1 with T periodic, then under $\delta_1 > \ldots > \delta_n$ with $2T,\ldots,2^nT$ periodic vibration, which **transits** on the final way γ) under δ_∞ into a *stochastic output* of Ch-m, under δ_∞ with an aperiodic, irregular jumping on a funny attractor. [Obviously, the Ch-m is not a random motion (as e.g. the BROWNIAN one) with only statistically measured parameters and truly without input data]. – b) A Ch-m is very *sensitive to* the *initial conditions* (IC), that is small differences in the IC can produce very great (enormous) divergencies in the final phenomena. – c) It bears a *loss of information* about IC, when the uncertainty $dA_0 = dx_0^2$ at time $t_0 = 0$ (in regular S) grows during t exponentially to $dA_t = dA_0 e^{ht}$ (in ch.S). – d) Its consequence $h = \frac{1}{t} \ln \frac{dA_t}{dA_0}$ is related (through the entropy) to the s.c. LJAPUNOV *exponent* (see in [2], [3]) measuring the divergency of trajectories in the phase plane $(x, \dot{x}, t)$. – e) Searching for the geometry of the (irregular become, s.c.) Ch-m, the s.c. '*strange attractor*' (Str-att) appears, as unusual (maze-like, multisheeted) structure in the phase space. – f) It is often measured by *fractal dimension* (fr.dim.). – g) A cross section of Str-att produced by the s.c. POINCARÉ *map* (Pc-map) a thread-like set of points shows also fr. properties. – h) The transition between *basin* of ch. and periodic motions in IC or parameter space is often qualified as *fr. basin boundary.*

1.3 Such and other properties of Ch-m were treated in detail in our papers [6]-[7] and mainly in our series of papers [3] (recommended also for postgraduate students and doctorands, too), therefore it is unnecessary to repeat them now. Obviously, it will be here sufficient to recall shortly the basic facts, notions, methods, etc., which are in a relation near enough with the fractal lines, dimensions, basin boundaries, etc. So they can help to fit – in this long 'fr. chapter' – into the mentioned series, (which has given till now only short information about the HAUSDORFF's definition).

2. Definition of the 'Capacity' as Fractal Dimension (Fr.Dim.)

2.1 A very intuitive (geometric) measure for the dimension of a set of points has been introduced by HAUSDORFF (7/4, [3], [5]). This is a general definition, which can furnish – occasionally – a fr. number, as the dimension

of the examined set, so it is suitable to classify the POINCARÉ map of numerous nlin. systems giving quantitative measure for the fr. properties of their Str-att. – We describe now the HAUSDORFF's *definition of the s.c. 'capacity'*, but later we will mention some other definition given e.g. by MANDELBROT, FARMER, etc.

2.2 Let us observe now a *set* S_d of points in the (integer) n-dimensional *space* S^n ($\supset S_d$), e.g. a uniform distribution of N_0 points a) along some $d = 1$ dim. (plane or space) curve G_1 in the space S^3, or b) N_0 uniformly distributed points on some $d = 2$ dim. surface $F_2 \subset S^3$. Then we try to *cover* this set of points with small n ($= 3$) dim. cubes of side $\varepsilon > 0$ (or spheres of radius $\varepsilon > 0$), namely using such covering cubes in minimal number $N(\varepsilon) < N_0$. If N_0 is large enough, then $N(\varepsilon)$ will scale for $d = 1, 2$ and for arbitrary d ($\leq n$) dim. – intuitively and approximately – as

$$N(\varepsilon) \approx 1/\varepsilon\,, \tag{1}$$

$$N(\varepsilon) \approx 1/\varepsilon^2\,, \tag{2}$$

$$N(\varepsilon) \approx 1/\varepsilon^d = (1/\varepsilon)^d \quad (\varepsilon, d > 0)\,. \tag{3}$$

There is expected a limit behaviour

$$N(\varepsilon) \approx (1/\varepsilon)^d \to +\infty \quad \text{at} \quad \varepsilon \to +0\,, \tag{4}$$

namely faster at larger $d > 0$ (connected with the information on G_1, F_2 and S_d's spatial placing, at increased accuracy for $\varepsilon \to +0$). The *Eqs.* (3)[1]–(4) show a natural way to the approaching value d got explicitly by logarithm of both sides:

$$\ln N(\varepsilon) \approx d \cdot \ln(1/\varepsilon)\,, \tag{5}$$

$$d \approx \ln N(\varepsilon)/\ln(1/\varepsilon)\,, \tag{6}$$

then to the exact value d_c (referring with a subscript to the name 'capacity') *defined* by the limit formula:

$$d_c = \lim_{\varepsilon \to +0} \frac{\ln N(\varepsilon)}{\ln(1/\varepsilon)}\,, \quad \text{with implicit requirement} \quad N_0 > N(\varepsilon) \to +\infty\,. \tag{7}$$

It gives in simple cases the usual *integer* dim. d ($= 1, 2, 3, \ldots$) (see the examples 1a–1c); but it furnishes in numerous chaotic cases non-integer = fraction result, sc. *fractal* dim. (see the examples 2–3).

2.3 Look at some simple, then complicated examples to calculate exactly the integer or fractal dim. of a set of points on a curve or surface.

1/a) Linear distribution points:

$$d = \ln N(\varepsilon)/\ln(1/\varepsilon) = \ln 10/\ln(1/0,1) = 1 \ldots\ldots \quad \text{(int.dim.)}\,.$$

[1] One can write more fully: $N(\varepsilon) \approx C(1/\varepsilon)^d$, but the limit $\varepsilon \to +0$ on $d \approx [\ln N(\varepsilon) + \ln C]/\ln(1/\varepsilon)$ makes disappear the term of C.

1/b) Linear distribution on a curve:

$$d = \ln N(\varepsilon)/\ln(1/\varepsilon) = \ln 10/\ln 10 = 1\ldots \quad \text{(int.dim.)}\,.$$

Fig. 1.

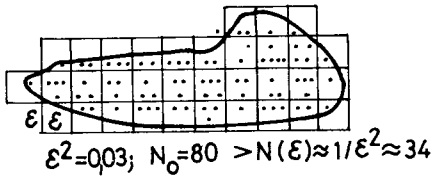

Fig. 2.

1/c) Planar distribution of points:

$$d = \ln N(\varepsilon)/\ln(1\varepsilon) = \ln 34/\ln 33^{\frac{1}{2}} =$$

$$= 2\cdot \ln 34/\ln 33 \approx 2\ldots \quad \text{(int.dim)}.$$

There was a sole step of the covering with a unique ε^2; it can be continued (with finer ε^2), expecting a better approach to 2 (*Fig. 3*).

2) KOCH *curve* (1904) treated in MANDELBROT's book (1977). The **increasing** geometric procedure α) sets out from an interval G_0 of length $L_0 = \varepsilon_0 = 1$, β) divides it into 3 segments of length $\varepsilon_1 = 1/3$ and γ) replaces the middle one by 2 segments of similar length 1/3; the new curve G_1 of $N_1 = 4$ sides has obviously the total length $L_1 = N_1\varepsilon_1 = 4/3$. The continuation happens by repeating of the former triple-step S_3 $(\alpha - \gamma)$ for all the 4 sides, namely the n^{th} S_3 results $N_n = 4^n$ segments of length $\varepsilon_n = (1/3)^n$ with the total length $L_n \triangleq N_n\varepsilon_n = (4/3)^n$. Tending $n \to +\infty$, so $G_n \to G$, $\varepsilon_n \to +0$, $N_n \to +\infty$ and $L_n = N_n\varepsilon_n \to +\infty$, then

$$d_c = \lim_{n\to\infty} \frac{\ln N_n}{\ln(1/\varepsilon_n)} = \lim_{n\to\infty} \frac{\ln 4}{\ln 3} = 1.26185\ldots \quad \text{(fr.dim.)}$$

and the fractional line G_n of N_n segments – looking fuzzy – becomes a continuous, but nowhere differentiable limit curve G (*Fig. 4*). This set of points $G_n \to G$ of dim. $d_c \approx 1.26$ appears as trying to cover more than a line, but reaching to fulfill less than an area only, having nevertheless some properties of area, as a young boy's scribbling with

coloured crayons on a piece of sidewalk. – We will find such fractal – like structures for basin boundaries of periodic attractors (see e.g. [5] p. 244) and for boundaries between periodic and Ch-m (see e.g. here, p.12) therefore this KOCH curve is very important for the nlin. dynamics.

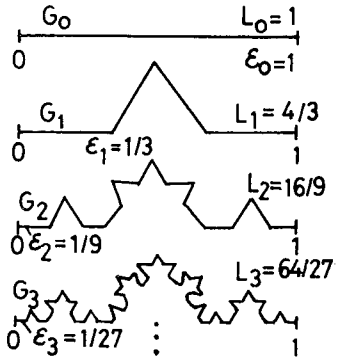

Fig. 3.

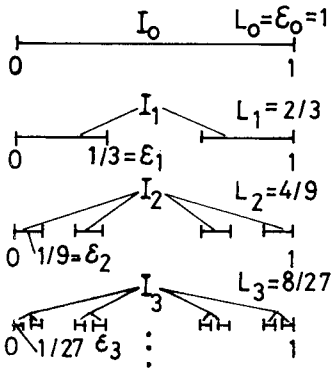

Fig. 4.

3) CANTOR *set* (discovered in 1883) can be produced by a **decreasing** geometric process. Namely, this also very significant concept for nlin. systems can be origined by repeated removing finer and finer pieces from the initial line (counter KOCH curve, by repeated complementing smaller and smaller segments to the initial interval). – The construction's procedure begins with a triple-step S_3: α) to take an interval I_0 of length $L_0 = \varepsilon_0 = 1$, β) to divide it into 3 parts of length $\varepsilon_1 = 1/3$ and γ) to omit the middle one and to keep the remaining $N_1 = 2$ parts as union I_1 with total length $L_1 = N_1\varepsilon_1 = 2/3$. – Continuation by repeating of S_3; after the n^{th} S_3, there is the remaining I_n with $N_n = 2^n$ segments of length $\varepsilon_n = (1/3)^n$ and total length

$L_n \overset{\wedge}{=} N_n\varepsilon_n = (2/3)^n$ (*Fig. 5*). At $n \to +\infty$, these limits appear: $I_n \to I$, $\varepsilon \to +0$, $N_n \to +\infty$, $L_n \to +0$, then

$$d_c = \lim_{n\to\infty} \frac{\ln N_n}{\ln(1/\varepsilon_n)} = \lim_{n\to\infty} \frac{n\ln 2}{\ln 2} = \frac{\ln 2}{\ln 3} = 0.63092\ldots \quad \text{(fr.dim.)}$$

Consequently, the infinite point-series I of dim $d_c = 0.63\ldots$ shows itself more, than a point (of dim. 0), but less than a line (of dim.1). On this discontinuous fr. set, one can generate a continuous fr. function, namely by integrating a distribution function of the total unit mass at the start on the total interval I_0, later on the remaining and decreasing CANTOR intervals $I_1, \ldots, I_n$, with increasing mass density. After the n^{th} step, when I_n consists of $N_n = 2^n$ parts of length $\varepsilon_n = (1/3)^n$, the density is $\varrho_n = (3/2)^n \overset{\wedge}{=} c_n$ for all the $N_n\varepsilon_n$-segments (obviously: $L_n\varrho_n \overset{\wedge}{=} N_n\varepsilon_n \cdot \varrho_n = 2^n(1/3)^n = 1$ total mass) and $\overset{\circ}{\varrho}_n = 0$ for all omitted (vacant) segments of $\overset{\circ}{I}_n$ $(\varepsilon_1, 2\varepsilon_2, \ldots, 2^n\varepsilon_n$; $\overset{\circ}{L}_n = \frac{1}{3}\frac{1-(2/3)^n}{1-2/3} = 1-(2/3)^n$; $L_n+\overset{\circ}{L}_n = (2/3)^n+[1-(2/3)^n] = 1 \overset{\wedge}{=} L_0)$. The mass on the interval $I_x = [0, x]$ at $x \in \overset{\circ}{I}_n$ will be calculated by integration

$$M_n(x) \overset{\wedge}{=} \int_0^x \varrho_n(\xi)d\xi = L'_n\varrho_n = N'\varepsilon_n\varrho_n = 2^\nu \cdot (1/2)^n = (1/2)^{n-\nu}$$

at $N' \overset{\wedge}{=} 2^\nu < 2^n \overset{\wedge}{=} N_n$, but at $\nu = n$ one has $M_n(1) = 2^n(1/2)^n = 1$ (*Fig. 6*).

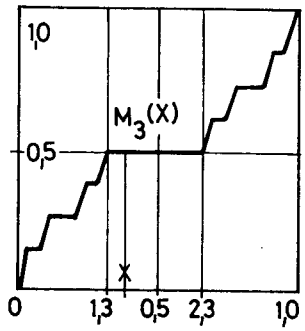

Fig. 5.

Its figure is a fractional, but continuous line consisting of oblique (increasing with $\tan\varphi = (3/2)^n$) and horizontal segments. – The limit curve at $n \to +\infty$ is the s.c. 'devil's staircase' $M(x)$ having $M'(x) = \varrho(x)\sum_{i=1}^{\infty}\delta(x-\xi_i)$.

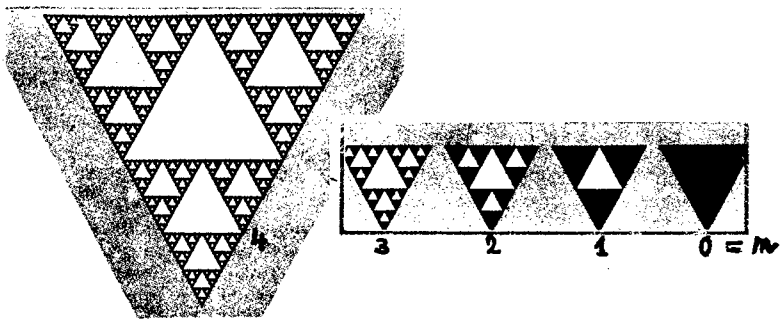

Fig. 6.

4) '**Decreasing**' triangular set: $T_0 = \frac{\sqrt{3}}{4}$, $T_1 = \frac{3}{4}T_0$, $T_2 = \frac{9}{16}T_0, \ldots$, $T_n = \left(\frac{3}{4}\right)^n$; $\varepsilon_n = (1/2)^n$, $N_n = 3^n$; $d_c = \ln 3/\ln 12 = 1{,}5737, \ldots$ (*Fig. 7*).

3. Alternate Definitions for the Fr.Dim.

3.1 The earlier introduced *capacity* d_c to measure the fr.dim. of Str-atts is a geometric metric (considering – without the frequency of orbit – the covering set of cubes or balls in phase space), but also a numeric one (counting the mentioned covering process often by computer). – The following alternate definitions – giving for many Str-atts roughly the same dim. – will be good controllers for the capacity d_c [5].

3.2 Pointwise dim. (Pw-dim.) On a long-time trajectory in phase space, we sign time-sampled points of motion in large number N_0, then place a sphere of measure r at some point ϱ_i of orbit and count the points in it: $N(r)$. The proportion $P(r, \varrho_i) = N(r, \varrho_i)/N_0$ gives us the (combinatorial) probability of finding a point in this sphere (from N_0 ones). – For a 1-dim. (closed periodic) orbit will be (at $r \to 0$, $N_0 \to \infty$): $P(r, \varrho_i) \approx br$; for a 2-dim. (toroidal, quasiperiodic) orbit: $P(r, \varrho_i) \approx br^2$; for a general case: $P(r, \varrho_i) \approx br^{d_p}$, consequ. [5]

$$\frac{\ln P}{\ln r} - \frac{\ln b}{\ln r} \approx d_p\,, \quad \text{finally} \quad d_p = \lim_{r \to 0} \frac{\ln P(r, \varrho_i)}{\ln r}\,. \tag{8}$$

For some attractor, d_p is independent of ϱ_i; but generally $d_p = d_p(\varrho_i)$, when it is suitable to count an *averaged Pw-dim.* on the randomly chosen set of points $\varrho_1, \ldots, \varrho_i, \ldots, \varrho_M$ at $M \ll N_0$ (e.g. distributed around the Str-att):

$$\frac{1}{M}\sum_{i=1}^{M} P(r, \varrho_i) \approx ar^{d_p}\,, \quad \ln \frac{1}{M}\sum_{i=1}^{M} P(r, \varrho_i) - \ln a \approx d_p \cdot \ln r\,,$$

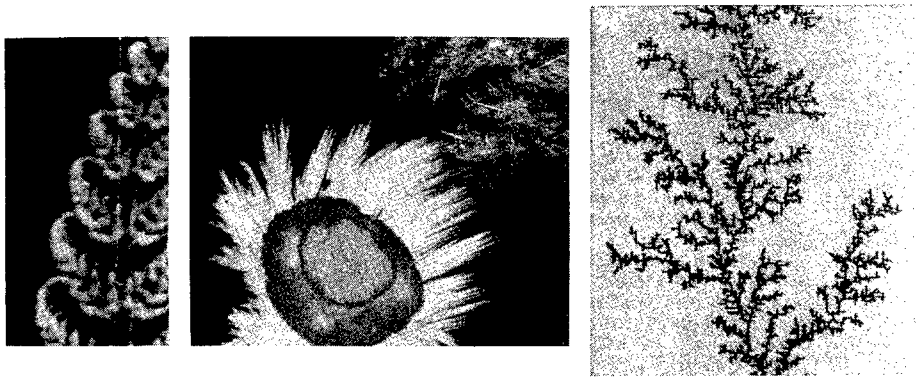

Fig. 7.

$$d_p = \lim_{r\to 0} \frac{\ln\left[\sum_i P(r, \varrho_i)/M\right]}{\ln r} \,. \tag{9}$$

Practically, at $N_0 \approx 10^3 \sim 10^4$, one use $M \approx 10^2 \sim 10^3$.

3.3 Correlation dim. (Cr-dim.). It is used successfully since 1983, mainly by experimentalists, they find it often as related to the Pw-dim.

We discretize the (continuous) set to one of N points $\{\hat{\varrho}_i\}_N$ in the phase space, then count the distances $s_{ij} = |\hat{\varrho}_i - \hat{\varrho}_j| \stackrel{\wedge}{=} \left[\sum_k (x_{ki} - x_{kj})^2\right]^{1/2}$ (or $s_{ij} = \sum_k |x_{ki} - x_{kj}|$) for the Cr-function [5]

$$C(r) = \lim_{N\to\infty} \frac{1}{N^2} \cdot \begin{pmatrix} \text{number of pairs } i,j \\ \text{with distances } s_{ij} < r \end{pmatrix} = \lim_{N\to\infty} \frac{1}{N^2} \cdot \sum_{i=1}^{N} \sum_{j=1}^{N} 1(r - s_{ij}) \,,$$

that is the number of points ϱ_j in each sphere of centre ϱ_i and radius r (where the unit spring function $1(r - s_{ij}) = \begin{cases} 1 & \text{at} \quad r > s_{ij} \\ 0 & \text{at} \quad r < s_{ij} \end{cases}$; the sum is performed here about every point, but at the Pw-dim. about $M \ll N_0$ ones only). For many Str-att, one can find a power law (for $r \to 0$)

$$C(r) \approx a r^{d_G} \,, \quad \text{from which the Cr-dim. originates :} \quad d_G = \lim_{r\to 0} \frac{\ln C(r)}{\ln r} \,. \tag{10}$$

3.4 Information dim. (Inf. dim.) This definition is similar to one of d_c, but it tries to take into account the frequency of visits each covering cube by the trajectory (assumed: it is long enough to cover effectively the Str-att). Having again a set of points N_0 to discretize uniformly the (continuous) trajectory and covering it with a set of N cubes of size ε, one counts the number of points N_i in each of N cubes and the probability P_i of finding a

point in the i^{th} cell:

$$P_i = N_i/N_0 \quad (N \ll N_0) \quad \sum_{i=1}^{N} P_i = 1 \,. \tag{11}$$

Then the information entropy (approached for small ε, too) appears so:

$$I(\varepsilon) = -\sum_{i=1}^{N} P_i \ln P_i \approx \ln(1/\varepsilon)^{d_1} = -d_I \ln \varepsilon \tag{12}$$

and from this the definition of Inf. dim. origines [5]:

$$d_I = \lim_{\varepsilon\to 0} \frac{I(\varepsilon)}{\ln(1/\varepsilon)} \stackrel{\wedge}{=} \lim_{\varepsilon\to 0} \frac{\sum_i P_i \ln P_i}{\ln \varepsilon} \,. \tag{13}$$

$I(\varepsilon)$ is a measure of the *unpredictability* in a system. – For uniform probability $P_i \stackrel{\wedge}{=} N_i/N_0 = 1/N \stackrel{\wedge}{=} P$, it has a *maximum*:

$$I(\varepsilon) \stackrel{\wedge}{=} -\sum_{i=1}^{N} P_i \ln P_i = -N \cdot P \ln P = N \cdot \frac{1}{N} \ln N = \ln N(\varepsilon) = \hat{I}(\varepsilon) \,, \tag{14}$$

moreover

$$\hat{d}_I \stackrel{\wedge}{=} \lim_{\varepsilon\to 0} \frac{\hat{I}(\varepsilon)}{\ln(1/\varepsilon)} = \lim_{\varepsilon\to 0} \frac{\ln N(\varepsilon)}{\ln(1/\varepsilon)} \stackrel{\wedge}{=} d_c \,; \tag{15}$$

as it is provable, $d_I \le d_c$ in general.
– For a sole filled (and each other empty) cube $N_1 = N_0$, $P_1 = 1$ (so at $i \neq 1$; $N_i = P_i = 0$), there is $I(\varepsilon) = -P_1 \ln P_1 = -1 \cdot \ln 1 = 0$, consequ. $d_I = \lim_{\varepsilon\to 0} \frac{0}{\ln(1/\varepsilon)} = 0$; this is the case of *maximal predictability*.

Let still be mentioned *the q^{th} order Inf. entropy and dim.* (1984; useful in statistical mechanics and inf. theory):

$$I_q(\varepsilon) = \frac{1}{1-q} \ln \sum_{i=1}^{N} p_i^q \,, \quad d_q = \lim_{\varepsilon\to 0} \frac{I_q(\varepsilon)}{\ln(1/\varepsilon)} \,. \tag{16}$$

Its cases $q = 0, 1, 2$ (with $q = 1 + \Delta q \to 1$ at $q \to 0$) make connection with d_c, d_I and d_G so [5]:

$$I_0 = \ln \sum_{i=1}^{N} P_i^0 = \ln N \cdot 1 = \ln N \stackrel{\wedge}{=} \hat{I}(\varepsilon) \,, \tag{17}$$

$$I_1 = \lim_{\Delta q\to 0} \frac{1}{\Delta q} \ln \sum_{i=1} P_i P_i^{\Delta q} = -\sum_{i=1}^{N} P_i \ln P_i \stackrel{\wedge}{=} I(\varepsilon) \,, \tag{18}$$

$$I_2 = -\ln \sum_{i=1}^{N} P_i^2 = \lim_{N_0\to 0} \ln 2 \cdot N_0 C(\varepsilon) \,. \tag{19}$$

Finally, it was proved (1983), that $d_G \leq d_I$ are lower bounds of d_c, however, they are very close for many known Str-atts:

$$d_G \leq d_I \leq d_c \,. \tag{20}$$

3.5 Fr.dim. based on LJAPUNOV **(Lj.) numbers & exponents.** As memorable, there exponents $\lambda_i = \ln L_i$ measure the (rate of the) velocity of 2 trajectories (going out from $S_0(\varepsilon)$: $|q_0' - q_0| \leq \varepsilon$ and) **diverging** on the attractor with $|q_n - \hat{q},| \to \infty$ (at $n \to \infty$), or **converging** off the attractor toward another one with $q_n \to \hat{q}_i$, (at $n \to \infty$). During this dynamical process, the initial conditions' sphere $S_0(\varepsilon)$ is imagined to deform into an ellipsoid (in 3 dim.). – At a chaotic 2 dim. map $\hat{\varrho}_{n+1} = \mathbf{f}(\hat{\varrho}_n)$, the circle $C_0(\varepsilon)$ deforms into an ellipse having – after M_ε steps of iteration – the main axes $\overline{L}_1$ and $\overline{L}_2$, where $\overline{L}_i > 0$ at $(i = 1,2)$ – as over the whole attractor averaged values – are the Lj. numbers, their logarithm $\overline{\lambda}_i = \ln \overline{L}_i$ the Lj. exponents. KAPLAN and YORK (1978) have proposed to calculate for a fr. attractor this Lj. *dim.*: [2]–[5]:

$$d_L = 1 + \frac{\ln \overline{L}_1}{\ln(1/\overline{L}_2)} = 1 - \frac{\overline{\lambda}_1}{\overline{\lambda}_2} \,. \tag{21}$$

A DE $\dot{\hat{\varrho}} = \mathbf{F}(\hat{\varrho}, t)$ of 4 dim. $(\hat{\varrho}, \dot{\hat{\varrho}} \in E_4)$ given for a dissipative system has a POINCARÉ map $\hat{\varrho}_{n+1} = \mathbf{f}(\hat{\varrho}_n)$ of **3 dim.** $(\hat{\varrho}_n; \hat{\varrho}_{n+1} \in E_3)$. For its Str-att, one can find

$$\overline{L}_1 > 1 \,, \quad \overline{L}_2 = 1 \,, \quad \overline{L}_3 < 1 \,, \tag{22}$$

that is the ellipsoid has tension, length-keeping, contraction in the 1^{st}, 2^{nd}, 3^{rd} main direction, resp. Because of dissipation, the ellipsoid's volume is less than the sphere's one, so that

$$\overline{L}_1\overline{L}_2\overline{L}_3 < 1 \,, \quad \text{but} \quad \overline{L}_1\overline{L}_2 > 1 \,. \tag{23}$$

This circumstance leads us to use the K. and Y. *formula* (as the special case $k = 2$ of their general one) for Lj. *dim.*:

$$d_L = 2 + \frac{\ln(\overline{L}_1 \cdot 1)}{\ln(1/\overline{L}_3)} \mathrel{\hat{=}} 2 + \frac{\overline{\lambda}_1}{\overline{\lambda}_3} \,, \tag{24}$$

where it is difficult to measure the contraction's Lj. number $\overline{L}_3$.

For an N-**dim.** POINCARÉ **map** of such a system and at the order

$$\overline{L}_1 > \overline{L}_2 > \ldots > \overline{L}_k > \ldots \overline{L}_N \quad \text{with} \quad \overline{L}_1\overline{L}_2 \ldots \overline{L}_k \geq 1 \,, \tag{25}$$

they have given for the Lj. *dim.* the following *general formula* [5]:

$$d_L = k + \frac{\ln(\overline{L}_1\overline{L}_2 \ldots \overline{L}_k)}{\ln(1/\overline{L}_{k+1})} \mathrel{\hat{=}} k - \frac{\overline{\lambda}_1 + \overline{\lambda}_2 + \ldots + \overline{\lambda}_k}{\overline{\lambda}_{k+1}} \,, \tag{26}$$

which is also a lower bound for d_c, that is

$$d_L \leq d_c \,. \tag{27}$$

Remarkable that FARMER (1983) has given for the *Btr* the following connection (at $\overline{\lambda}_a = \overline{\lambda}_b = \overline{\lambda}$):

$$d_I = d_L = 1 + \frac{\ln(1/\alpha) + (1-\alpha)\ln[1/(1-\alpha)]}{\ln(1/\overline{\lambda}) + (1-\alpha)\ln(1/\overline{\lambda})} \overset{\wedge}{=} 1 + \frac{H(\alpha)}{\ln(1/\overline{\lambda})}\,; \tag{28}$$

moreover at $\alpha = 1 - \alpha = 1/2$ and $H(\alpha) = \ln 2$, one obtains:

$$d_I = d_L = d_c \,, \tag{29}$$

and the map is like the horseshoe, or CANTOR map. – Worth mentioning that the studied dynamical process can lead to a *nonuniform* POINCARÉ *map*, when the different fr.dims often yield different results.

3.6A *The nature* exhibits fr. geometry in rich variety. Fr. curves (as fractioned lines consisting of straight pieces with free length and direction): a) border the coastal region of oceans, seas, lakes, b) similarly one of (pen)isle countries (as Island, England, Norway, etc.) (with longer frontier at finer measuring). Such (often randomlike) fr. formations appear (in the plane or space): c) on the ice of lake, as clefts; d) at the lightning, as trace lines of discharge; e) the contour line of mountain chains (looking from far); f) on the snowflake, as its contour and surface; g) on the frost – works of window, as strange figures; h) at the leaves' falling in windy autumn, as layered spread of foliage; i) fleecy clouds on the sky; j) the (randomly) ramifying of certain plants (e.g. cauliflower), bushes (e.g. blackberry); k) similar spread of weeds among the plants; l) sinking down sand grains during a sand storm; etc. [2], [5]. (*Fig. 8*).

3.6B *The artists'* sensitiveness to the fr. properties is remarkable. E.g. at the beginning of the century, a) the impressionists have used coloured points to make perceptible different effects in the space; b) in its 2nd half, VASARELLY and others are using a rich world of colours and fitted geometric forms for various effects of space. c) Today, some textile designers create fr. figures for ladies' wear [2], [5].

4. Fractal Basin Boundaries

4.1 Attractors and their basins. In most *lin.* systems (given e.g. by a IDE), there is just one possible motion for certain input and one attractor:

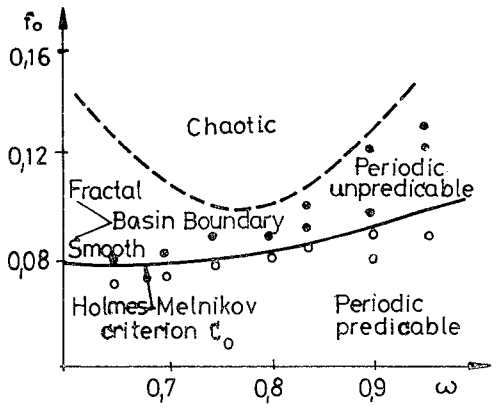

Fig. 8.

the equilibrium point. However, in *nlin.* systems (given e.g. by a nl.DE), more motions can occur depending on the input parameter and more attractors, too: equilibrium positions, periodic or limit cycle motions. These last ones are interesting now for us.

The range of values taken up by certain input or control parameter, for which the motion tends toward a given attractor, is called a *basin of attraction* in the parameter's space.

If there are two (or more) attractors, then their frontier-giving transition from one basin to (an)other – is called a *basin boundary.* – In *lin.* systems, it is expected, as a smooth, continuous line or surface and when its parameters are away from the input ones then their small uncertainties will not affect the outcome. – However, as the research has proved it, many *nlin.* systems exhibit nonsmooth, but fractal basin boundary; its existence is an essential part in the behaviour of nlin. systems. Small uncertainties in input, or other parameters may cause uncertainties in the outcome, so the predictability of motion can be impossible. – The (*Fig. 9*) shows certain smooth (continuously traced) and fractal (dotted lined) basin boundary, namely the fractal one for the HOLMES-MELNIKOV criterion ($f_0 > \frac{\gamma\sqrt{2}}{3\pi\omega}\cosh\frac{\pi\omega}{\sqrt{2}} \mathrel{\hat{=}} C_0$) at the two-well potential problem ($\ddot{x} = -\gamma\dot{x} + x(1 - x^2)/2 + f_0\cos\omega t$), the smooth one for the counter case ($f_0 \leq C_0$).

4.2 Let be mentioned the *complex map* $\overset{\circ}{L}$ to the series of regular complex function having a complex parameter ζ [2] [4]:

$$z_{n+1} \mathrel{\hat{=}} x_{n+1} + iy_{n+1} = (x_n^2 - y_n^2 + \xi) + i(2x_n y_n + \eta) \mathrel{\hat{=}} z_n^2 + \zeta\,.$$

The (black) domain of a) called as MANDELBROT set is the *fr. basin* of a parameter ζ, for which the long iteration (at $n \to \infty$) will remain bounded: $|z_{n+1}| < K$; the boundary of this domain shows fr. properties. – At

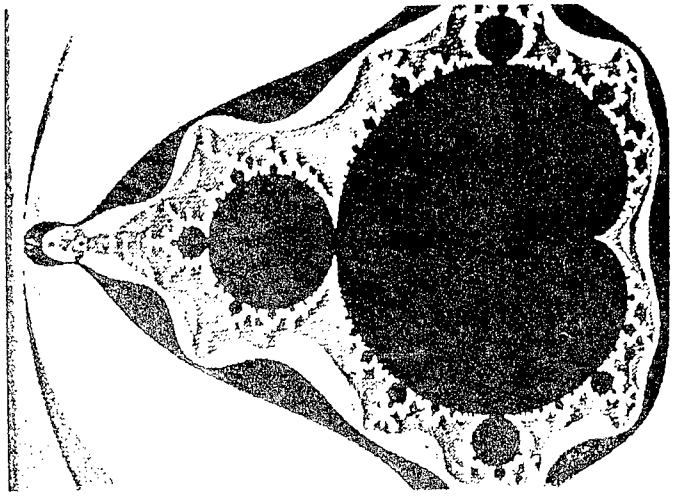

Fig. 9-a

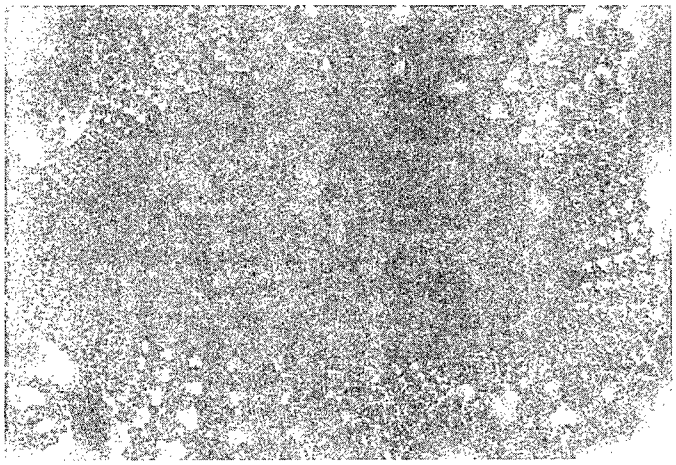

Fig. 9-b.

POINCARÉ map written by irregular complex functions

$$z_{n+1} \stackrel{\wedge}{=} x_{n+1} + iy_{n+1} = u(x_n, y_n) + iv(x_n, y_n) \stackrel{\wedge}{=} f(z_n) \,,$$

one can meet a map b), which is different from a) in details, but related in central role of the fr. basin (here an oval one) and its fr. boundary (*Figs. 10*, and *11*).

5. Control of Chaotic Motions (Ch-m) into Periodic Ones

5.1 As it was stated (e.g. in 1.1), a Ch-m[2] cannot be predicted into future. Therefore the applied sciences (e.g. the appl. math.-phys.-biology-chemistry, etc.) intended recently to keep a firm hand on such a motion and reduce it possibly into a regular one. In the last 3–5 years, the researches have proved that the Ch. systems can be controlled really, that is their *Ch-m* can be moderated into a *periodic one.*

In research institutes of various applied sciences, mainly interdisciplinary teams have found several '**control algorithms**' (CA) for such purposes. Of course, these CA look very specific with strongly different details, but yet one can state some general steps St_k of common quality; such are e.g.: St_1 **diagnostic step**: one observes – with suitable feedback, or measuring tool – 'just where is walking the Ch. system S', that is in which direction and measure are deviating its control parameter (C_p) values from their normal ones; – St_2 **correcting step**: one betters the Ch-S's behaviour by small perturbations of the mentioned C_p, to drive its Ch-m towards a periodic one; $St_{i>2}$, **repeating steps** of St_1 and St_2, too, for hindering S from reverting to the Ch [7].

5.2 Stay here some example!

1) It is obvious, that the *medical treatment* of an ill person can be considered, as a CA (it is suggested also by our naming of St_i). There is now the illness, as Ch; S_1 happens by a clinical thermometer, ECG, blood test, etc.; St_2 happens by prescribed medicines, dietary meal, gargling, inhaling, hydrotherapy, etc.: $St_{i>2}$ are the repetition of St_1 and St_2; the restored normal state is the health.
2) Let be mentioned *some successful CA* from the last years! – a) OTT–GREBORI–YORKE (Maryland) CA (having St-type steps), which was the beginner of such experiences. – b) DITTO–RAUESEO–SPANO (Navy) C, which reduced the Ch-m of an elastic band in magnetic field into a regular one. – c) R. ROY and team (Georgia) increased the energy product of a solid laser – by slowing up its Ch – onto 10–15 times. – d) SHOWALTER and team with Hung. cooperation [7] examined resultsfully– a simple CA to regulate the chemical Ch etc.

5.3 Let us close this paper with the hope that the applied mathematics – in cooperation with other applied sciences – can promote surely *the quick development and the industrial propagation of this recent branch 'CA of Ch-m'*, namely by more fine and profound discovery of Ch-m (and C_p, sequential bifurcations, Str-att, fr.lines–dimensions–basin boundaries), by elaboration of optimal CA for various Ch systems, etc. The expected success of the 'controlled chaos' promises *a giant practical importance for the next decades.*

[2] which is signed e.g. just by fr. properties.

References

[1] ARNOLD, A. V.: Közönséges differenciálegyenletek. – A diff. egyenletek elméletének geometriai fejezetei. – Ford. oroszból, Műszaki Könyvkiadó, Budapest, 1987-88. (In Hungarian).
[2] SZÉPFALUSSY, P. – TÉL, T. (editors): A káosz. Akadémiai Kiadó, Budapest, 1982.
[3] FAZEKAS, F.: *Chaotic Behaviour Caused by Bifurcation at Nonlinear Dynamic Systems.* Part I) BAM-556/88 (L). Part II) BAM-587/88 (LI). Part III) BAM-638 (LII). Part IV-V) BAM-639 (LIII). Technical University of Budapest.
[4] ENGELBRECHT, J.: Order and Chaos in Nonlinear Wave Motion. Postgraduate lectures at the TU-Bp, 1988.
[5] MOON, F. C.: Chaotic Vibrations, I. Wiley, New York, 1988.
[6] FAZEKAS, F.: Papers of Lectures on the Chaos Held at the Congresses, Vrnjac Banja, 1988. Zakopane, 1988. TF of TU-Bp., 1988. U-Trieste, 1989, Skopje, 1989, TU-Košice, 1989.
[7] GÁSPÁR, V. A.: *A megszelidített káosz.* NSz, Bp., 1993.

PERIODICA POLYTECHNICA SER. TRANSP. ENG. VOL. 23, NO. 1-2, PP. 89-105 (1995)

COMPUTER SIMULATION STUDY OF THE INFLUENCE OF TOOTH ERRORS ON GEAR DYNAMIC BEHAVIOUR

János MÁRIALIGETI

Department of Machine Elements
Technical University of Budapest
H-1521, Hungary

Received: November 1, 1994

Abstract

The origin of the excitation effects of gear train is briefly discussed and an adequate tooth spring system model is presented, which enables to take into consideration the important exiting effects, due from the mesh. The model is especially adapted for computer simulation studies. Making use of this tooth mesh substituting model, the basic tooth vibration features are discussed, based on simulation results. Influence of the mesh irregularities, being always present, even in the case of ideal toothing, is presented. Further on, the effect of the manufacturing errors on gear dynamic behaviour is analyzed by the Furier development of the tooth stiffness functions on one hand, and the vibration characteristics are studied under quasi stationary rolling down conditions, based on computer simulation results, on the other hand.

Keywords: gear dynamic, computer simulation, non-linear vibration, parametric excitation, tooth errors.

1. Introduction

The gear transmissions are one of the mostly applied power transmission elements in mechanical drive systems. In the case of their application in vehicle transmissions, they are generally subjected to random load conditions, varying in a wide range of load levels and excitation frequencies. The schematic model of a drive system is represented on *Fig. 1.* The gear box on the input is connected to the prime mover, providing a variable $T_1(t)$ input torque and on the output it is coupled to the final drive, presenting a variable $T_2(t)$ load as well, where t is the time. Both are varying in the load and in the frequency range, too.

The gear trains as active vibration exciting elements can have important effect on the dynamic behaviour of the whole transmission system. They influence the load histories on the connected parts on one side and their own load conditions on the other side. On *Fig. 1* $s(\varphi_1)$ refers to the vibration exciting effect, as a function of the input φ_1 angular displacement.

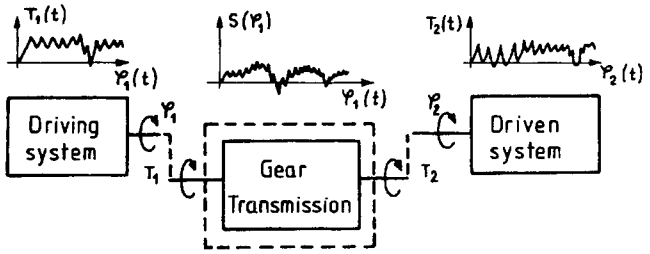

Fig. 1. Schematic representation of a vehicle drive system

Because of the complexity of the problem, numerical simulation technics can be applied for system and for element characteristic analysis and optimisation [1, 2].

In this contribution, some basic aspects of the non-linear vibrations of gear trains are studied and some simulation results are presented for gears with ideal normal and modified involute profiles and for gears with manufacturing errors, as base circle and pitch error.

2. The Origin of the Vibration Exciting Effects of Gears

The main vibration exciting effects of gears can be originated by two main groups [3,4]:

- The effects caused by the stiffness variation of the teeth, on two levels, namely the stiffness variation as the function of the contact point location of the mating single tooth pairs and the alternating number of teeth being actually in mesh. They are called generally as dynamic effects.
- The effects introduced by contact irregularities at the beginning and at the end of the pressure line, even in the case of ideal geometry, and the exciting effects introduced by manufacturing errors and intended profile modifications, the latter for improving gear characteristics. They are called generally as cinematic excitation effects.

Other parameters as the friction influence are generally less important.

In the case of ideal tooth meshing, assuming that the teeth under load do not deform, the stiffness variation can be described in the function of the drive gear angular displacement, φ_1, as a simple periodic function, $s(\varphi_1)$, where the period is determined by the angular displacement corresponding to a single tooth contact length, $\Omega_z = \gamma_{1b}$. At that model, the abrupt stiffness change is accepted at the end points φ_{A_i} and φ_{E_i} of the pressure line, see *Fig. 2a*. The load influence on the meshing characteristics is fully neglected, so the resulting vibration is linear; no load influence is present.

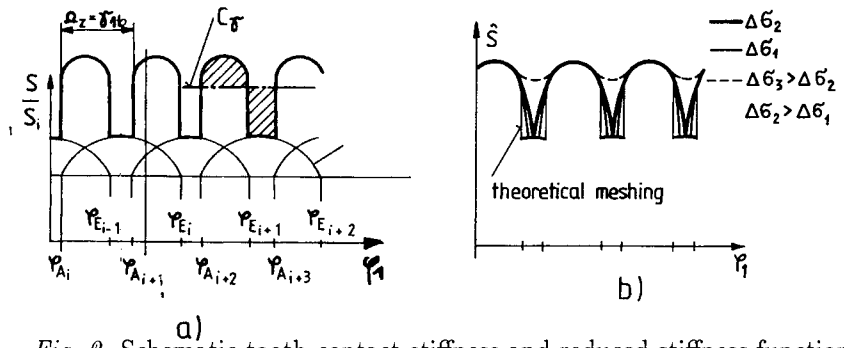

Fig. 2. Schematic tooth contact stiffness and reduced stiffness functions

However, even in the case of ideal tooth geometry, assuming elastic tooth deformations under load, the tooth contact length varies in the function of the load, so the stiffness function must be replaced by a two variable function, $\hat{s}(\varphi_1; F_N/b)$, where F_N/b is the specific tooth normal load, F_N stands for the tooth normal force, and b is the tooth length. The $\hat{s}$ *reduced stiffness function* [4] contains already the load influence, so the resulting vibration will not be linear. On the *Fig. 2b*, the load dependent stiffness variation is schematically represented for *ideal geometry and realistic tooth meshing*, i.e. the tooth deformations are taken into consideration. $\Delta\sigma$ refers to the specific load as parameter. If real tooth with fabrication error is considered, the period of the $\hat{s}(\varphi_1; F_N/b)$ function is determined by the angular displacement of the drive gear, corresponding to the all possible combinations of contact of the drive and of the driven gear tooth profiles.

The tooth fabrication errors, as pitch, profile, etc. errors, result in the non-uniform rotation transmission, see for ex. *Fig. 3* for the profile error, resulting non-linear effects, too. The influence of the intended profile modification is load dependent as well.

Further non-linear feature is introduced by the non-linear single tooth pair force-deflection characteristic at any fixed contact point, resulting variable stiffness in the function of the load, see for ex. [5]. On the *Fig. 4*, single tooth pair force-deflection curve is schematically represented, where w stands for the tooth deflection. The theoretical, linear force-deflection curve is indicated as a thin line.

The linear vibration model, discussed in detail by many authors, is convenient for qualitative studies, or in the case of constant load drives, if the specific load is in the middle or high load range. In vehicle drive systems, however, characterised by important load variations, the load dependent effects must be taken into consideration, so the non-linear gear vibration properties are of prime importance.

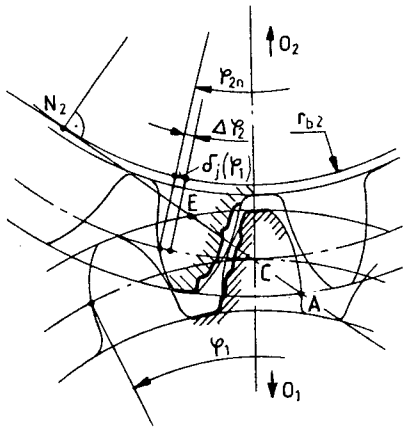

Fig. 3. Real tooth profile meshing (schematic)

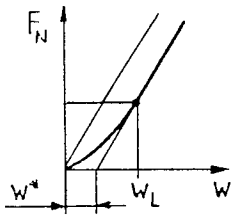

Fig. 4. Non-linear single tooth pair force-deflection curve

3. Gear Train Modelling and Basic Tooth Dynamic Behaviour

3.1. The Gear Train Model

For the study of the gear dynamic behaviour, a two mass model is applied, see *Fig. 5a*, where the two rotating masses are coupled by a system of springs, replacing the real tooth mesh, see *Fig. 5b*, where T_1, T_2 are the torques, r_{b1}, r_{b2} are the base circle radii, φ_1, φ_2 are the real angular positions, z_1, z_2 are the number of teeth, J_1, J_2 are the moments of inertia, i_n is the *nominal ratio*, $\bar{s}_i\ (\varphi_1)$ is the single tooth pair stiffness, K_j is the damping coefficient, h is the backlash. *Contact function* $\delta_j\ (\varphi_1)$ [4], corresponds to the j-th tooth profile pair combination, and gives the travel along the pressure line, corresponding to angular error $\Delta\varphi_2 = \varphi_{2n} - \varphi_2$ of the driven gear, in the case of zero load, only the j-th tooth pair being in contact, where $\varphi_{2n} = \varphi_1/i_n$ is the nominal angular position. F_z and F_D are the elastic and the damping force components of the tooth normal force. The values with mark correspond to the reverse torque transmission.

The model enables the handling of the reverse torque transmission case, and the individual treatment of the different tooth pair characteristics, so single

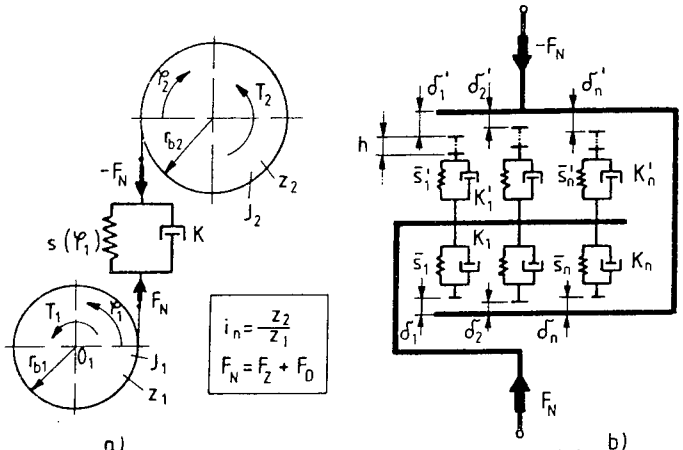

Fig. 5. The gear train two mass model

tooth error influences can be modelled as well.

The equation, corresponding to the system takes the following form:

$$J_1\ddot{\varphi}_1 + \left[\sum_{j=1}^{n} K_j \cdot \left(\Delta\dot{\sigma} - \dot{\delta}_j(\varphi_1)\right)\right] \cdot r_{b1} + \quad r_{b1} \cdot \hat{s}(\varphi_1; \Delta\sigma) \cdot \Delta\sigma = T_1(t),$$

$$J_2\ddot{\varphi}_2 + \left[\sum_{j=1}^{n} K_j \cdot \left(\Delta\dot{\sigma} - \dot{\delta}_j(\varphi_1)\right)\right] \cdot r_{b2} + \quad r_{b2} \cdot \hat{s}(\varphi_1; \Delta\sigma) \cdot \Delta\sigma = -T_2(t) \quad (1)$$

where the points stand for the time derivatives, $\Delta\sigma = r_{b1} \cdot \varphi_1 - r_{b2} \cdot \varphi_2$ is the travel error of the wheel measured on the pressure line, corresponding to the actual angular position, relative to the nominal angular position, so the term $\hat{s}(\varphi_1; \Delta\sigma) \cdot \Delta\sigma$ gives directly the actual elastic total force in the tooth contact.

The $\hat{s}(\varphi_1; \Delta\sigma)$ reduced stiffness function contains all vibration exciting effects, and formally can be applied as multiplication factor with the actual deformation. In the general form, it can be developed by its Fourier components:

$$\hat{s}(\varphi_1; \Delta\sigma) = C_0(\Delta\sigma) + \sum_{k=1}^{\infty} C_k(\Delta\sigma) \cdot \cos\left(\frac{2\pi}{\Omega} \cdot k\varphi_1 + \nu_k\right) \quad (2)$$

where the load dependence is symbolised by the actual 'deflection' value $\Delta\sigma$ C_0 is the load dependent average, C_k is the k-th Fourier component, Ω is the basic period, and ν_k stands for the phase angle.

As it is known, this vibration exciting type belongs to the group of the *rheo-non-linear* vibrations [6]. Because of the composed parametric excitation function, *Eq.* (2), analytic solutions are not possible. The convenient way for the study of the dynamic behaviour is the computer simulation.

Further on, the basic vibration properties of a simplified system will be presented.

3.2. Basic Dynamic Behaviour.

The basic vibration properties of a simple one mass system with harmonic excitation can be studied by the *stability chart*, see ex. [6].

Introducing into the *Eq.* (2) an $\Omega = 2\pi$ periodic excitation function with $k = 1, \nu_k = 0$ and assuming a load independent case, we get a simple cosine type excitation, see *Fig. 6*, where $\tau = \omega_1 \cdot t$ is a dimensionless parameter, ω_1 being the input angular speed. Reducing the system of *Eq.* (2) into a one mass system [7], the resulting homogeneous differential equation is a rheo-linear, Matthieu type one.

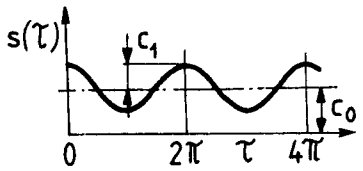

Fig. 6. Simple cosine type excitation function

The ω_s system eigenfrequency in this case is $\omega_s = \sqrt{C_0/m}$, where $C_0 = c_y$ is the *gear engagement spring stiffness* [8], and m is the reduced mass of the one mass system. The tooth angular frequency $\omega_z = \omega_1 \cdot z_1 = 2\pi f_z$, where f_z is the tooth frequency. It can be concluded from the stability chart, that at ω_1 input speeds of:

$$\omega_1 = \frac{2 \cdot \omega_s}{\upsilon}; \quad \upsilon = 1, 2, ...\infty \tag{3}$$

resonance points develop. In the gearing technics, the resonance point corresponding to $\upsilon = 2$ is called as main resonance. Introducing the N dimensionless number by:

$$N = \frac{\omega_1 \cdot z_1}{\omega_s} = \frac{2}{\upsilon} \tag{4}$$

the resonance points are at $N = 2, 1, (2/3), 1/2, (2/5)....$, and the main resonance corresponds to the value of $N = 1$. The N values in parenthesis,

corresponding to the odd values of v, are generally not important, and do not develop in the presence of damping.

The *excitation intensity* can be characterised by the $C_k' = C_k/C_0$ *excitation intensity factor*. Greater intensities give broader resonance regions, characterised by more intensive vibrations, even in the case of the presence of damping and inversely.

For the simulation study of gear vibration, one can generate by computer simulation quasi stationary resonance curves, by simulating an acceleration process at a given nominal static specific tooth normal load, from n_1 zero speed over the main resonance point. The diagram ordinate on the resonance curves is the dimensionless V_Σ value, the *contact force magnification factor*, defined by the following equation:

$$V_\Sigma = \max ..._{\gamma_{1b}} \{V_\Sigma(\varphi_1)\} \; ; \qquad V_\Sigma(\varphi_1) = \frac{\sum_{j=1}^{n} \frac{F_{Nj}(\varphi_1)}{b}}{\frac{F_N}{b}} \tag{5}$$

where F_N/b is the total constant specific load on the teeth, and F_{Nj}/b is the real dynamic specific tooth load on the individual tooth in mesh, n is the number of teeth actually in mesh, γ_{1b} is the rotation angle on the drive gear, corresponding to one tooth mesh.

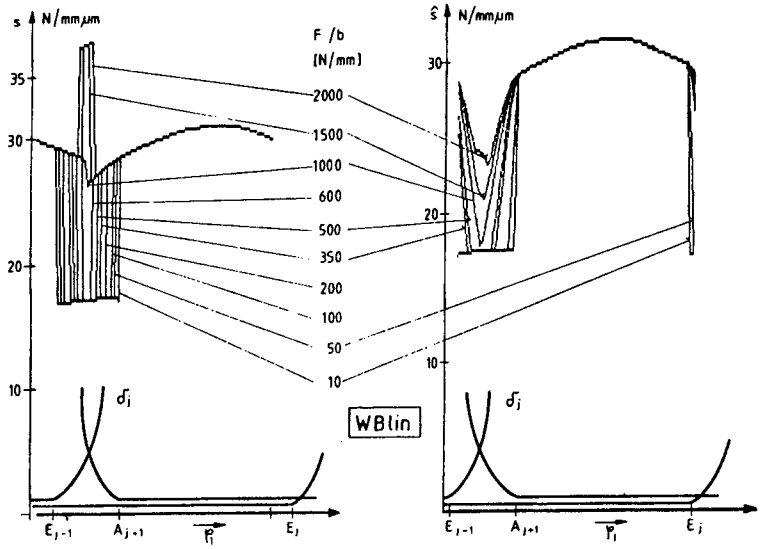

Fig. 7. Stiffness functions for an ideal gear train, with real meshing

For real gear vibration excitation functions, *Eq.* (2), generally the $k \neq 1$, nevertheless the basic characteristics of the parametric vibrations can be fairly well represented with an ideal gear train model.

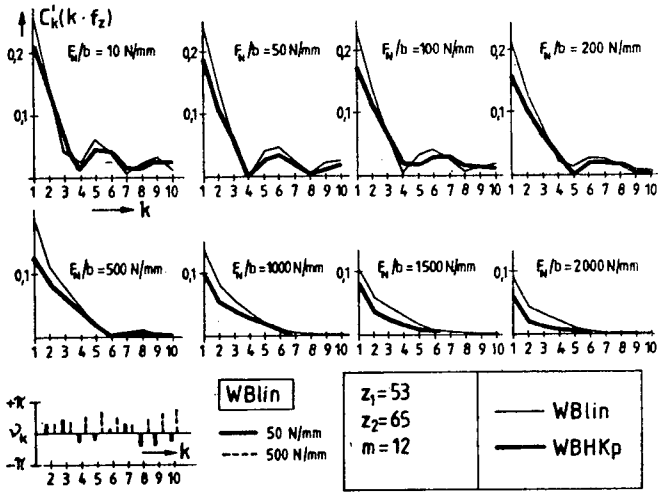

Fig. 8. Vibration exciting intensity components for ideal gear with real meshing

To demonstrate the basic behaviour of a rheo-linear system as a reference one, an ideal gear train model behaviour is simulated, with a quasi stationary acceleration process. A linear single tooth pair force-deflection characteristic, so constant stiffness at each contact point is applied. Evidently, the stiffness values vary from point to point. Further on, the code WBlin refers to this type of stiffness characteristic. The tooth deformations, so the load dependent pressure line length is taken into the calculation, see *Fig. 2b*. Consequently, the system is not exactly linear, but at a constant specific load, it can be accepted as a good approximation.

Fig. 7 represents the $\hat{s}\ (\varphi_1; F_N/b)$ reduced stiffness function, which is the excitation one, and the $s\ (\varphi_1; F_N/b)$ function, which represents the stiffness variation. The latter determines the system eigenfrequency. The nominal (at zero load) contact ratio for this train is $\varepsilon_\alpha = 1,7$, so at high specific load values the $\varepsilon_\alpha > 2$. The δ_j *contact functions* for the individual teeth enable to follow the mesh conditions of the gears [4]. *Fig. 8* shows the reduced Fourier components of the excitation function, the C'_k excitation intensity factors. The code WBlin refers to a linear single tooth stiffness characteristic.

Fig. 9a represents the resonance curve for this gear variant. For the simulation, the $h = 0$ backlash value was chosen, for avoiding the non-linearities involved in the case of tooth flank separations. A fairly low, $D_z = 0.007$ Lehr damping ratio was chosen, to assure the development of the resonance points.

The gear and other parameters are given on the Figure. The marked N values show the resonance locations. At lower speeds, even in the case of a small damping, the resonances cannot develop. The relatively small

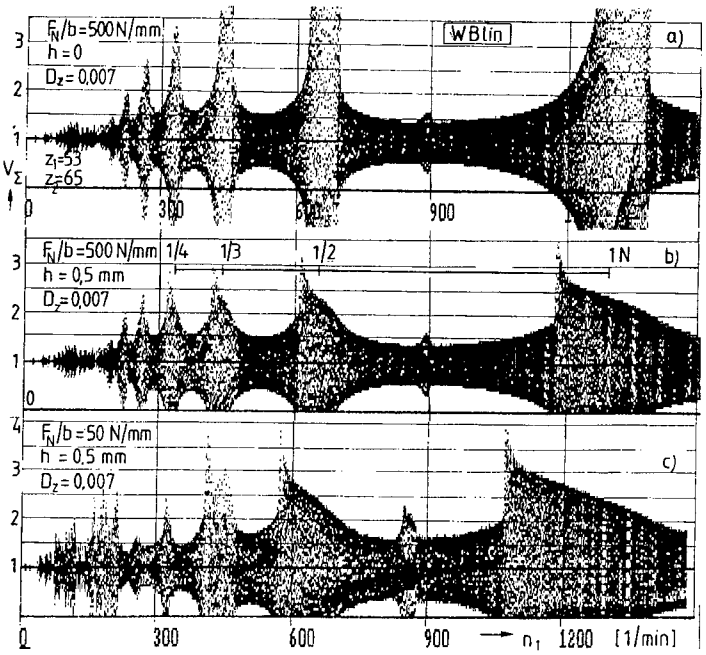

Fig. 9. Resonance curves for ideal gear, real meshing, with low damping ratio

elevations at $n_1 = 900/\text{min}$ refer to the resonance at $N = 2/3$. The Figure shows that at lower speeds the vibrations are relatively reduced, but at the value of about 200/min, important vibrations are present. Especially the resonances at N=1,1/2,1/3, 1/4...are important.

Further on, several parameters, introducing non-linearity, are studied.

4. Non-linear Vibrations in the Case of Ideal Gear Geometry

For the study of the effects of some basic gear parameters and meshing properties introducing non-linearity, the previously applied real gear train with ideal geometry was chosen. Real tooth engagement was applied in all cases.

The real tooth engagement means that the pressure line length is load dependent, so the reduced stiffness function, so the excitation properties vary in the function of the load. Further on, the variable contact length influences the average damping as well. So, the influence of the nominal load, the realistic backlash and the non-linear single tooth characteristic was studied. For all cases, quasi stationary acceleration or deceleration processes were simulated and the ratio of the contact force magnification factor was calculated, see *Eq.* (5).

Fig. 9b represent the basic effect of the backlash, involving important

non-linearity. For the sake of the better representation of the basic features, the previously applied damping ratio was applied. The $V_{\Sigma} = 0$ values indicate the separation of the tooth flanks, enabled by the presence of the backlash. Characteristic non-linear resonance shapes develop, with reduced peak values, as compared to the case of *Fig. 9a*. Because of the average stiffness reducing effect of the backlash, the resonance regions are at lower speeds. *Fig. 9c* represents the influence of the nominal specific load, in accordance with the reduced stiffness exciting components on *Fig. 8*. The increase of the vibrations at the resonance points involves increased tooth flank separations, so the resonance locations move to the direction of lower speeds. Because of the increased C'_k values, the vibrations are more intensive, with increased contact force elevation factors.

Fig. 10 presents the simulation results for the same gear train, with backlash and realistic damping ratio, in the case of WBlin, linear single tooth pair stiffness characteristic. At lower nominal specific load values the tooth flank separation remains at the resonance points, however, at higher specific loads it disappears. The peak values are generally lower as in the cases of small damping, and the higher order resonances tend to disappear. At F_N/b=1000 N/mm specific nominal load, the contact force magnification factors are considerably reduced, as it follows from the vibration exciting intensity factors.

The *Fig. 10b* shows a deceleration process. The opposite running direction of the main resonance point results in the broadening of the resonance region, and it extends to the resonance at N=1/2. This feature is well known in the field of the non-linear vibrations.

On *Fig. 12* the influence of the non-linear single tooth pair stiffness characteristic is presented. The applied stiffness curve type is as it is on the *Fig. 4*, with a progressive beginning section, and linear later. The stiffness reducing effect of the gear body design (as gear rim) was taken into account too [8]. The code for this single tooth pair stiffness characteristic is WBHKp. The reduced stiffness and stiffness function show important changes, related to the WBlin case, see *Fig. 11*. The Fourier components of the vibration exciting intensity are shown on *Fig. 8*.
Based on the resonance curves on *Fig. 12*, one can see that the vibration effects are smoother than for the WBlin case, see *Fig. 10*. The origin of it is the smooth beginning part of the single tooth pair stiffness curve, the smaller average stiffness and the increased contact ratio, resulting higher average damping. The load influence, however, is expressed.

At F_n/b=50 N/mm specific load, no tooth flank separation occurs, and the main resonance points are at lower speed, because at that load, the small stiffness region of the characteristic curve dominates. The resonances are reduced, too, related to the WBlin case. At high specific load values the contact force magnification factors decrease.

Based on the results of the simulations, one can state that even in the case of ideal tooth geometry, important non-linear behaviour is found. Con-

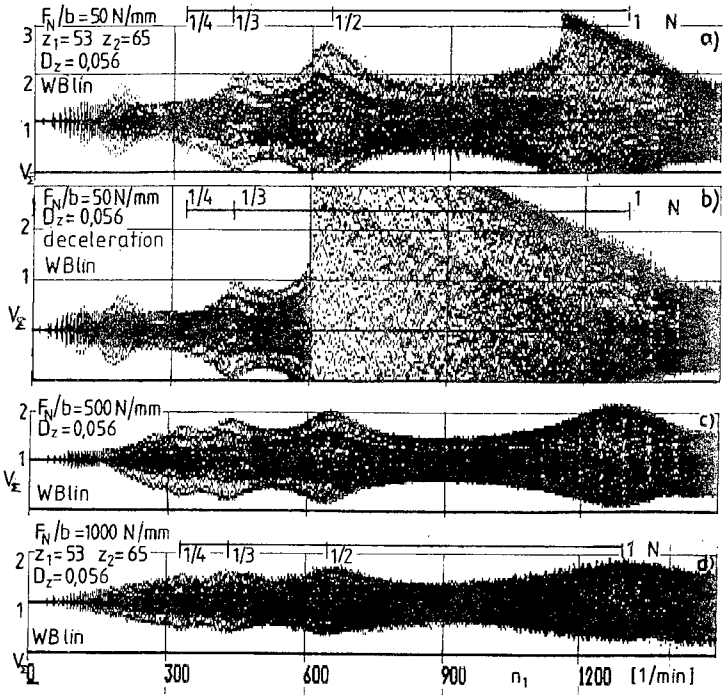

Fig. 10. Resonance curves for gear train with ideal geometry, real meshing and normal damping

sequently, in gear applications, characterised by important load variations, the non-linear effects can not be neglected.

5. Dynamic Behaviour in the Case of Gears with Profile Error

For the study of the profile error influence, the same gear train was applied. The profile error was taken onto the drive gear, as a base circle error on each tooth, of $f_{h\alpha} = -20$ μm, which corresponds to a DIN7 (ISO) quality class [9]. This driver was rolled together with the driven gear, having ideal tooth geometry.

On *Fig. 13* the reduced stiffness and the stiffness functions with the C'_k components, and the contact functions are shown, for linear single tooth stiffness characteristic (WBlin). The $\hat{s}$ excitation function changes considerably, related to the ideal geometry, especially at lower specific load levels. The C'_k excitation intensity factors increase similarly, especially at low specific load levels.

On *Fig. 14a* an h=0 backlash value was applied, for the sake of com-

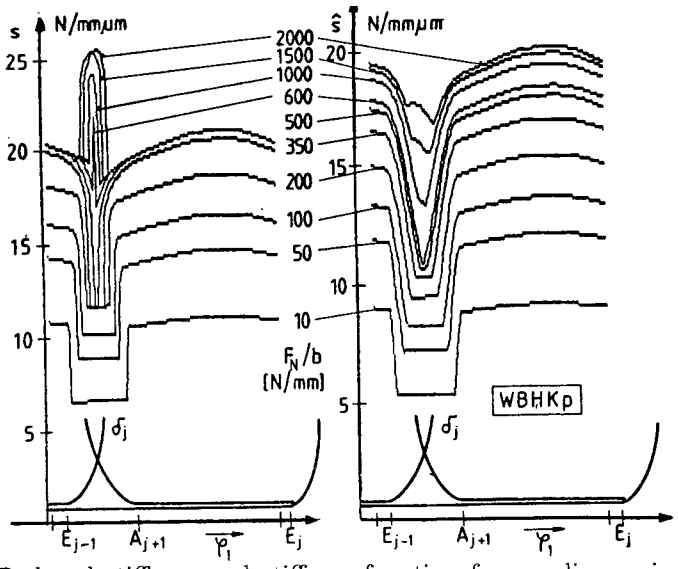

Fig. 11. Reduced stiffness and stiffness function for non-linear single tooth pair stiffness characteristic

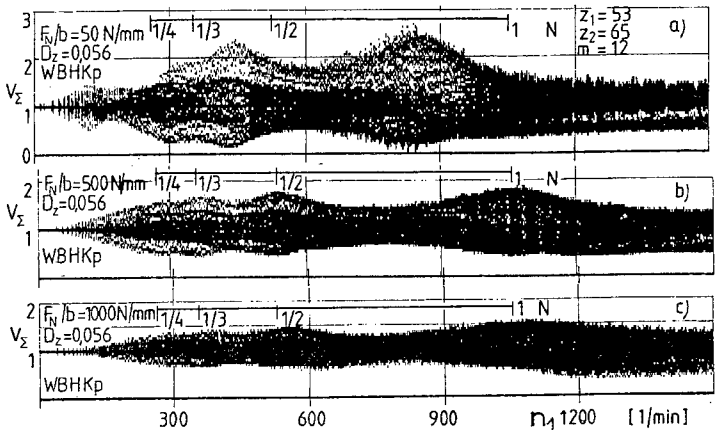

Fig. 12. Resonance curves for non-linear single tooth force-deflection characteristic

parison of the results on *Fig. 7a*. In spite of the normal damping, important vibrations develop, with an expressed hardening type non-linear resonance at the main resonance point. The *Fig. 14b* represents the resonance curve at the same specific load level as previously, with backlash. Because of the important vibration effects, tooth flank separations occur practically on the hole speed region, with important softening type non-linear resonances.

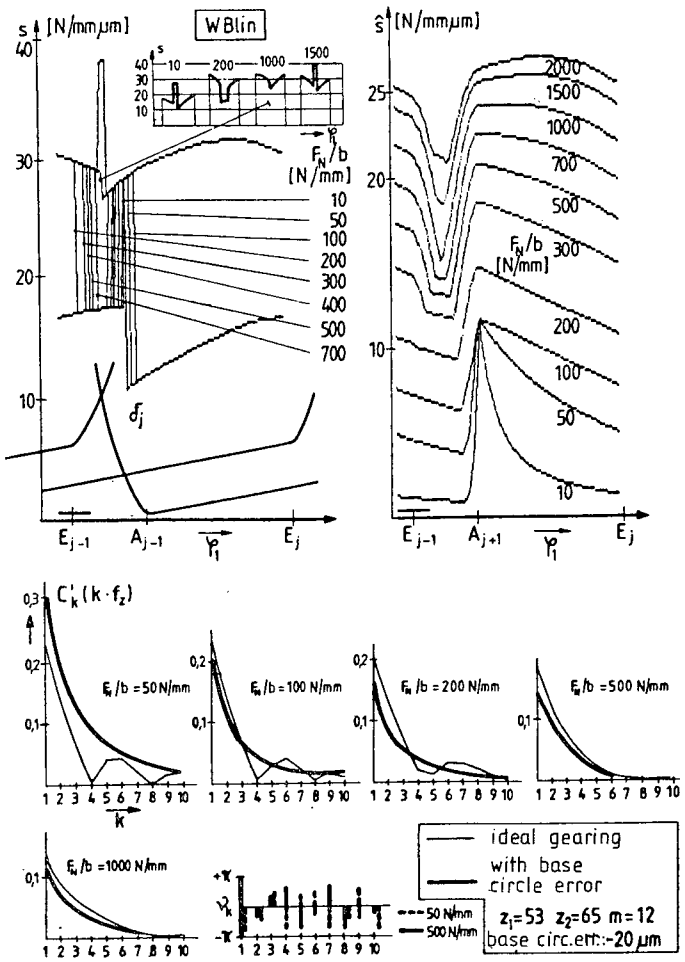

Fig. 13. Reduced stiffness and stiffness function for gear train with base circle error

The real resonance point locations do not correspond to the nominal ones, see *Fig. 14a*.

At higher load levels, the vibration extremities are decreased, but they are greater than for the ideal gear. Based on the simulation results, one can state that the greater vibration intensities, especially at lower specific load levels, result in increased dynamic loads, which is magnified by the decreased average damping, due to the real contact ratio decrease. Important non-linear characteristics dominate the vibrations. At higher load levels the general vibration shape is similar to the ideal case, see *Fig. 14c* and *9b*, at low damping ratio. At normal damping, however, characteristic differences are found, see *Fig. 14d* and *Fig. 10c*.

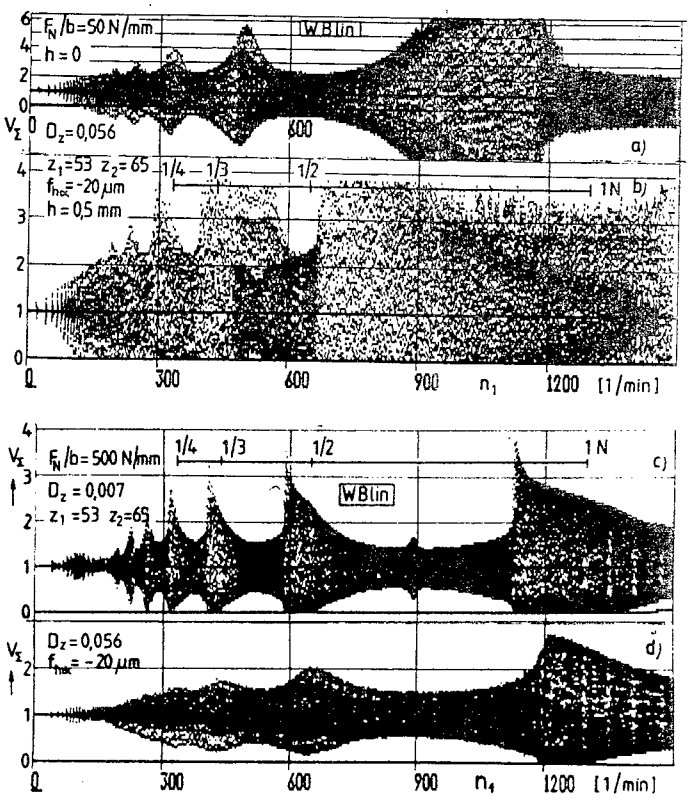

Fig. 14. Resonance curves for a gear train with base circle error

6. The Influence of the Pitch Error

For the study of the pitch error influence, $f_{pbr} = \pm 0.02$ mm error was taken on all drive gear teeth. For creating this type of error, it is enough to displace each second tooth profile; it results automatically an opposite sign pitch error with the following tooth flank. For the simulation, this gear was taken into meshing with a driven wheel of ideal tooth geometry, and WBlin type single tooth pair force-deflection characteristic was applied. The resulting reduced stiffness and the stiffness functions and the δ_j contact functions are presented on *Fig. 15.* The C'_k intensity components are represented on *Fig. 16.*

The basic period angle of the excitation and the stiffness function is now the double as previously. This corresponds to the fact that each second tooth is displaced with the given pitch error, giving so a double period. That is why new C'_k components appear, see *Fig. 16.* The k' values on *Fig. 16*

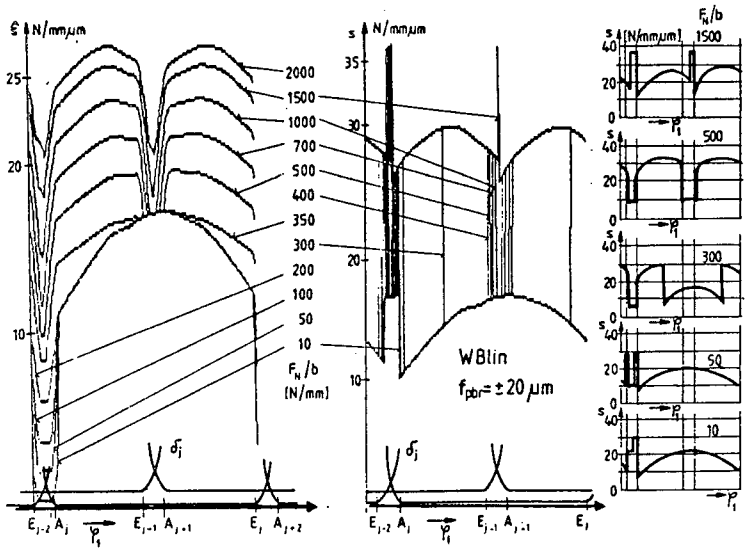

Fig. 15. Reduced stiffness and stiffness functions for a gear train with pitch error

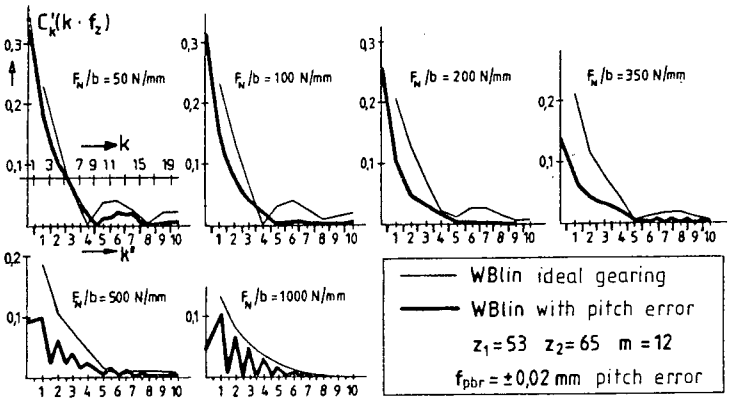

Fig. 16. Fourier components of the reduced stiffness function for gear with pitch error

refer to the Fourier indexes of the ideal tooth geometry. For the sake of comparison, the ideal gear component is indicated, too.

For the better presentation of the basic vibration characteristics, a simulation was realised with a low damping ratio, see *Fig. 17a*. In accordance with the new C'_k vibration excitation intensity factors, new resonance points appear; the resonance curve shape differs considerably from that for ideal gear

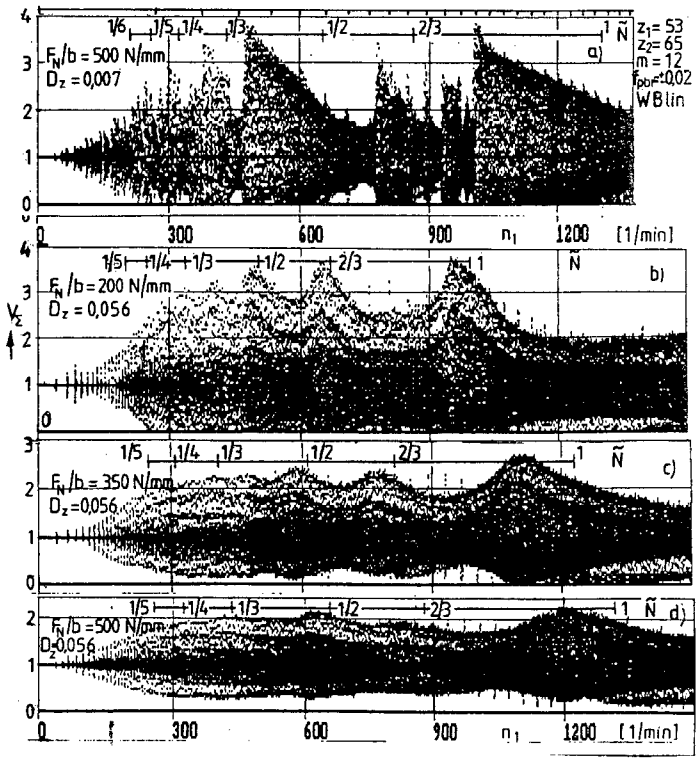

Fig. 17. Resonance curves for gear train with pitch error

geometry, see *Fig. 9a*. This characteristic remains even at higher damping ratios, see *Fig. 17bcd*. Above the input speed about n_I=200/min., the vibration peaks remain practically at the level of the resonance points. The maximum values at the main resonance point remain practically on the same level. So, intensive vibration is found on the whole speed region. An interesting result for that case that the resonances at $\tilde{N}$ =2/3 appear, which was not the case for normal gears.

The $\tilde{N}$ values on *Fig. 17* are similar to the previously defined N values, but they are calculated with the actual average stiffness, belonging to the given specific load.

7. Conclusions, Future Work

The simulation results of gear train dynamic analysis presented in this paper have shown ,that even in the case of ideal tooth geometry, important non-linear effects develop, if the real tooth meshing conditions are taken into consideration. Similarly, the tooth errors involve important load dependent features. For enabling the treatment of these phenomena, a complex dynamic model is needed and careful tooth meshing analysis is to carry out. On the other side, the single tooth pair force-deflection curve type influences considerably the dynamic behaviour of the gear train, too.

Future work is needed for the study of the dynamic behaviour in the case of realistic gears with randomly distributed fabrication errors, and under continuously variable load conditions.

References

[1] MICHELBERGER, P. – ZOBORY, I.: Operation Loading Conditions of Ground Vehicles – Analysis of Load History. *Proceedings ASME Winter Annual Meeting*, Dallas, New York, 1990, pp. 175-182.
[2] ZOBORY, I.: The Forecasting of the Load Histories in the Drive Systems of Railway Traction Vehicles by Stochastic Simulation, Based on a System Dynamic Model. TU. Budapest, Dep. of Railway Vehicles. Research Report. 1992.
[3] NIEMANN, G. – WINTER, H.: Machine Elements, Bd. II. Springer Vlg. Berlin, Heidelberg, New-York. 1985. (In German.)
[4] MÁRIALIGETI, J.: Simulation Model of Gear Tooth Stiffness Function with Manufacturing Errors. *Periodica Polytechnica Ser. Transp. Eng.* Vol. 18. Nos 1-2. (1990) pp. 157–173.
[5] WINTER, H. – PODLESNIK, B.: Tooth Stiffness Characteristics of Gears. Part 2. *Antriebstechnik*, Vol. 22. (1983) Nr. 5. pp. 51–57.
[6] KLOTTER, K.: Vibration Theory. Bd. 1. Springer Vlg. Berlin, Heidelberg, New-York. 1980. (In German.)
[7] MÁRIALIGETI, J.: C. Sc. Thesis. Budapest, 1990. (In Hungarian.)
[8] Calculation of the Load Capacity of Gears. DIN 3990. (In German.)
[9] Tolerances for Gears. DIN 3961. 3962. 3963. (In German.)

PERIODICA POLYTECHNICA SER. TRANSP. ENG. VOL. 23, NO. 1-2, PP. 107-114 (1995)

FLEXIBLE BUS STRUCTURES OBTAINED BY THE METHOD OF STATIC CONDENSATION

Dezső SZŐKE

Department of Mechanics
Faculty of Transportation Engineering
Technical University of Budapest
H-1521 Budapest, Hungary
e-mail: dezso@kme.bme.hu

Received: November 13, 1994

Abstract

The determination of dynamic responses (accelerations, stresses) of linear systems with large number of degrees of freedom costs much work and time. Practically the same results can be obtained by using an appropriate method by which the given dynamic system can be reduced achieving less cost and time required for computation.

Retaining the structure of physical model the static reduction is the most frequently applied process. Elaboration of lumped mass matrix of bus and commercial vehicle models is heuristic, therefore only the stiffness matrix of the given system is problematic.

Considering the computational possibilities there are more ways to determine the stiffness matrix of a simplified model. A reduced stiffness matrix, elaborated from the results of dynamic analysis of finite element models, is competitive from the point of view of accuracy and computational costs.

Keywords: FEM analysis, structural dynamics, static condensation, vehicle dynamics.

1. Introduction

Concerning the calculated outputs of dynamic systems the increase of degrees of freedom (DOF) causes several problems, such as: the computational time increases exponentially, where the power term is about 3 and 4, and on the other hand the punctuality of computation is reduced. The reason of these failures is the more segmented, detailed model. Therefore the time or frequency domain functions can be calculated with smaller time or frequency sampling intervals and required time to calculate the independent variable, as the answer function is proportional with the 2nd-3rd power of the unknown functional.

By increasing the DOF of model, the information obtained by the computation also increases. Although the information must be considered very carefully, hence the possibility to measure data on a real system is very much limited in comparison with the calculated points of available model. The results obtained from computation are adjusted according to real measurements.

From the afore-mentioned facts it is clear that in the selection of the number of unknown parameters the designers should be careful, hence the computational facilities allow us much freedom. Therefore the models designed for static modelling must be simplified for dynamic analysis. From the reduction technics the method of static condensation is the most known. A practical implementation is shown in this paper, used to model vehicle undercarriage systems.

2. Dynamic Structure of Vehicle Undercarriage Systems

The description of the deformation of vehicles, vehicle undercarriages is based very often on the concept of discontinuity modelling. The required parameters, such as the mass, stiffness and damping parameters are sought from finite element (FEM) modelling. For example the mechanical model of a bus structure can be represented by 300–500 nodes, where each node has six DOF.

In the calculation of dynamic signals the number of DOF can be reduced significantly, on the one hand to half, if the nodes only modell mass points, and on the other hand to a further one third, if only the vertical dynamics of vehicle are considered. Here we suppose that from the vertical excitation no lateral force exaggeration exists, hence no lateral vibration occurs. (A small scale lateral displacement can only occur due to three-dimensional geometrical and stiffness constraints of the model). The DOF of dynamic model therefore is equal with the number of nodes.

The knowledge of mass distribution of system may lead to further simplifications. The size of useful load can be compared with the own mass of vehicle, where both loads are acting on the main frame of the vehicle. During the modelling phase the designers ought to concentrate on the exact description of the, before mentioned phenomena concerning the dynamic impacts. Then the dynamic models of buses could be described by 140–200 DOF.

Although, we can state without going into details that the global equations of motion of a bus can be described with appropriate 40–60 DOF, moreover if we only consider the bending modes then this number can be reduced to further 8–12, which results in two times smaller DOF.

3. Derivation of Stiffness Matrix of the Simplified Dynamic Model

After the selection of the unknown parameters of dynamic model the system matrices of the static finite element model have to be transformed into the dynamic freedoms. In the following, only the reduced stiffness matrix

is considered. In theory the solution is simple: after the participation of stiffness matrix the unimportant unknowns of the dynamic calculation are eliminated (static condensation, Guyan algorithm):

$$\begin{bmatrix} \mathbf{S}_{11} & \mathbf{S}_{12} \\ \mathbf{S}_{21} & \mathbf{S}_{22} \end{bmatrix} = \begin{bmatrix} \mathbf{x}_1 \\ \mathbf{x}_2 \end{bmatrix} = \begin{bmatrix} \mathbf{F} \\ \mathbf{0} \end{bmatrix}, \tag{1}$$

$$\mathbf{x}_2 = -\mathbf{S}_{22}^{-1}\mathbf{S}_{21}\mathbf{x}_1 , \tag{2}$$

$$\mathbf{S}_{red}\mathbf{x}_1 = \mathbf{F} , \tag{3}$$

$$\mathbf{S}_{red} = \mathbf{S}_{11} - \mathbf{S}_{12}\mathbf{S}_{22}^{-1}\mathbf{S}_{21} . \tag{4}$$

The implementation of reduced stiffness matrix is not problemless, hence the FEM programs existing in the market have no such option, moreover the stiffness matrix of the system has no access. The stiffness matrix of dynamic systems thus can only be sought from the optional facilities of FEM programs. It means that the elements of the condensed matrix are built up from 5 digit, rounded results of the internal calculations. Although this data file consists the errors of numerical calculation, too.

The stiffness matrix of the dynamic model can be determined based on the concepts of

a, kinematic load,
b, flexibility matrix and inverse matrix theorems or instead of the concept of static load the matrix can be obtained as a result of dynamic analysis, as
c, the combination of eigenvectors and eigenvalues.

Concerning the above mentioned methods the *c* variant has given the best results obtained from the tests made on different underframe structures. This method needs less work and computational time and the obtained results are satisfactory concerning numerical punctuality, too (the comparison of different methods is summarized and presented at the GAMM'94 Conference in Braunschweig).

The meaning of stiffness matrix reduction based on the knowledge of modal parameters (eigenvalue and eigenvector) is as follows:

- the eigenvalue analysis of a mechanical system can only be done, if the mass matrix is non-singular.

If this condition is satisfied, then the system has to be transformed into the place of degrees of freedoms of the non-zero elements of the mass matrix, which means static condensation.

$$\begin{bmatrix} \mathbf{M}_1 & \mathbf{0} \\ \mathbf{0} & \mathbf{0} \end{bmatrix} \begin{bmatrix} \ddot{\mathbf{x}}_1 \\ \ddot{\mathbf{x}}_2 \end{bmatrix} + \begin{bmatrix} \mathbf{S}_{11} & \mathbf{S}_{12} \\ \mathbf{S}_{21} & \mathbf{S}_{22} \end{bmatrix} \begin{bmatrix} \mathbf{x}_1 \\ \mathbf{x}_2 \end{bmatrix} = \begin{bmatrix} \mathbf{0} \\ \mathbf{0} \end{bmatrix}, \tag{5}$$

$$\mathbf{x}_2 = -\mathbf{S}_{22}^{-1}\mathbf{S}_{21}\mathbf{x}_1 , \tag{6}$$

$$\mathbf{M}_1\ddot{\mathbf{x}}_1 + \mathbf{S}_{red}\mathbf{x}_1 = \mathbf{0}\,, \tag{7}$$

$$\mathbf{S}_{red} = \mathbf{S}_{11} - \mathbf{S}_{12}\mathbf{S}_{22}^{-1}\mathbf{S}_{21}\,. \tag{8}$$

The solution of eigenvalue problem simply means the determination of the modal parameters of the simplified model. From the results, the missing elements of eigenvalues and that of the reduced mass matrix can be calculated by the inverse transformation method. If the mass matrix of the simplified model is identic, then the equation of motion described in the subcoordinate system is as follows:

$$\mathbf{T}^T\mathbf{E}\mathbf{T}\ddot{\mathbf{q}} + \mathbf{T}^T\mathbf{S}_{red}\mathbf{T}\mathbf{q} = \mathbf{0}\,, \tag{9}$$

$$\mathbf{E}\ddot{\mathbf{q}} + \Lambda\mathbf{q} = \mathbf{0}\,, \tag{10}$$

from which the searched condensed stiffness matrix:

$$\mathbf{S}_{red} = \mathbf{T}\Lambda\mathbf{T}^T\,, \tag{11}$$

where

Λ – diagonal matrix, consisting the eigenvalues (square values of own frequencies),

$\mathbf{T}$ – normated eigenvector matrix sought from the non zero elements of mass matrix.

The way to determine the reduced stiffness matrix is as follows: in the places of degrees of freedoms to be reduced, identity mass distribution is considered and then the eigenvalue problem is solved as an option of FEM analysis. At the end, when the modal parameters are selected, the matrix is built up and the required operation is carried out.

4. Numerical Investigation and its Results

In the afore-mentioned paragraph the obtained condensed matrix can have different errors, such as the errors of the numerical procedure, which can be introduced through the process of condensation of mass matrix, the iteration procedure of eigenvalue analysis and from the truncated and rounded presentation of modal parameters (eigenvalue, eigenvector) in the data sheet of FEM analysis. While the error mentioned at last can be approximated, the errors of numerical calculation are unknown (besides the eigenvalues).

In the evaluation procedure of reduced mass matrix punctuality, the static equilibrium equations can be considered as the basis. If the flexible constraints of the system are removed then a free system is obtained, whose stiffness matrix only has internal contact forces. The force system of the kinematical loads existing in the rows of the stiffness matrix must fulfill the conditions of weight point and moment. This means that the sum of the

elements in the rows of the matrix and the moments calculated to the weight points must be zero. Although the satisfaction of the equilibrium condition is only a necessary condition. Further information can be obtained to the reliability of the condensed stiffness matrix, if the modal parameters are calculated to the free systems, too. Without going into details it is evident that the eigenvectors used as kinematical loads must fulfill the equilibrium conditions. The shape of eigenvectors, the number of nodes, i.e. lines, and its situation given for a construction (for example bus system), gives additional information for the experts in order to check the computed results. Hence, in this way the contents of errors can be detected.

The numerical analysis is carried out for a grid system of a bus and in the other hand four FEM bus models were under investigation by the application of SUPERSAP software package. The reduction has been made in the vertical plane of the underframe of the vehicles, according to the imagined vertical deformations of beam elements.

This flexible beam represents the average reduced stiffness of logitudinal underframe structures, incorporating the effect of lateral beams, too. Then the global bending stiffness parameters are given.

The eigenvalue problem is only solved to the free system consisting a grid structure. The applied FEM program is only capable to handle the modal parameters of constrained system, therefore the model is fixed with small value of stiffness.

The goal of investigation is to prove the applicability of the mentioned theorem. The most important information of the given figures in the appendix can be summarized as:

- the DOF of the system and its reduced counterpart,
- the size of the elements of reduced matrix,
- the geometrical location of weight point and
- the sum of errors in one row of the matrix, which is defined as the sum of elements and their moments.

5. Conclusions

1. The reduced stiffness matrix practically satisfies the equilibrium conditions. The values of the sums derived in every row have not reached the size of rounded errors.
   For example concerning the grid model of bus system, the maximal rounded error 0.5, due to the 5 digit displaying (while in case of 5th order approximation, the roundoff error is 5), while the error consequence concerning the moment is not else than the maximal distance multiplied by the value of error $0.5^*480 = 290$.
2. Concerning the last model the values of errors are greater and the sum of moments shows a large scale deviation in a range, which can

be located geometrically. The probability of this phenomenon can be found in the fault of FEM program made for statistical analysis. This comes from the investigation so that the errors deduced for the moment are very close to the already determined values by the application of kinematical load (a, variant). Although by this the usefulness of the concept, i.e. that the matrix is derived by the modal approach can be counteracted with the results obtained by the static condensation method, moreover it can be deduced that the relative error is within the range of round off errors.

3. The above statements are concerned with the simplification of an order of two models, therefore one can conlude that such a large size of reduction can be used in numerical way.

References

[1] SZŐKE, D.: Zusammensetzung der reduzierten Steifigkeitsmatrix, *GAMM Tagung* 1994, Braunschweig.

6. Appendix A

Model of the side wall of the bus

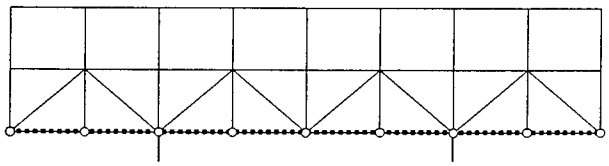

static model: 171 DOF
dynamic model: 9 DOF

S_{max}= 5.5180E4 S_{min}= 121.6 [·10 N/cm] x_{max}= 480 [cm]
max. round off error: Δ F= 0.5 Δ M= 240

DOF	1	2	3	4	5	6	7	8	9
Δ F	0.37	-0.77	0.96	-0.55	0.23	-0.55	0.96	-0.77	0.37
Δ M	41	-135	102	-28	0.0	28	-102	135	-41

FE model of the Midi-bus

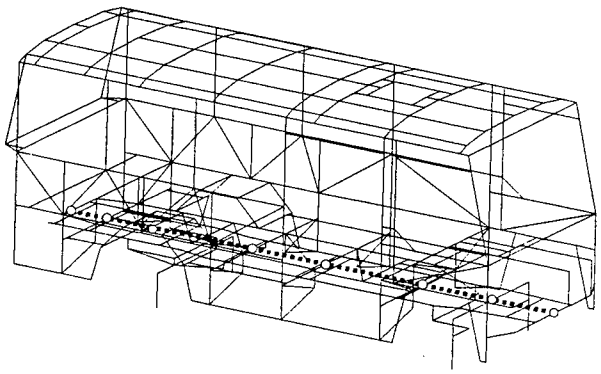

static model: 1969 DOF
dynamic model: 8 DOF

S_{max}= 6.4682E4 S_{min}= 1.0784 [·10 N/cm] x_{max}=330 [cm]
max. round off error: Δ F= 0.5 Δ M= 165

DOF	1	2	3	4	5	6	7	8
Δ F	-0.05	0.03	-0.02	0.36	-0.56	0.36	-0.02	-0.08
Δ M	-4	16	-95	140	-85	81	-67	13

FE model of the citybus (vers. A.)

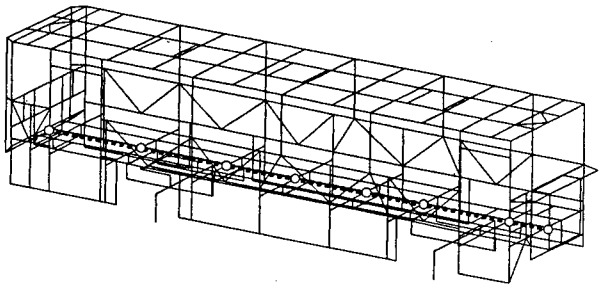

static model: 1737 DOF
dynamic model: 8 DOF

S_{max}= 6.9082E4 S_{min}= 9.7424 [·10 N/cm] x_{max}= 527 [cm]
max. round off error: Δ F= 0.5 Δ M= 263

DOF	1	2	3	4	5	6	7	8
Δ F	0.06	-0.11	0.19	0.36	-1.08	0.98	-0.28	0.03
Δ M	-29	82	-225	296	-277	191	-102	43

FE model of the citybus (vers. B.)

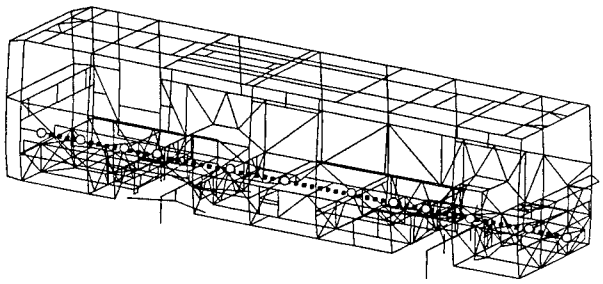

static model: 2668 DOF
dynamic model: 12 DOF

S_{max}= 1.7078E5 S_{min}= 5.3274 [·10 N/cm] x_{max}= 517 [cm]
max. round off error: Δ F= 5 Δ M= 2.58E3

DOF	1	2	3	4	5	6	7	8	9	10	11	12	
Δ F	0.09	-0.08	0.64	-0.19	-0.76	0.74	0.42	-1.33	3.31	-2.21	-0.74	0.84	
Δ M	-0.58	-1.51	2.91	-0.94	0.14	-0.18	0.14	-0.24	0.50	-0.24	0.07	-0.07	·E4
ΔM_A	-0.57	-1.53	2.91	-0.92	0.12	-0.16	0.13	-0.22	0.39	-0.15	0.08	-0.08	·E4

PERIODICA POLYTECHNICA SER. TRANSP. ENG. VOL. 23, NO. 1-2, PP. 115-122 (1995)

RESPONSE SPECTRUM ANALYSIS OF LARGE VEHICLE SYSTEMS

István KUTI

Department of Mechanics
Faculty of Transportation Engineering
Technical University of Budapest
H-1521 Budapest, Hungary

Received: November 30, 1994

Abstract

The dimensioning of vehicle body structures for service fatigue life is a highly complicated task in its every stage. Namely the appropriate structural modelling for dynamic analysis and the elaboration of realistic loading and design conditions (loading and design spectra) for the total duration of their life. In this paper the dynamic analysis of a bus is presented as a feasibility study using finite element model of large number of degrees of freedom.

Keywords: large vehicle models, modelling by finite elements, dynamic analysis, simulation of road profiles, evaluation of response spectra.

1. Introduction

The failure of mechanical structures due to material fatigue is usually originated from local yields (dislocations) in the material. Prediction of fatigue life of one or more elements of a large mechanical system necessitates the precise knowledge of the position and process (in time) of local stress concentrations producing errors or deterioration of it. This fact demands the application of well-detailed structural, usually finite element models of large number of degrees of freedom. A number of Hungarian researchers have successfully studied the theoretical, computational and measuring aspects of this problem ([1], [2], [3]), etc.). However, the actual calculations have been carried out on smaller mechanical models since earlier there were no satisfactory computational possibilities. Nowadays some developments can be observed in this area namely some of the professional finite element programs are currently available (NASTRAN, COSMOS/M, ANSYS, etc.). When the number of degrees of freedom of a finite element model is about some thousands the most useful way is the application one of these finite element programs.

Each phase of strength calculation of vehicle body structures for service fatigue life is a very complex and complicated task. First phase is the determination of representative sets of loads that are valid for the total duration of life of vehicles. These loads, for example, originate from the

roughness of different kinds of roads, manoeuvres like steering, acceleration or braking and from the excitation of the engine and power transmission. Moreover the payload is usually changed during the service life of a vehicle. Second phase is the elaboration of an appropriate vehicle structural model. Actually a vehicle body can be described as damped linear elastic system while the behaviour of suspensions and tyres are non-linear (damping and stiffness characteristics). Having determined the required vehicle responses the last phase is the fatigue life calculation itself.

For the reliable strength calculation for service fatigue life of vehicles experimental data are indispensable. Considering the input loads it is necessary to know the (measured) excitations of different roads and their expected rate of occurrence during the vehicle life of duration. Besides the road roughness measurements there are publications in the modelling of road profiles and surfaces ([4], [5]) since it is not so easy to measure parallel tracks below left and right wheels simultaneously. Moreover the designers are much more interested in the expected behaviour of vehicles over a large number of roads of the same class than in their detailed behaviour on a particular road. In the second phase especially the determination of the stiffness and damping characteristics of tyres as well as the damping of vehicle bodies requires measured data. At last, in the third phase, the elaboration of design fatigue curves requires experiments [6].

In this paper dynamic analysis of a bus structure is carried out by finite element method using the COSMOS/M finite element program. The number of degrees of freedom of the applied finite element model is 1852. Excitations are derived from two-dimensional power spectral density function which describes the roughness of road surface in vertical direction.

2. Simulation of Road Excitations

Measuring parallel road profiles simultaneously is always a very complicated and difficult operation. Final (road profile) data from measurements are usually carried out indirectly after filtering, signal analysis and unavoidable data transformations. Therefore there are numbers of attempts for the spectral representation of road surfaces ([4], [5]). In the road surface simulation we follow the method contained by paper [5] in which it is proved that from

$$G(n_x, n_y) = \frac{0.5 G_0}{\sqrt{n_x^2 + n_y^2}}\,, \tag{1}$$

the two dimensional power spectral density (psd.) function, the next one dimensional psd. function can be derived for random description of road profiles

$$G_1(n) = \frac{G_0}{n^2}\,. \tag{2}$$

In the previous equations G_0 is constant moreover n_x, n_y and n are spatial wave numbers.

In paper [4] for the random representation of road profiles the relationship

$$G_1(n) = \frac{G_0}{n^{2.5}}, \tag{3}$$

is suggested where $0.01 \leq n \leq 10$ cycles/m and values for G_0 are as follows,

motor way : $G_0 = 3 + 50 \times 10^{-8}$,
major road : $G_0 = 3 + 800 \times 10^{-8}$,
minor road : $G_0 = 50 + 3000 \times 10^{-8}$,

where $G_1(n)$ is the spectral density of road roughness in m^3/cycle and the n the unit of n is cycle/m. The unit of G_0 is compatible with other quantities in *Eq.* (3). It can be proved by direct calculation that the results in paper [5] are applicable for the *Eq.* (3). Having applied it we get the two dimensional psd. function

$$G(n_x, n_y) = \frac{G_0}{1.748\sqrt{n_x^2 + n_y^2}^{3.5}} \tag{4}$$

that will be used for the isotropic description of road surface roughness.

When a professional finite element program is applied the user is constrained by its possibilities. In case of the most finite element programs similarly to COSMOS/M the response spectrum analysis can only be performed for diagonal input spectrum matrix that is the cross spectra are assumed to be zero. Therefore it may not be applied directly for road surface excitations since cross spectra among left and right wheels are not negligible. This difficulty is overcome when the psd. functions of tracks below the wheels are represented by their realizations along the road in the function of driving distance. Using SHINOZUKA's method [7] the road profile realizations can be simulated from the psd. function given by *Eq.* (4) besides the value of $G_0 = 50 \times 10^{-8}$ which corresponds to major roads of better quality (*Fig. 1*).

3. Model Elaboration

The discussed finite element model shown in *Fig. 2* is elaborated on the basis of an actual bus. Frame structures of bus bodies usually have linear elastic properties, however, the behaviour of suspension systems and tyres is non-linear. In some cases these nonlinearities may not be neglected, for example in the case of stability problems or studying the effect of extreme road irregularities, etc. In other cases the characteristics of suspensions and tyres can be approximated by linear ones with acceptable errors when road vehicles travel on country roads of good or average quality with constant speed. Linearization of these characteristics is based on their nominal operating data released by manufacturers.

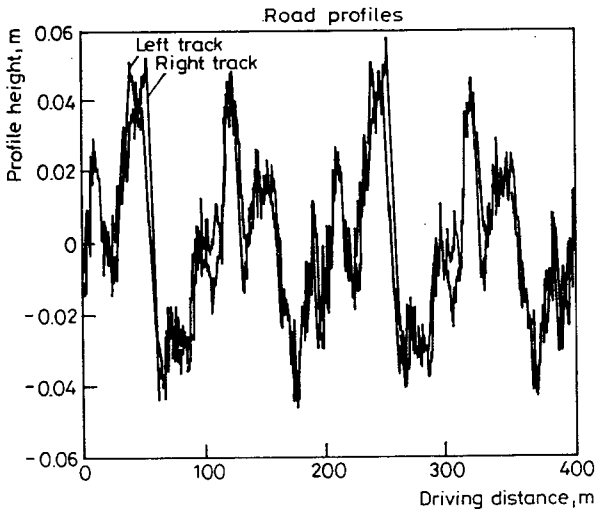

Fig. 1. Simulated road realizations below left and right wheels

The continuously distributed mass of the studied bus is divided into nodes in a manner that its mass matrix is a lumped one. As it was mentioned above the stiffness and damping of suspensions and tyres is approximated by linear characteristics while structural damping of bus body as Raleigh's damping is taken into consideration assumed to be proportional to the stiffness matrix. Kinematic excitations of road roughness in the function of time are derived from the simulated road profile realizations assuming constant travelling speed of 20 m/s. Time delay between front and rear wheels is considered.

Number of degrees of freedom of the studied finite element model is 1852 and the number of nodes and mass points is 325 and 207, respectively. The number of beam elements is 533 and 128 shell elements are built in the body of the bus model.

4. Dynamic Analysis and Results

In service, bus bodies among others are subjected to the vertical excitation of road surface roughness describing as a stationary random process. Actually the applied time history functions for excitations are derived from the road profile realisations of this random process. In compliance with it the response stress-time history functions can also be considered as realisations of a stationary random process. Being in the possession of fatigue design curves these stress time history functions can be used for the estimation of the average fatigue life [8].

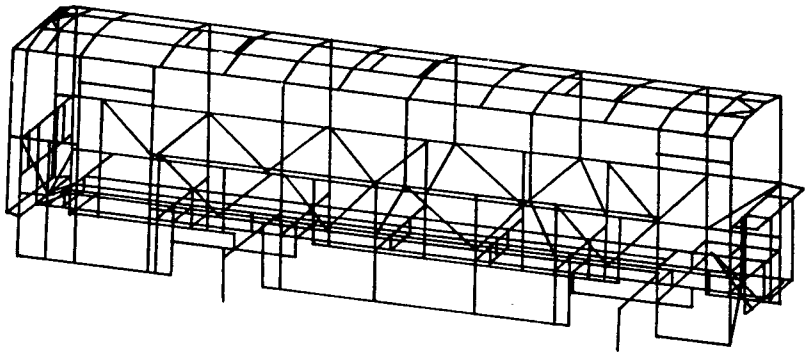

Fig. 2. Wire network sketch of the studied finite element model

Calculations of stress time history functions are carried out by the modal time history analysis module of COSMOS/M in two phases. In the first phase the lower 45 undamped natural frequencies and mode shapes are calculated up to 20 Hz. This upper limit of natural frequencies is enough to a correct dynamic stress analysis. Then, in the second phase, using these natural frequencies and mode shapes the stress-time functions are calculated in the required equidistant time points. The effect of the concentrated viscous dampers, built in the finite element model, is calculated in each time step by an iterative process. Similarly the material damping of the bus structure is taken into consideration during the second phase of the dynamic analysis. In *Figs. 3* and *4* the resultant of axial stresses (from bending moments and axial forces) and the shear stress (from torsion) can be seen respectively, arising at one end of a beam element located in the left side longitudinal web of the chassis of the bus. These stress-time history functions are made only for illustrations. In case of actual calculations the lengths of the considered time intervals can be increased to the required lengths.

If statistical nature of response stress records is necessary there is possibility to generate their power spectral density functions using Fourier transformations. For example in *Fig. 5* the power spectral density function of the axial stress record is demonstrated which is shown in *Fig. 3*. On the basis of power spectral density functions the standard deviations of response stresses can also be calculated. In case of the presented axial stress the magnitude of its standard deviation is 8.227×10^6 [N/m^2].

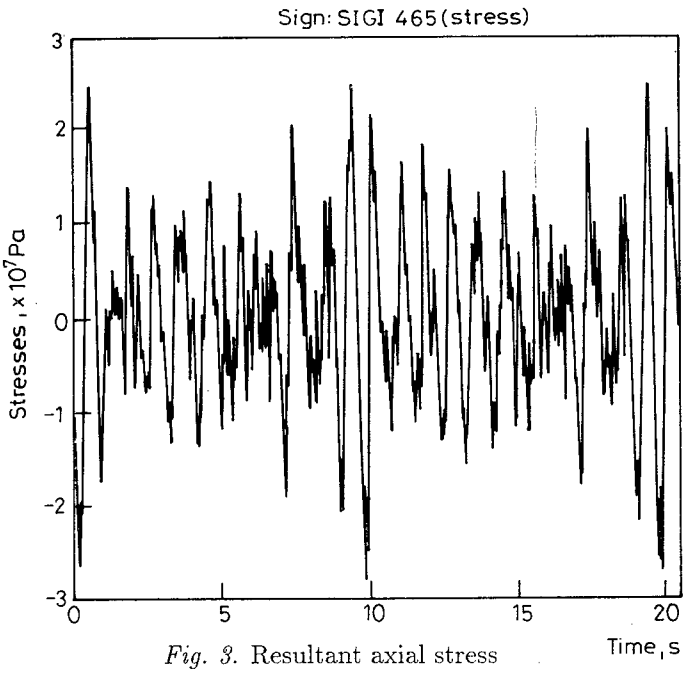

Fig. 3. Resultant axial stress

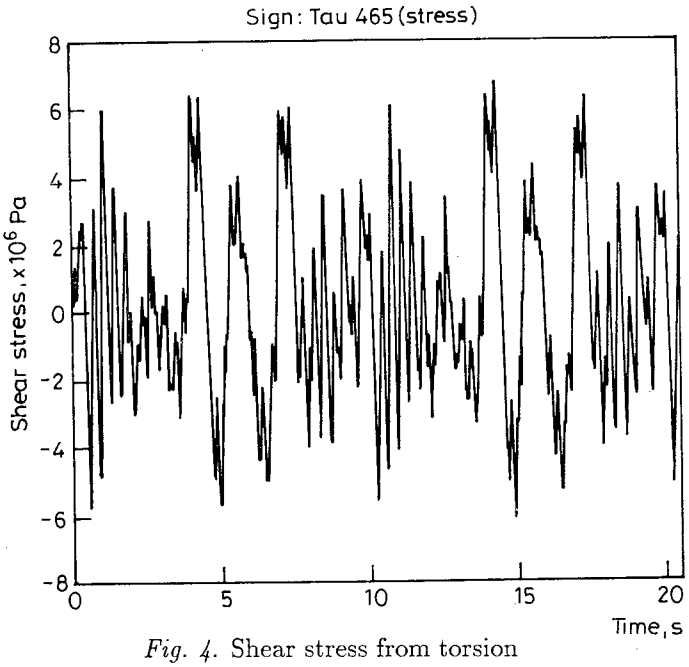

Fig. 4. Shear stress from torsion

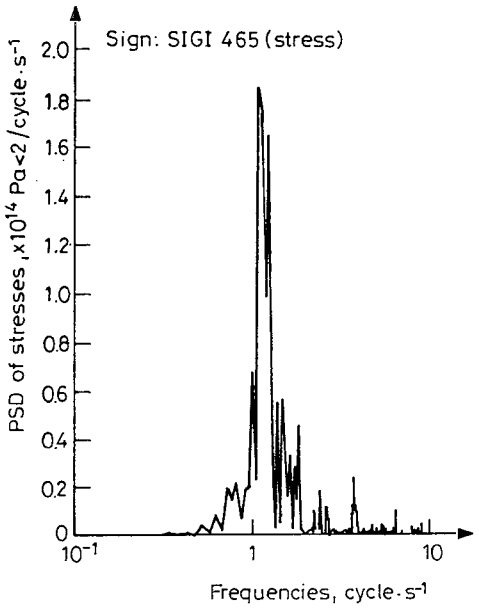

Fig. 5.

5. Conclusions and Future Tasks

The analysis presented in this paper has shown the potential applicability of one of the professional finite element programs for the calculation of fatigue life of large vehicle structures considering vertical excitations of road surface roughness.

In future there are a lot of problems to solve, for example:

- Determination of representative sets of roads that characterize the realistic road excitations for the total duration of life of vehicles. (By measurements and on the basis of literature data.)
- Determination by measurements of material damping in bus body structures.
- Theoretical and numerical study of the accuracy of linear approximation of the non-linear suspension and tyre characteristics, etc.
- Detailed modelling of the reaction of the passengers, etc.

References

[1] MICHELBERGER, P. – KERESZTES, A. – HORVÁTH, S. (1984): Modelling Problems in the Dynamic Design of Autobuses, *Proc. of Int. Conf. on Vehicle Structures, I. Mech. E. Conf.*, pp. 195–200.

[2] MATOLCSY, M. (1978): The Service Strength and Life of Bus Frame Structures, *Proc. of XVII Fisita Congress*, Budapest, Vol. II., pp. 1081–1114.

[3] FARKAS, M. – FRITZ, J. – MICHELBERGER, P. (1981): On the Effect of Stochastic Road Profiles on Vehicles Travelling with Varying Speed, *Acta Techn. Hung.* Vol. 91, No. 3–4.

[4] KAMASH, K. M. A. – ROBSON, J. D. (1978): The Application of Isotropy in Road Surface Modelling, *Journal of Sound and Vibration*, Vol. 57, No. 1, pp. 89–100.

[5] PELLEGRINO, E. – TORNAR, U. (1987): A Mathematical Model of Road Excitation, *Proc. of the Second Workshop on Road Vehicle Systems and Related Mathematics*, ICI Torino, pp. 7–26.

[6] GRUBISIC, V. (1994): Determination of Load for Design and Testing, *Int. J. of Vehicle Design*, Vol. 15, No. 1/2, pp. 8–26.

[7] SHINOZUKA, M. (1972): Digital Simulation of Random Processes and its Applications, *Journal of Sound and Vibration*, Vol. 25, No. 1, pp. 111–128.

[8] KACENA, W. J. – JONES, P. J. (1976): Fatigue Prediction of Structures Subjected to Random Vibration, *Shock and Vibration Bulletin*, No. 46, pp. 87–96.

INDEX

INFORMATION FOR AUTHORS

Submitting a Manuscript for Publication. Submission of a paper to this journal implies that it represents original work previously not published elsewhere, and that it is not being considered elsewhere for publication. If accepted for publication, the copyright is passed to the publisher: the paper must not be published elsewhere in the same form, in any language, without written consent of the executive editor. The first author will receive 50 free reprints.

Manuscripts should be submitted in English in two copies to the editors' office (see inner front cover). Good office duplicated copies of the text are acceptable.

Periodica Polytechnica is typeset using the TEX program with the AMSTEX macro package. Therefore, authors are encouraged to submit their contribution after acceptance in this form too, or at least the text of the article in a simple ASCII file (e. g. via email or on a floppy diskette, readable on an IBM compatible PC). By this solution most of the typesetting errors can be avoided, and publishing time can be reduced. An AMSTEX style file with a sample TEX source file is also available upon request.

Compilation and Typing of Manuscripts. Contributions should be typed or printed in double spacing (24 pt spacing when using text processors), on A4 paper. One page may contain not more than 10 corrections (paints do not count).

The maximum length of the manuscript is 30 standard pages (25 lines, with 50 characters in a line), including illustrations and tables. When more characters are typed on a page, the allowed page number is reduced accordingly.

When using a text processor, please use a (preferably English) spelling checker before the final printing.

Use one side of the sheet only. Paragraphs are to be indented by 5 spaces and not to be preceded by a blank line.

A correctly compiled manuscript should contain the following items:

(1) Title page giving: the suggested running header (max. 50 characters) for the odd typeset pages; the title (short, with subheading if necessary); the name(s) of the author(s); affiliation (institution, firm etc.) of the author(s), in English, with mailing address, telefax and phone numbers and email address; grants, scholarships etc. during the research (in a footnote); an informative abstract of not more than 200 words with 3-5 keywords;
(2) Textual part of the contribution with a list of references;
(3) A separate sheet listing all figure captions and table headers;
(4) Illustrations and tables (please put your name on each sheet), at least one set of illustrations in very good quality for reproduction.

Abstract. A summary or abstract of about 100-200 words should be provided on the title page. This should be readable without reference to the article or to the list of references, and should indicate the scope of the contribution, including the main conclusions and essential original content.

Keywords are to be given for the purpose of data bases and abstracting; avoid too general keywords which provide no help in literature searching.

General rules for the text. Chapters are to be numbered with Arabic numbers in decimal hierarchy.

Wherever possible, mathematical equations should be typewritten, with subscripts and superscripts clearly shown. Metric (SI) units are to be used, other units may be given in parentheses. Equations must be numbered on the right side, in parentheses. Handwritten or rare mathematical, Greek and other symbols should be identified or even explained if necessary in the margin. Letters denoting quantities are to be distinguished by different setting both in the formulae and in the text. Remember the rule that scalar quantities are to be denoted by italics (underline by hand in your manuscript), vectors by lower case bold type letters (underline doubled), and matrices by bold capitals (underline doubled). Dimensions (like cm, Ohm, V etc.) and standard function names (sin, ln, P etc.) are to be typeset in Roman typefaces (not in italics). A few important words may be distinguished by italic setting (underline).

Illustrations and Tables. Graphs, charts and other line illustrations should be drawn neatly in Indian ink, or printed by a laser printer. Computer printouts can only be used if they are of excellent quality. Figures should be submitted in an adequate size for camera-ready pages in size 1.2:1. Suggested line thicknesses: 0.18–0.35–0.4 mm or 0.5–0.7–1.14 pt. Letter sizes: 0.4 mm (10 pt). All figures should be numbered with consecutive Arabic numbers, have descriptive captions, and be referred to in the text. Captions should be self-explanatory, not merely labels. Figures must not contain lengthy texts; use captions instead.

Number tables consecutively with Arabic numbers and give each a descriptive caption at the top. If possible avoid vertical rules in tables. Tables should be preferably submitted in camera-ready form.

The earliest acceptable position of figures and tables is to be indicated in the left margin.

References. In the text references should be made by the author's surname and year of publication in parentheses, e.g. (Earl et al, 1988) or ...was given by Kiss and Small (1986a). Where more than one publication by an author in one year is referred to, the year should be followed by a suffix letter (1986a, 1986b etc.), the same suffix being given in the reference list. For the style of the reference list, which is to be given in alphabetical order, see the examples below for journal articles, conference papers and books.

Earl, J., Kis, I. and Török, I. (1988): Partial Discharge Measurement in Cables. *Periodica Polytechnica Ser. Electrical Engineering*, Vol. 32, No. 4, pp. 133–138.

Kiss, S. and Small, A. B. (1986a): Roundoff Errors in FFT. *Proc. 5th IEEE Symposium on Signal Processing*, Boston (MA), May 3–5, 1986. New York, NY, IEEE Press, CH0092-2875/86, pp. 3.5–3.9.

Kiss, S. and Small, A. B. (1986b): Ellenállások (Resistances). Budapest, Tankönyvkiadó. pp. 533–535. (in Hungarian)

More detailed guidelines for authors, with hints for the preparation of figures and with a sample page, are available from the editors' office (see inner front cover).

CONTENTS